Copyright Warning & Restrictions

The copyright law of the United States (Title 17, United States Code) governs the making of photocopies or other reproductions of copyrighted material.

Under certain conditions specified in the law, libraries and archives are authorized to furnish a photocopy or other reproduction. One of these specified conditions is that the photocopy or reproduction is not to be "used for any purpose other than private study, scholarship, or research." If a, user makes a request for, or later uses, a photocopy or reproduction for purposes in excess of "fair use" that user may be liable for copyright infringement,

This institution reserves the right to refuse to accept a copying order if, in its judgment, fulfillment of the order would involve violation of copyright law.

Please Note: The author retains the copyright while the New Jersey Institute of Technology reserves the right to distribute this thesis or dissertation

Printing note: If you do not wish to print this page, then select "Pages from: first page # to: last page #" on the print dialog screen

ABSTRACT

BATCH AND CONTINUOUS PRODUCTION OF STABLE DENSE SUSPENSIONS OF DRUG NANOPARTICLES IN A WET STIRRED MEDIA MILL

by
Afolawemi Afolabi

One way to improve the bioavailability of poorly water-soluble drugs is to reduce particle size of drug crystals down to nanoscale via wet stirred media milling. An increase in total surface area per mass loading of the drug and specific surface area as well as reduced external mass transfer resistance allow a faster dissolution of the poorly-water soluble drug from nanocrystals. To prevent aggregation of nanoparticles, polymers and surfactants are dissolved in water acting as stabilizers via adsorption onto the drug crystals.

In the last two decades, ample experimental data were generated in the area of wet stirred media milling for the production of drug nanoparticle suspensions. However, a fundamental scientific/engineering understanding of various aspects of this process is still lacking. These challenges include elucidation of the governing mechanism(s) during nanoparticle formation and physical stabilization of the nanosuspension with the use of polymers and surfactants (formulation parameters), understanding the impact of process parameters in the context of first-principle-based models, and production of truly nanosized drug particles (10–100 nm) with acceptable physical stability and minimal contamination with the media. Recirculation mode of milling operation, where the drug suspension in a holding tank continuously circulates through the stirred media mill, has been commonly used in lab, pilot, and commercial scales. Although the recirculation is continuous, the recirculation operation mode is overall a batch operation, requiring significant number of batches for a large-volume pharmaceutical product. Hence, development and investigation of a truly continuous process should offer significant advantages. To explain the impact of some of the processing parameters, stress intensity and stress number concepts were widely used in literature, which do not account for the effect of suspension viscosity explicitly. The impact of the processing parameters has not been explained in a predictive and reliable manner.

In this dissertation, a comprehensive investigation of the production of Griseofulvin nanosuspensions in a wet stirred media mill operating in both the recirculation and continuous modes has been conducted to address the aforementioned fundamental challenges. Griseofulvin has been selected as a model poorly water-soluble BCS Class II drug. Impact of various formulation parameters such as stabilizer type and loading as well as processing parameters such as rotor speed, bead loading, bead size, suspension flow rate and drug loading was studied. A major novelty of the present contribution is that the impact of processing and formulation parameters has been analyzed and interpreted using a combined experimental–theoretical (microhydrodynamic model) approach. Such a comprehensive approach allowed us to intensify the process for the production of sub-100 nm drug particles, which could not be produced with top-down approaches in the literature so far. In addition, a multi-pass mode of continuous operation was developed and the so-called "Rehbinder effect", which has not been shown for the breakage of drug particles, was also elucidated. The dissertation work (1) indicated the need for a minimum polymeric stabilizer-to-drug ratio for proper stabilization of drug nanosuspensions as dictated by polymer adsorption and synergistic interactions between a polymeric stabilizer and a surfactant, (2) demonstrated the existence of an optimum polymer concentration from a breakage rate perspective in the presence of a surfactant, which results from the competing effects of viscous dampening and enhanced steric stabilization at higher polymer concentration, (3) developed fundamental understanding of the breakage dynamics–processing–formulation relationships and rationalized preparation of a single highly drug-loaded batch (20% or higher) instead of multiple dilute batches, (4) designed an intensified process for faster preparation of sub-100 nm particles with reduced specific energy consumption and media wear (i.e. minimal drug contamination), and (5) provided first evidence for the proof of Rehbinder effect during the milling of drugs. Not only do the polymers and surfactants allow proper physical stabilization of the nanoparticles in the suspensions, but they also do facilitate drug particle breakage. This dissertation also discusses applications of nanosuspensions and practical issues encountered during wet media milling.

BATCH AND CONTINUOUS PRODUCTION OF STABLE DENSE SUSPENSIONS OF DRUG NANOPARTICLES IN A WET STIRRED MEDIA MILL

by
Afolawemi Afolabi

A Dissertation
Submitted to the Faculty of
New Jersey Institute of Technology
in Partial Fulfillment of the Requirements for the Degree of
Doctor of Philosophy in Chemical Engineering

Otto H. York Department of
Chemical, Biological and Pharmaceutical Engineering

August 2013

.

APPROVAL PAGE

BATCH AND CONTINUOUS PRODUCTION OF STABLE DENSE SUSPENSIONS OF DRUG NANOPARTICLES IN A WET STIRRED MEDIA MILL

Afolawemi Afolabi

Dr. Ecevit A. Bilgili, Dissertation Advisor — Date
Assistant Professor of Chemical, Biological, and Pharmaceutical Engineering, NJIT

Dr. Robert B. Barat, Committee Member — Date
Professor of Chemical, Biological, and Pharmaceutical Engineering, NJIT

Dr. Edward L. Dreizin, Committee Member — Date
Professor of Chemical, Biological, and Pharmaceutical Engineering, NJIT

Dr. Zafar Iqbal, Committee Member — Date
Research Professor of Chemistry and Environmental Science, NJIT

Dr. Rennan Pan, Committee Member — Date
Director, Glaxosmithkline (GSK), Collegeville, PA

BIOGRAPHICAL SKETCH

Author: Afolawemi Afolabi

Degree: Doctor of Philosophy

Date: August 2013

Undergraduate and Graduate Education:

- Doctor of Philosophy in Chemical Engineering,
  New Jersey Institute of Technology, Newark, NJ, 2013

- Bachelor of Science in Chemical Engineering,
  New Jersey Institute of Technology, Newark, NJ, 2009

Major: Chemical Engineering

Publications:

Azad, M., Afolabi, A., Patel N., Davé, R., Bilgili, E., (2013). "Preparation of Stable Colloidal Suspensions of Superdisintegrants via Wet Stirred Media Milling" Particuology, Accepted.

Bilgili, E., Afolabi, A., (2012). "A Combined Microhydrodynamics–Polymer Adsorption Analysis for Elucidation of the Roles of Stabilizers in Wet Stirred Media Milling." Int. J. Pharm., 439, 193–206.

Monterio, A., Afolabi, A., Bilgili, E., (2013). "Continuous Production of Drug Nanoparticle Suspensions via Wet Stirred Media Milling: A Fresh Look at the Rehbinder Effect." Drug Dev. Ind. Pharm., 39, 266–283.

Afolabi, A., Akinlabi, O., E. Bilgili, "Impact of Process Parameters on the Breakage Dynamics of BCS Class II Drugs during Wet Media Milling: A Microhydrodynamic View," Eur.J. Pharm.Sci., Under Review.

Chettiannan, R., Afolabi, A., Yaragudi, N., Davé, R., Bilgili, E., "Fast Production of Drug Suspensions with Sub - 100 nm Particles and Minimal Media Contamination via Intensified Wet Media Milling" Int. J. Pharm., Submitted.

Conference Presentations and Poster Sessions:

Afolabi, A., Bilgili, E., "Batch and Continuous Production of Stable Drug Nanoparticle Suspensions via Wet Stirred Media Milling," Annu. Meet., NSBE Oral Competition, Indianapolis, IN March 29, 2013 **(3rd place winner)**.

Afolabi, A., Akinlabi, O., E. Bilgili, "Impact of Process Parameters on the Breakage Dynamics of BCS Class II Drugs during Wet Media Milling: A Microhydrodynamic View," Annu. Meet. NJ ISPE Poster Competition, Johnson & Johnson, New Brunswick, NJ April 18, 2013 **(2nd place winner)**.

Afolabi, A., Bilgili, E., "A Microhydrodynamic Analysis of Wet Stirred Media Milling for Production of Stable Drug Nanoparticle Suspensions," Annu. Meet. AIChE, Paper No: 655b, Pittsburgh, PA, Oct.-Nov. 2012.

Azad, M., Afolabi, A., Davé, R., Bilgili, E., "Preparation of Co-Ground Drug-Superdisintegrant Nanosuspensions As a Precursor to the Production of Fast Dissolving Surfactant-Free Nanocomposite Microparticles," Annu. Meet. AIChE, Paper No: 631d, Pittsburgh, PA, Oct.-Nov. 2012.

Bilgili, E., Afolabi, A., "Impact of Processing and Formulation Parameters on Drug Nanoparticle Suspensions Produced via Wet Stirred Media Milling," Annu. Meet. AIChE, Paper No: 397b, Minneapolis, MN, Oct. 2011.

Bilgili, E., Afolabi, A., "Continuous Production of Stable Drug Nanoparticle Suspensions via Wet Stirred Media Milling," Annu. Meet. AIChE, Paper No: 506a, Minneapolis, MN, Oct. 2011.

Elele, E., Shen, Y., Boppana, R., Afolabi, A., Bilgili, E. A., Khusid, B., "Electrodeless Electro-Hydrodynamic Printing of Nano-Suspensions for Personalized Medicines," 65th Annu. Meet. APS, Paper No: A30.00007, San Diego, CA, Nov. 2012.

To the Most High God, the Alpha and Omega, the Beginning and the End, which is, and which was, and which is to come, the Almighty

ACKNOWLEDGMENTS

My deepest gratitude and appreciation goes to my dissertation advisor Dr. Ecevit A. Bilgili, for his unending support, understanding, guidance, and for exposing me to the field of particle technology. His advisement is crucial to the success of this dissertation. Special thanks are given to Dr. Robert B. Barat, Dr. Edward L. Dreizin, Dr. Zafar Iqbal, and Dr. Rennan Pan for their invaluable advisements and contributions as committee members.

I would like to acknowledge Dr. Rajesh Davé who was always a great source of wisdom and financial support provided for me from the National Science Foundation Engineering Research Center for Structured Organic Particulate Systems through the Grant EEC-0540855. I would also like to acknowledge the financial support of the Otto York Department of Chemical, Biological and Pharmaceutical Engineering. Special thanks are given to Boehringer-Ingelheim for the unrestricted research grant and NJIT SEED funding in establishment of the particle engineering laboratory.

I would like to give me sincere and deepest thanks to my whole family: my parents, Ajibola and Abisade; my brothers, Abolasade and Ajibolu; my aunties, Modupe and Adesumola; their husbands, Mustafa and Abimbola; their children, Christina, David, Daniel, and Esther; my sister-in-law, Abimbola and her family; and to all of my extended family and friends not mentioned above. Your sacrifices, unending support and achievements have shaped me into the man I am today, and I deeply thank you for all you have done.

I would also like to thank Alex Monteiro, Naveen Yaragudi, Dr. Catharina Knieke, Dr. Ravikumar Chettiannan and the rest of our group for the help.

TABLE OF CONTENTS

TABLE OF CONTENTS
(Continued)

TABLE OF CONTENTS
(Continued)

Chapter **Page**

TABLE OF CONTENTS
(Continued)

LIST OF TABLES

LIST OF TABLES
(Continued)

Table **Page**

.

LIST OF FIGURES

LIST OF FIGURES
(Continued)

Figure **Page**

LIST OF FIGURES
(Continued)

Figure **Page**

LIST OF FIGURES
(Continued)

Figure **Page**

LIST OF FIGURES
(Continued)

Figure **Page**

LIST OF FIGURES
(Continued)

LIST OF SYMBOLS

a	average frequency of drug particle compressions, Hz
A_1, A_2	parameters of the empirical model fit in Eq. (4.3), s
A_3	parameters of the empirical model fit in Eq. (4.3), $s^{2.6}/m^{2.6}$
A_{eff}	effective Hamaker constant, J
c	volumetric concentration of the beads, –
D	stirrer tip diameter, m
d	particle diameter (size), m
d_1, d_2	core particle diameter, m
d_b	milling bead diameter, m
d_{lim}	limiting particle size of the drug particles, m
e	elementary charge, 1.6022×10^{-19} C
E	cumulative energy consumption by the slurry, J
E^*	specific energy consumption per unit mass of drug suspension, J/kg
Eu	stirrer Euler number, –
F	milling intensity factor for same bead size in Eq. (4.2), $m^{2.6}/s^{2.6}$
F	milling intensity factor for different bead size in Eq. (5.4), $m^{0.6}/s^{2.6}$
F_b^n	average maximum normal force during collision of two identical elastic beads, N
k	restitution coefficient for bead–bead collisions, –
k_B	Boltzmann's constant, 1.3806×10^{-23} J/K
K	coefficient obtained from an empirical correlation, –
m_s	mass of the drug suspension in the milling chamber, kg
n	Initial number of particles, –
p	probability to be caught between the beads for a single drug particle, –
P	power applied by the mill motor, W
P_s	specific energy, J/kg

PSD	particle size distribution
P_w	power applied by the mill stirrer per unit volume, W/m^3
Q	volumetric flow rate of the drug suspension, m^3/s
r	center to center distance between the particles, m
R	radius, m
R^*	half of harmonic mean size of the bead and drug particles, m
Re	stirrer Reynolds number, –
R_{diss}	dissipation (effective drag) coefficient of the bead, –
R_{diss0}	dissipation coefficient when relative motion of the bead–liquid is absent, –
s	surface to surface separation distance between two particles, m
SSR	sum-of-squared residuals
t	milling time, s
T	temperature , 298 K
u	stirrer tip speed, m/s
u_b	average bead oscillation velocity, m/s
V	interaction potential, J
$V_{attractive}$	van der Waals interaction potential, J
$V_{repulsive}$	Electrostatic interactions potential, J
V_{steric}	Steric interaction potential, J
V_{total}	Net interaction potential, J
V_m	volume of the milling chamber, m^3
Y	Young's modulus, Pa
Y^*	reduced elastic modulus for the bead–drug contact, Pa

Greek letters

Δ	Cumulative variable, –
α	radius of the contact circle formed at the contact of two beads, m
δ	shell thickness, m

ε_d	Dielectric constant, –
ε	volumetric drug loading in the drug suspension, –
ε_{coll}	energy dissipation rate due to partially inelastic bead–bead collisions, W/m^3
ε_{ht}	power spent on shear of equivalent liquid of the slurry at the same shear rate but calculated (measured) as if no beads were present in the flow, W/m^3
ε_m	non-dimensional bead–bead gap thickness at which the lubrication force stops increasing and becomes a constant, –
ε_o	Permittivity of free space, 8.854×10^{-12} $A^2.s^4/m^3.kg$
ε_{tot}	total energy dissipation rate, W/m^3
ε_{visc}	energy dissipation rate due to both the liquid–beads viscous friction and lubrication, W/m^3
γ	coefficient for bead–drug particle contact, –
γ^*	shear rate, 1/s
η	Poisson's ratio, –
η_{app}	apparent viscosity, kg/m·s
κ	Debye length, m
λ	material-dependent factor in Eq. (4.1), $kg/m^{3.6}\cdot s^{0.4}$
λ	material-dependent factor for different bead size in Eq. (5.3), $kg/m^{1.6}\cdot s^{0.4}$
μ_o	Permeability of free space, 1.26×10^{-6} $kg/s^2.A^2$
μ_L	apparent shear viscosity of the equivalent fluid, kg/m·s
ν	frequency of single-bead oscillations, Hz
Π	energy dissipation rate attributed to the deformation of drug particles per unit volume, W/m^3
θ	granular temperature, m^2/s^2
ρ	density, kg/m^3
ρ_g	grafting density, molecules/m^2

σ_b^{max}	maximum contact pressure at the center of the contact circle, Pa
σ_y	contact pressure in a drug particle when the fully plastic condition is obtained, Pa
τ	shear stress, Pa
τ_p	characteristic time constant of the process, s
ψ_o	surface potential, V
ζ	zeta potential, V

Indices

b	beads
g	grafting
L	equivalent liquid (milled drug suspension)
p	drug particle
y	yield
50	50% passing size (median size) of the cumulative distribution, m
90	90% passing size of the cumulative distribution, m

CHAPTER 1

INTRODUCTION

1.1 Background and Motivation

Fast and efficient development of pharmaceutical formulations containing poorly water-soluble drug particles is of great interest to the pharmaceutical industry (Date and Patravale, 2004). By some estimates, 60% of drug candidates currently under investigation can be classified as Biopharmaceutical Classification System (BCS) Class II, for which the bioavailability is limited by the dissolution rate. Recent advances in combinatorial chemistry aided the discovery of new drug molecules with such low solubility characteristics (Muller and Peters, 1998; Niwa et al., 2011). Few approaches that have been employed to improve drug solubility are the use of co-solvents or salt/pro-drug formation (Merisko-Liversidge and Liversidge, 2011), reduction of particle size of the drugs (Merisko-Liversidge and Liversidge, 2011) and amorphous solid formation by methods such as hot melt extrusion (Leuner and Dressman, 2000), super cooling of the melt, rapid precipitation from solution (e.g., during freeze-drying or spray drying) (Hancock and Zografi, 1997). While amorphous solids have higher solubility and dissolution rates, they are generally less stable physically and chemically than their corresponding crystal forms.

A popular approach for the bioavailability enhancement of poorly water-soluble drugs is particle size reduction. Reduction in particle size leads to an increase in the specific surface area of the drug particles which in turn improves the dissolution rate as per the modified version of Noyes-Whitney equation (Noyes and Whitney, 1897).

$$\frac{dm}{dt} = k_0 A(C_S - C) \tag{1.1}$$

Here, k_0 is the overall solute transfer coefficient defined by $1/k_0 = 1/k_i + 1/k_c$, where k_i and k_c are the interface rearrangement constant and the external mass transfer coefficient respectively, C_s is the saturation solubility, C is the concentration in the bulk solution, A is the total surface area, and m is the amount dissolved at time t. Upon a decrease in particle size, the saturation solubility C_s increases according to the Ostwald-Freundlich equation and results in an increased dissolution rate in the nanoparticle size domain (Florence & Attwood, 1981). The increase in saturation solubility and surface area is important for dissolution of the nanoparticles (typically particles smaller than 1 μm, prevalent within the pharmaceutical terminology); while the increase in surface area and decrease in the thickness of diffusion layer around the microparticles (Bisrat & Nystorm, 1988) contribute to the higher dissolution rates of the microparticles (particles typically in the size range 1–10 μm).

Ultrafine particles (or nanoparticles) can be produced either by the so-called top-down approach, which includes jet milling (Chan et al., 2002), high pressure homogenization (Kamiya et al., 2009), and stirred media milling (Bilgili et al., 2004, 2006); or by the bottom-up approach (Anais et al., 2009; Chiou et al., 2008) which involves building up particles by precipitation of dissolved molecules. Wet media milling has been the most popular approach of producing nanocrystals with four products Rapamune® (Wyeth), Emend® (Merck), Tricor® (Abbott), and Megace® (Par Pharmaceutical) currently on the market, which make use of Elan's Nanocrystal Technology® (Liversidge et al., 1992). During wet stirred media milling, an aqueous

suspension containing drug particles and dissolved stabilizers (polymer and/or surfactant) as well as hard beads (media) is stirred at high speed by a rotor. Repeated stressing of the micron-sized drug particles that are captured between the colliding beads causes breakage and eventually production of nanoparticles provided that milling is continued for sufficient time. The milled particles in nanosuspensions (suspensions with median size typically less than a micron) interact significantly with the neighboring particles through van der Waals (interparticle) forces, hydrophobic forces, etc. due to their large surface area (Israelachvili, 1992). The attractive interparticle forces can ultimately result in particle aggregation if the suspensions are not properly stabilized. Stabilization can be achieved using polymers, surfactants or a combination of both; however, the particle growth can also occur in the suspension by Ostwald ripening during storage (Wu et al., 2011). Therefore, from a stability perspective as well as patient preference/compliance perspective, the general practice in pharmaceutical industry is to dry these suspensions into powders and incorporate them into solid dosage forms via standard pharmaceutical unit operations such as blending, milling, capsule filling, and tabletting.

1.1.1 Physical Stability of Wet-Media Milled Suspensions

In general, physical stabilization of suspensions can be achieved either by electrostatic, steric or electrosteric interactions (Kim, 2004; Napper, 1970). During electrostatic stabilization, the surface of the particles is equally charged (e.g. by the formation or adsorption of ions) so that repulsion forces emerge, which can overcome the attractive van der Waals forces between the particles. Steric stabilization results from the adsorption of polymers or larger monomers onto the particles' surface. If the adsorbed polymer contains charged groups, steric and electrostatic components act simultaneously,

which is typically described as electrosteric stabilization. To protect drug particles against aggregation, formulators commonly use stabilizers like polymer(s) and/or surfactant(s).

A review by Van Eerdenbrugh et al. (2008) lists various polymers and surfactants and their concentrations used for the stabilization of drug nanoparticle suspensions. Few systematic studies on the stabilizing capability of adsorbed polymers suggest the importance of hydrophobicity of the polymers (Lee et al., 2005, 2008) and surface energy difference between drug particles and polymers (Choi et al., 2005; Lee et al., 2008). Investigation of the polymer adsorption on drug nanoparticles in aqueous suspensions has led to insight into the steric stabilization capability of the polymers and selection of optimum polymer concentration (Choi et al., 2008; Lee, 2003; Panmai and Deshpande, 2003; Sepassi et al., 2007). Despite these advances, it is still not possible to *predict*, based solely on first principles and mechanistic understanding, an optimal stabilizer type/concentration for a given drug that ensures proper short- and long-term physical stability of the drug nanoparticle suspensions. This task is usually carried out by stabilizer screening studies at the bench-scale (Kesisoglou et al., 2007; Van Eerdenbrugh et al., 2008), where milling dynamics, process cycle times, and scale-up effects are not of any concern.

1.1.2 Breakage Dynamics and Microhydrodynamics

Milling in a planetary mill (Van Eerdenbrugh et al., 2009) or in a ball mill (e.g. Lee, 2003; Lee and Cheng, 2006; Liversidge and Cundy, 1995; Merisko-Liversidge et al., 1996; Van Eerdenbrugh et al., 2007), both making use of vials containing drug suspensions with various stabilizers, has previously been described for their capability in obtaining nanoparticles. These mills are regarded as medium or low-energy mills; hence,

suspension flow and microhydrodynamics are quite different in these mills than in the wet *stirred media mills.* It is not surprising to see that the nanoparticles are produced after several hours to a few days of milling even at the bench scale with suspension quantities on the order of ~10 ml. In other screening studies, wet stirred media mills are used: e.g. the Nanomill® System (e.g. Kesisoglou et al., 2007). However, the impact of stabilizers on the microhydrodynamics has not been reported. More importantly, as pointed out by Bhakay et al. (2011), most wet media milling work in pharmaceutical literature either disregarded the breakage kinetics (rate) completely (as in Ain-Ai and Gupta, 2008; Cerdeira et al., 2010; Choi et al., 2005; Liversidge and Cundy, 1995; Tanaka et al., 2009; Van Eerdenbrugh et al., 2008, 2009) or did not characterize the breakage kinetics and its relationship to the stabilizers quantitatively (as in Lee, 2003; Lee et al., 2005, 2008; Choi et al., 2008; Deng et al., 2008).

While scant information is available regarding the impact of stabilizers on the breakage rate during wet stirred media milling, the microhydrodynamics, which is the study of the fluctuating motion of the beads in sheared suspensions, has not been investigated at all. The milling process has been largely treated as a "black-box" in pharmaceutical literature. The recent advances in wet media milling of non-pharmaceutical materials are summarized here. It is known that high solids loading results in high suspension viscosity, which could dampen the collision speed of the milling beads (viscous dampening) and reduce the breakage rate (Knieke et al., 2010; Mende et al., 2003). Knieke et al. (2010) provided a semi-theoretical model based on the kinematic equations describing the relative motion of undeformed spheres (beads). However, their model does not allow calculation of the bead oscillation velocity and

frequency (microhydrodynamic parameters), which fundamentally determine the breakage rate along with the material properties in a wet stirred media mill (Eskin et al., 2005a, 2005b). Using the well-known kinetic theory of granular flows and the fundamental granular energy balance (Gidaspow et al., 1994), Eskin et al. (2005a, 2005b) developed a microhydrodynamic model on the basis that the power spent on stirring the mill rotor dissipates through bead–suspension viscous friction, lubrication, and partially inelastic collisions of the beads. This model was used to study the effects of stirring speed, beads loading, and bead size on the microhydrodynamic parameters in a mixing tank with Rushton type paddles, which provided significant insight into the experimentally observed impact of these process parameters on the bead collision dynamics. However, this model has not been applied to the wet stirred media milling of drug suspensions with the objective of elucidating the impact of stabilizers such as viscous dampening of the polymers on the breakage rate.

1.1.3 Impact of Wet Milling Process Parameters

Although ample experimental data exists on pharmaceutical nanoparticles production and their stabilization via wet media milling, the impact of process parameters on the breakage kinetics and its relation to the microhydrodynamics has not been reported. Considering that the breakage kinetics determines the process cycle times and production rate for a desired fineness of the nanosuspension, it is fair to remark that a significant gap exists in the pharmaceutical engineering literature regarding the dynamics of the wet media milling process. As wet media milling process is time-consuming, costly, and energy-intensive (Kawatra, 2006) and the breakage kinetics determines the cycle time

and production rate for a desired fineness, milling process design and optimization entails a good understanding of the breakage kinetics and its controlling process parameters.

Process parameters such as stirrer speed, bead loading, and drug loading can significantly affect the breakage rate and milling time required in a wet stirred media milling process. In a recent review paper, Peltonen and Hirvonen (2010) summarized various process parameters and their ranges investigated in wet media milling processes. While Peltonen and Hirvonen (2010) and the references cited therein provide great understanding of the impact of stabilization and formulation, little fundamental understanding of the impact of process parameters is available at the beads scale (microhydrodynamics). In a more recent work, Ghosh et al. (2012) present the effects of stirrer speed, bead size, and drug content on the final milled suspension; however, the impact of these parameters on the breakage kinetics was not investigated. Singare et al. (2010) and Singh et al. (2011) used a statistical design of experiments with a response surface methodology (RSM) with the goal of optimizing the process parameters including milling speed and time. However, no information regarding the breakage kinetics was presented explicitly. In general, the statistically-based designs of experiments such as those in Singare et al. (2010) and Singh et al. (2011) do not provide significant physical insight at the beads scale as to how the process parameters affect the breakage kinetics.

1.1.4 Preparation of Sub-100 nm Drug Particles with Minimal Contamination

It is understood that faster particle breakage reduces the milling time required for desired particle fineness and energy consumption, and can be achieved by the right selection of mill process parameters such as bead size, bead load, stirrer speed, and suspension flow rate. Influence of these operating parameters on the specific energy consumption and

product fineness has been studied previously through experiments and empirical models (Fadhel and Frances, 2001; Stehr, 1984; Tüzün et al., 1995). However, the combined effect of these parameters on breakage kinetics leading to the preparation of fine drug nanoparticles at a shorter time is not addressed. Therefore, a detailed strategy or methodology for combining different mill process parameters has to be developed which could lead to an intensified process for the faster production of fine drug nanoparticles with reduced specific energy consumption.

In pharmaceutical applications, the demand for using fine drug nanoparticles with size as low as possible is increasing steadily, as fine drug nanoparticles offers a much faster dissolution rate, and also result in rapid onset of therapeutic action (Muller et al., 2006). Most importantly, drug nanoparticles with size < 100 nm renders feasible and efficient sterile filtration of aqueous drug nanosuspensions, and allows higher loading for reduced injection volume in parenteral dosage forms (Baert et al., 2009; Xiong et al., 2008). In addition to the nanosuspension dosage form, nanocomposite microparticles made of very small size drug nanoparticles offer rapid redispersion of particles at an increase drug loading in a given mass of dosage (Bhakay et al., 2013). Therefore, it is important to prepare drug nanosuspensions with size as small as possible (< 100 nm) to achieve enhanced efficacy in various pharmaceutical applications. By varying the process parameters, several researchers have prepared inorganic nanoparticles in the size range of 10–100 nm using WSSM technique. For example, 20–50 nm Magenta pigment (Bilgili et al., 2004, 2006), 50 nm Al_2O_3 (Stenger et al., 2005), 50 nm $BaSO_4$ (Patel et al., 2012), and 30–40 nm quartz, calcite and dolomite (Wang et al., 2006) have been prepared. However, an investigation on the effect of process parameters for the preparation of drug

nanoparticles having < 100 nm has not been attempted so far. From the current search in literature, only using smaller initial drug particle size and at low batch volume, the drug nanoparticles with a typical median size of 136 nm and above have been produced via WSMM. It is to be noted that the preparation of drug particles with < 100 nm size is a challenging task, especially if the mill is desired to operate with the large initial particle size, high batch volume (> 200 ml at the bench scale), and high drug load > 10 % (w/w).

Despite the fact that drug nanoparticles with size as small as possible is of great interest in pharmaceutical application, drug product contamination introduced by typical bead wear (for example, e.g., yttrium stabilized zirconia) at intensified process conditions is a major concern and is yet to be investigated. Due to the high turbulence during the wet stirred media milling process, wear is generated, between grinding beads and grinding bead/milling chamber and transferred into the related drug products as undesirable contamination (Juhnke et al., 2012; Peltonen and Hirvonen, 2010). In general, toxicity data and contamination levels from ceramics is unknown and needs to be quantified according to the current regulatory concepts and permitted daily exposures for oral, parenteral, pulmonary and topical administration (Juhnke et al., 2012).

A literature review by Juhnke et al. (2012) lists several earlier publications that explored the generation of wear from grinding beads. Few systematic studies on the generation of grinding bead wear was investigated via the wet milling of alumina particles with yttrium stabilized beads along with fused corundum beads (Mende and Schwedes, 2006; Breitung-Faes and Kwade, 2008). The generation of wear was characterized by a gravimetric method, including washing, drying and weighing of the grinding media to determine the overall weight loss. Adam et al. (2008) investigated the

wet media of zirconia with grinding beads made from zircon silicate as well as a grinding chamber and a stirrer made from zirconia. The generation of wear from grinding beads was characterized by determining elemental silicium using inductively coupled plasma atomic emission spectrometry. Ohnishi et al. (2010) investigated the use of grinding beads made from silica doped and undoped yttrium stabilized zirconia during wet milling of barium titanate. The doped silica had a lower wear as compared to the un-doped grinding media. Several material combinations of grinding beads and milling chamber with respect to the overall generated wear during the production of fenofibrate nanosuspensions by wet media milling has also been investigated (Stein et al., 2010). Stein et al. (2010) investigated the use of various grinding beads made from glass, polyamide, polycarbonate, polystyrene, stainless steel and zirconia as well as milling chambers made from polyamide, polyurethane, stainless steel and zirconia. Wear generated by the grinding beads was characterized by a gravimetric method. Despite these advances, for a given drug, it is still not possible to *predict drug contaminations levels*, based solely on the mill process parameters such as bead size, bead load, stirrer speed, and suspension flow rate.

1.1.5 Continuous Production of Drug Nanoparticles and Rehbinder Effect

In all major chemical industries, continuous processing is widely used for large-scale production. There is a growing interest in moving all pharmaceutical unit operations in drug product manufacture from batch processes to continuous processes. Recent publications on continuous mixing have made the case for the feasibility of continuous drug product manufacture (see e.g. Berthiaux et al., 2008; Vanarase et al., 2010a, 2010b). This manufacturing strategy could bring the pharmaceutical industry advantages such as

consistent and improved product quality, reduced waste, lower inventory and equipment costs, easy scale-up, flexibility, and short cycle times. Pharmaceutical unit operations such as tabletting, roller compaction, and capsule filling are already performed semi-continuously; whereas mixing; wet milling, most granulations, drying, and tablet coating are usually performed in the batch/recirculation mode. Although ample experimental studies of batch and recirculation mode of wet media milling exist in literature, little effort has been devoted to the cascade or multi-pass continuous modes. In the area of continuous wet stirred media milling of drugs, there are only a couple of patents available (Holland et al., 2006; Verhoff et al., 2003). Feasibility of nanomilling Fenofibrate using a wet stirred media mill operating in single-pass mode was presented (Verhoff et al., 2003); however, the figures and examples provided only described recirculation milling. Another patent (Holland et al., 2006) presents what is believed to be the first documentation of cascade continuous mode of wet media milling of drugs, where Nabumetone nanoparticles were produced using five media mills in series. In both cases, only the final median particle size was provided; procedural details were missing, and the breakage dynamics was not studied.

During wet media milling of materials, stabilizers such as polymer(s) and/or surfactant(s), also known as grinding aids, can affect or play a major role in three phenomena: stabilization of the suspension and proper dispersion of the product particles, microhydrodynamics during media milling as affected by suspension rheology, and particle strength. However, it is interesting to note that most pharmaceuticals literature on wet media milling focused on the first phenomena, i.e., stabilization and proper dispersion of the particles, thus largely neglecting the impact of the stabilizers on the

microhydrodynamics and the particle strength (associated with the Rehbinder effect). Rehbinder effect is described as the facilitation of crystal cleavage and decrease in hardness of crystals caused by surfactant solutions, and can be explained by the weakening of bonds in the crystal surface layer due to adsorption and lowering of the specific surface free energy (Rehbinder and Shchukin, 1972; Shchukin, 1999, 2006). Rehbinder effect manifests itself as facilitated breakage of crystals and enhanced breakage rate in the presence of surface-active agents (El-Shall and Somasundaran, 1984). There exists no prior work as to whether Rehbinder effect arises during the wet media milling of drugs owing to the use of such agents as stabilizers.

1.2 Objectives and Major Research Tasks

Nanoparticle suspensions (nanosuspensions) of poorly water-soluble drugs are prepared with the ultimate goal of increasing the dissolution rate and bioavailability of such drugs. This dissertation work aims to achieve the following objectives: (1) develop a fundamental understanding of the impact of various stabilizers, i.e., polymers and surfactants, on the breakage kinetics, microhydrodynamics, and suspension rheology/stability; (2) investigate the impact of various milling parameters on the breakage kinetics and explain the findings from a microhydrodynamic perspective; (3) design an intensified process for faster preparation of sub-100 nm particles with reduced specific energy consumption and media wear (i.e. minimal drug contamination); (4) develop a continuous milling methodology that can mimick true cascade continuos milling operation; and (5) explore if Rehbinder effect plays any role during the milling of drugs.

In this dissertation, a comprehensive investigation of the production of Griseofulvin nanosuspensions in a wet stirred media mill operating in both the recirculation and continuous modes has been conducted to achieve the afore-mentioned objectives. Griseofulvin was selected as a model poorly water-soluble BCS Class II drug. Impact of various formulation parameters such as stabilizer type and loading as well as processing parameters such as rotor speed, bead loading, bead size, suspension flow rate and drug loading were studied. A major novelty of the present contribution is that the impact of processing and formulation parameters has been analyzed and interpreted using a combined experimental–theoretical (microhydrodynamic model) approach. Such a comprehensive approach allowed us to intensify the process for the production of sub-100 nm drug particles, which could not be produced with top-down approaches in the literature so far. In addition, a multi-pass mode of continuous operation was developed and the so-called "Rehbinder effect", which has not been shown for the breakage of drug particles, was also investigated. The five major objectives stated above have been divided into four Chapters and are discussed in the dissertation outline.

1.3 Dissertation Outline

The dissertation work is presented in seven chapters. Chapter 1 begins with a review of what has been done in literature followed by the objectives and outline of the dissertation. Chapter 2 discusses the theoretical framework used in the current work. Chapter 3 explores the roles of various stabilizers such as polymers and surfactants during the wet milling of drugs. Chapter 4 investigates the impact of processing parameters on the breakage kinetics using a combined experimental–microhydrodynamic model approach.

Chapter 5 presents an intensified process for the production of sub-100 nm particles and how such a process is designed in view of the microhydrodynamic model. The contamination of the drug product during milling was also investigated in Chapter 5. In Chapter 6, the continuous production of drug nanoparticles suspension was investigated with a fresh look at the Rehbinder effect. Chapter 7 gives an overall summary and conclusion of the current work. Potential future work is discussed in Chapter 8.

CHAPTER 2

THEORETICAL BACKGROUND

2.1 Fundamentals of Interparticle Interactions and Stabilization of Drug Particles against Aggregation

2.1.1 Fundamentals of Interparticle Interactions

Several interparticle forces or interactions come into play when two colloidal particles approach one another. The extent of interaction between two colloidal particles is determined by how rapidly the approach occurs. The colloidal behavior which is dependent on the surface properties of the particles affects both the state of aggregation along with the suspension rheology.

2.1.1.1 van der Waals Interactions. The most attractive van der Waals forces is the interaction between induced dipoles, which arise due to orientation effects between molecules with permanent dipoles or induction effects in neutral particles (Hunter, 1986). Particle stressing and/or deformation as a result of two colliding beads can lead to aggregation of particles during milling. The attractive van der Waals interaction energy, V_a is given by (Russel et al., 1987).

$$V_a = -\frac{1}{6k_BT} A_{eff} \left[\frac{d_1 d_2}{2\left\{ r^2 - \left(\frac{d_1 + d_2}{2} \right)^2 \right\}} + \frac{d_1 d_2}{2\left\{ r^2 - \left(\frac{d_1 - d_2}{2} \right)^2 \right\}} + \ln \left\{ \frac{r^2 - \left(\frac{d_1 + d_2}{2} \right)^2}{r^2 - \left(\frac{d_1 - d_2}{2} \right)^2} \right\} \right] \qquad (2.1)$$

where k_B is Boltzmann's constant, T is absolute temperature, A_{eff} is the effective Hamaker constant, d_1 and d_2 are the core diameters of the two particles, which can be of different

size, and *r* is the center to center distance between the particles. Whenever an aggregate of two or more particles is formed, the resultant aggregate is considered to be a spherical particle of volume equal to the sum of the constituents (Kumar et al., 2010).

2.1.1.2 Electrostatic Interactions. Electrostatic repulsion energy (V_e) between two particles is calculated using the expression below. (Hunter, 1987; Lee et al., 1998; Ohshima, 1995)

$$V_e = 2\pi \frac{d_1 d_2}{d_1 + d_2} \varepsilon\varepsilon_o \psi_o^2 \ln\left\{1 + \exp\left(-\kappa s\right)\right\} \quad \text{for} \quad 0.5d\kappa > 5 \tag{2.2}$$

$$V_e = \pi d_1 d_2 Y_1 Y_2 \varepsilon\varepsilon_o \left(\frac{k_B T}{e}\right)^2 \frac{\exp\left(-\kappa s\right)}{s + \frac{d_1 + d_2}{2}} \quad \text{for} \quad 0.5d\kappa < 5 \tag{2.3}$$

where

$$Y_i = \frac{8\tanh\left(\frac{e\psi_o}{4k_B T}\right)}{1 + \left[1 - \frac{\kappa d_i + 1}{\left(\kappa \frac{d_i}{2} + 1\right)^2} \tanh^2\left(\frac{e\psi_o}{4k_B T}\right)\right]^{\frac{1}{2}}}$$

where subscript *i* indicates 1, 2; e is elementary charge, ε is the dielectric constant of the medium (water), ε_o is the permittivity of free space, ψ_o is the surface potential and κ is Debye length. The surface potential ψ_o can be approximated by measuring values of the ζ - potential.

In general, the repulsion potential during electrostatic interactions is generated from electrical double layer (EDL) (see schematic in Appendix A (Figure A.1)). The

EDL is sensitive to the ion concentration in the system (i.e. the ions move freely under the influence of electrical and thermal forces in the so called diffuse layer). Upon an increase in the ion strength, the thickness of the EDL decreases due to screening of the surface charge (Kim, 2004). This effect leads to a decrease in the repulsion potential and an increase in the attractive potential (van der Waals interaction) (i.e. the vulnerability of dispersed particles to form aggregates). Zeta (ζ) potential is the electric potential at the shear plane and is the representative of the surface charge (see schematic in Appendix A (Figure A.2)).

2.1.1.3 Steric Interactions. Attractive van der Waals and electrostatic interactions often fail to describe the all interactions; steric repulsion energy between polymer coated spherical nanoparticles is given by (Rosensweig, 1985)

$$V_s = \frac{1}{2}\pi d^2 \rho_g \left[2 - \frac{l+2}{t} \ln\left[\frac{1+t}{1+\frac{l}{2}} \right] - \frac{l}{t} \right] \qquad (s/2\delta) \le 1 \qquad (2.4)$$

$$V_s = 0 \qquad (s/2\delta) > 1 \qquad (2.5)$$

where ρ_g is the grafting density (i.e. the number of stabilizing groups bound to the particle surface), s is the surface to surface separation distance, δ is the thickness of the polymer chain (shell) and d is the average core diameter of the two solid particles (see schematic in Appendix A (Figure A.3). Steric interaction between two particles of diameters d_1 and d_2 can be calculated using average core diameter $d = (d_1 + d_2)/2$ (Castro et al., 2008). In addition, $l = 2s/d$ and $t = 2\delta/d$ have been defined (see schematic in Appendix A (Figure A.3)).

The net interaction potential energy (V_{total}) can be calculated by summing all the above individual interaction potentials. This is governed by van der Waals (V_a), steric (V_s), and electrostatic (V_e) interactions and is discussed next further in the next section by the DLVO theory.

2.1.2 Stabilization of Drug Particles against Aggregation

The physical stability of poorly water-soluble drug nanosuspensions produced by wet media milling must be preserved against aggregation and ripening during the production and storage. Milled drug particles with mean sizes below 1 μm show a strong tendency to aggregate due to a high number concentration (given solid loading), small interparticle distances, enhanced Brownian motion, and relatively high surface energy (Bruno et al., 1996; Knieke et al., 2009; Lee, 2003; Sommer et al., 2006). During milling, repeated stressing of the micron-sized drug particles that are captured between the colliding beads increases the turbulent shear, which can cause a high collision rate among the particles and in turn high aggregation rate (Barthelmes et al., 2003; Peukert et al., 2005; Su et al., 2004). The physical stability during the storage of the nanosuspensions is affected by the sedimentation (gravity), Ostwald ripening, Brownian motion, along with van der Waals interactions (see section 2.1.1.1). Based on the physical stability of the suspension, it is known that drug particles below 1 μm can be stabilized electrostatically due to unipolar charging of particles; sterically by the adsorption of polymers on the particle surface; or electrosterically by a combination of both electrostatic and steric mechanism (see schematic of various forms of stabilization in Appendix A (Figure A.4)).

2.1.2.1 Electrostatic Stabilization. *The DLVO-Theory*: The net interaction potential (V_{total}) between particles is the result of repulsion forces ($V_{repulsive}$) due to the electric double layer (electrostatic interaction) and attraction due to the van der Waals interaction ($V_{attractive}$). The superposition of the van der Waals interaction and electrostatic repulsion can be traced back to the independent research of Derjaguin and Landau (1941) as well as Verwey and Overbeek (1948) and is known as DLVO theory (see schematic in Appendix A (Figure A.5)). Mostly the repulsive steric interaction is also included so that the net interaction energy consists out of:

$$V_{total} = V_{repulsive} + V_{attractive} + V_{steric} \tag{2.6}$$

The probability of a particle to overcome the energy barrier leads to more aggregation due to the attractive interaction (see schematic in appendx A (Figure A.5)). For this case, attraction is very strong and redispersion of the particles is almost impossible (i.e. strong aggregate formation). If repulsive forces are large enough, the suspension can remain well dispersed.

2.1.2.2 Steric Stabilization. Unlike electrostatic stabilization, the influence of steric stabilization on the energy barrier is complex to interpret. However, it can be understood mainly through the adsorption or chemisorption of polymer chains on the surface of the particles (Napper, 1977). If the concentration of the polymer is high (i.e. increase in the polymer layer thickness), the attractive forces will be suppressed and the surface coverage of the polymer on the particle will be high (Fleer et al., 1938). When two particles coated with polymer approach each other, one can distinguish them by three distance regimes (Davies and Binner, 2000). At large distances between the particles, no overlap of the polymer is observed. For this case, no repulsive forces are acting. At a

close distance, an overlap of the polymer chains is observed, for solvents, a densification of the polymer chains is detected and solvent molecules are depleted out of the overlap area into the solvent (Wu et al. 2011). In a good solvent, the entanglement of polymer chains is unfavorable, strong enthalpic interaction (good solvation) between the solvent and the stabilizing segment of the stabilizer is the key factor to achieve steric stabilization and prevent particles from aggregation in the medium (Kim, 2004; Nutan and Reddy, 2009). The chemical potential of the solvent molecules is higher than in the bulk solvent, resulting in an increase of the osmotic pressure and yielding a positive contribution to the net interaction potential (V_{total}) (i.e. the reason for the repulsion). For the third case, particles approach each other closer to the compressed polymer layer. The compression forces in addition to the osmotic forces have to be considered.

2.1.2.3 Electrosteric Stabilization. Electrosteric stabilization occurs, if the adsorbed polymer contains charged groups, steric and electrostatic components act simultaneously. Basically, the development of a double layer is formed when the non-polar ends of the polymers adsorb favorably on hydrophobic particles in polar surroundings, while the polar ends reach into the polar solvent (Klimpel, 1999). Consequently, the concentration of the ionic charge should be optimal to avoid suppression of the double layer. The stabilization is strengthened by the polymer layer due to the steric effect suggesting that the principle of the DLVO theory can be applied.

2.1.3 Comparison: Steric Stabilization vs. Electrostatic Stabilization

Steric stabilization offers several distinct advantages over electrostatic stabilization.

- Steric stabilization is comparatively insensitive to the presence of electrolytes because the dimensions of non-ionic chains vary relatively little with the electrolyte

concentration. This contrasts sharply with the electrical double layers, which are strongly dependent upon the ionic strength (Hunter, 1986). This accounts for the coagulation of electrostatically stabilized dispersions on the addition of electrolyte.

- Steric stabilization is equally effective in both aqueous and non-aqueous dispersion media. This contrasts with electrostatic stabilization, which is relatively ineffective in non-polar dispersion media.
- Steric stabilization is equally effective at both high and low volume fractions/concentrations of the dispersed phase, the high volume fraction dispersions displaying relatively low viscosities.
- Sterically stabilized suspensions can be often be flocculated reversibly whereas this is less common with electrostatically stabilized suspensions.
- Sterically stabilized suspensions frequently display good freeze-thaw stability, which can be a desirable attribute in some practical application (e.g. paint system).

Despite all these advantages, there exist several significant disadvantages for the application in wet stirred media milling. High molecular weight polymers affect the suspension rheology during the milling process which could dampen the collision speed of the milling beads (viscous dampening), resulting in a reduced breakage rate. Moreover, the adsorbed polymers can be desorbed from the particle surface by the high shear forces during milling. However, the most critical issue and disadvantage is due to the unknown adsorption kinetics for high molecular weight molecules.

2.2 Impact of Apparent Shear Viscosity on Suspension Rheology in Wet Stirred Media Mills

It is known that both a high solids loading and particle–particle interactions results in high suspension viscosity. High solids loading could dampen the collision speed of the milling beads (viscous dampening), resulting in a reduced breakage rate (Knieke et al., 2010; Mende et al., 2003) while particle-particle interactions can increase the rate of aggregation. Suspension viscosity affects the microhydrodynamics, which is the study of the fluctuating motion of the beads during the media milling process. It is therefore necessary to measure the rheological properties of the milled suspension.

The rheological behavior of suspensions is determined by the shear stress function $\tau(\gamma^*)$ or alternatively the shear viscosity function $\eta_{app}(\gamma^*)$ which has to be measured in stationary shear experiments. The two functions are connected by a constitutive equation for the shear stress (Hunter, 1986). Here, γ^* is the shear rate, which is applied by the rheometer, and $\eta_{app}(\gamma^*)$ a characteristic material function which describes the flow behavior of the fluid. The typical flow characteristic of suspensions is further explained in Appendix B.

2.3 Analysis of the Breakage Kinetics

When particle breakage governs the dynamics of a wet media milling process as opposed to particle growth/aggregation in a properly stabilized suspension, the median particle size d_{50} decreases in time t monotonically and approaches/attains a limiting value provided milling is continued for a prolonged time. The evolution can be described by a first-order exponential decay function as follows (Bilgili et al., 2008; Strazisar and Runovc, 1996; Varinot et al., 1999):

$$d_{50}(t) = d_{\lim} + [d_{50}(0) - d_{\lim}]\exp(-t/\tau_p) \tag{2.7}$$

where $d_{\lim}$ is the limiting median particle size, τ_p is a characteristic time constant of the process, and $d_{50}(0)$ is the initial median particle size. A lower τ_p corresponds to faster breakage of the particles and a higher overall apparent breakage rate, which will be shortly referred to as the breakage rate throughout the rest of this dissertation. To estimate $d_{\lim}$ and τ_p, Eq. (2.7) was fitted to the measured median size data via minimization of the following sum of squared residuals (SSR):

$$\text{SSR} = \sum_{i=1}^{n} \left[\log_{10}\left(d_{50i}^{\text{exp}}\right) - \log_{10}\left(d_{50i}^{\text{mod}}\right)\right]^2 \tag{2.8}$$

where the superscripts 'exp' and 'mod' refer to experiment and model, respectively. The median sizes at different time points were indexed by i (i = 1, 2, …, n). SigmaPlot's (Version 11) nonlinear regression wizard, which has a built-in Marquardt-Levenberg algorithm, was used for the minimization. Preliminary analysis indicated that large particles with as-received median particle size broke faster initially (within first minute) than the particles produced after one minute or first turnover or pass. Therefore, Eq. (2.7) with a single time constant τ_p was not able to fit the whole experimental data governed by two or potentially more characteristic time constants (Cho et al., 1996). Hence, initial median particle size at 0^{th} min was discarded, thus making the 1^{st} min median size the initial size for better fitting capability, which is in line with prior studies (Varinot et al., 1999; Bilgili and Afolabi, 2012).

2.4 Microhydrodynamic Analysis

Based on the kinetic theory of granular flows and the fundamental granular energy balance (Gidaspow et al., 1994), Eskin et al. (2005a and 2005b) developed a model to calculate the mean velocity of the milling bead oscillations (fluctuations) in a well-mixed slurry. The salient features of this model are presented here and readers are referred to Eskin et al. (2005a) for the full set of assumptions and the development of their model. It is assumed that the power input by the mill rotor in a wet stirred media mill is uniformly applied throughout the whole volume of the slurry and equals the total energy dissipation rate. The power input dissipates through fluctuating motions of the beads and liquid–beads viscous friction at the micro-scale; hence, the total energy dissipation rate (ε_{tot}) is given by

$$\varepsilon_{tot} = P_w = \varepsilon_{visc} + \varepsilon_{coll} \tag{2.9}$$

where P_w is the power applied by the rotor per unit volume, ε_{visc} is the energy dissipation rate due to both the liquid–beads viscous friction and lubrication, and ε_{coll} is the energy dissipation rate due to partially inelastic bead–bead collisions. Numerical simulations performed by Eskin et al. (2005a, 2005b) and Bilgili's research group (not shown here for brevity) indicate that ε_{visc} is much greater than ε_{coll}, making the viscous friction–lubrication the main energy dissipation mechanism.

In its current form, Eq. (2.9) can be used for a suspension undergoing turbulent motion, which is characterized by the stirrer Reynolds number ($Re = ND^2\rho_L/\mu_L$) greater than 35000 (Kawatra, 2006). Re value between 120 and 35000 describes a laminar–turbulent transition region and a Re value less than 120 describes a laminar region. In Re definition, N is the rotor speed, D is the rotor's tip diameter, ρ_L is the density of the

equivalent liquid, and μ_L is the apparent shear viscosity of the equivalent fluid. Eskin et al. (2005a, 2005b) considered the equivalent liquid to be water (~1 cP); therefore, their numerical simulations considered the turbulent motion. On the other hand, most drug suspensions with polymeric stabilizers have orders of magnitude higher viscosity than water and can exhibit a flow behavior in the transition region. As commonly assumed in the wet stirred media milling literature (refer to Kawatra, 2006), the equivalent liquid was taken as the milled suspension. The shear viscosity obtained at a shear rate of 1000 1/s was taken as the μ_L value. Although the shear rate in media mills could exceed this value, earlier work (Bernhardt et al., 1999; Knieke et al., 2010) considered 1000 1/s to be a representative value because the shear viscosity did not change drastically above 1000 1/s and it can be reliably measured by most rheometers. Re values were calculated with the equivalent liquid properties of the milled suspensions. In this dissertation, unless otherwise indicated, Re typically ranged from 1000–35000; thus, the flow was in the transition region in most runs.

Since Eq. (2.9) does not consider the energy dissipation due to friction between "liquid layers", which becomes more pertinent in the transition region, a new term should be added to the right-hand-side. Eskin and Miller (2008) included such a term ε_{ht} in the granular energy balance for a slurry flow in fractures. ε_{ht} is defined as the power spent on shearing equivalent fluid of the slurry (beads–drug suspension here) at the same shear rate but calculated or measured as if no particles (beads here) were present in the slurry. Then, following Eskin et al. (2005a, 2008), Eq. (2.9) can be modified as

$$P_w = \varepsilon_{visc} + \varepsilon_{coll} + \varepsilon_{ht} \tag{2.10}$$

$$P_w = \frac{54\mu_L c\theta R_{diss}}{{d_b}^2} + \frac{12}{d_b\sqrt{\pi}}\left(1-k^2\right)\left[\frac{1-0.5c}{(1-c)^3}\right]c^2\rho_b\theta^{3/2} + \varepsilon_{ht} \tag{2.11}$$

where c is the beads volumetric concentration, R_{diss} is the dissipation or effective drag coefficient, d_{b} is the average bead size (taken as the median size of the bead), ρ_{b} is the density of the beads (measured to be ~6000 kg/m^3), k is the restitution coefficient for the bead–bead collisions (taken from Tatsumi et al., 2009), and θ is the granular temperature defined as the bead–liquid relative mean-square velocity. The dissipation coefficient R_{diss} is given by Wylie et al. (2003) as

$$R_{\text{diss}} = R_{\text{diss0}}(c) + K(c)\, d_{\text{b}}\rho_{\text{L}}\theta^{1/2}/\mu_{\text{L}} \tag{2.12}$$

ρ_{L} is the density of the equivalent liquid, K is a coefficient expressed as an empirical correlation of bead concentration c expressed as

$$K(c) = \left(0.096 + 0.142c^{0.212}\right)/(1-c)^{4.454} \tag{2.13}$$

R_{diss0} is the dissipation coefficient taking into account squeezing in the equivalent liquid film between two approaching beads and is expressed as follows:

$$R_{\text{diss0}}(c) = k_1(c) - k_2(c)\ln\varepsilon_{\text{m}} \tag{2.14}$$

In Eq. (2.14), ε_{m} is the non-dimensional bead–bead gap thickness at which the lubrication force stops increasing and becomes a constant. According to Sangani et al. (1996), ε_{m} can be taken as 0.003. k_1 and k_2 in Eq. (2.14) are computed using

$$k_1(c) = 1 + 3\sqrt{c/2} + (135/64)c\ln c + 11.26c(1 - 5.1c + 16.57c^2 - 21.77c^3) \tag{2.15}$$

$$k_2(c) = c\left(1-0.5c\right)/(1-c)^3 \tag{2.16}$$

Using the equivalent liquid properties (ρ_{L} and μ_{L}), power input values in the presence and absence of the beads (P_{w} and ε_{ht}), and the aforementioned bead parameters, Eq. (2.11) is

solved for the granular temperature (θ) using MATLAB's fsolve function. The average bead oscillation velocity (u_b) and the frequency of single-bead oscillation (ν) are determined using the calculated θ value from

$$u_b = \sqrt{\frac{8\theta}{\pi}} \quad \text{and} \quad \nu = \frac{24c}{d_b}\left[\frac{1-0.5c}{(1-c)^3}\right]\sqrt{\frac{\theta}{\pi}} \tag{2.17}$$

The microhydrodynamic parameters (θ, u_b, and ν) determine the intensity and frequency of the bead–bead collisions, and thus the number of compression events and compression forces to which the drug particles are subjected during the milling. At the micro-scale (beads scale), these parameters are good predictors of the breakage rate for a given material (Eskin et al. 2005b).

Eskin et al. (2005b) advanced the earlier microhydrodynamic model (Eskin et al. 2005a) by considering the elastic contact deformation of the beads along with the elastic–perfectly plastic deformation of the particles caught between the beads. While the beads frequently collide due to their fluctuating motions in a slurry, which are characterized by θ, u_b, and ν, the beads capture and compress (deform) the particles to be milled. Based on Hertzian theory of elastic impact, the average maximum normal force F_b^n during collision of two identical elastic beads, the radius of the contact circle formed at the contact of two beads α_b, and the maximum contact pressure at the center of the contact circle σ_b^{max} (see schematic of bead–bead interaction in Appendix A (Figure A.6)) were calculated using

$$F_b^n = 1.96\left(\frac{Y_b}{1-\eta_b^2}\right)^{2/5}\rho_b^{3/5}R_b^2\theta^{3/5} \tag{2.18}$$

$$\alpha_b = \left[\frac{3}{4}\frac{\left(1-\eta_b^2\right)}{Y_b}R_b F_b^n\right]^{1/3} \tag{2.19}$$

$$\sigma_{\mathrm{b}}^{\max} = \frac{3}{2}\frac{F_{\mathrm{b}}^{n}}{\pi\alpha_{\mathrm{b}}^{2}} \tag{2.20}$$

where Y_{b}, and η_{b} are the Young's modulus and Poisson's ratio of the bead material. (yttrium stabilized zirconia here), and were taken from the literature as 200 GPa and 0.2, respectively (Ashby, 1999; Srikar et al., 2004); R_{b} is the bead radius and was taken as half of d_{b}. The probability p of a single particle with radius R_{p} being caught between beads was estimated as the ratio of the volume containing the caught particles to the volume of milled drug suspension falling on a pair of the milling beads and is expressed as

$$p = 0.97\frac{c}{1-c}\left[\frac{\rho_{\mathrm{b}}\left(1-\eta_{\mathrm{b}}^{2}\right)}{Y_{\mathrm{b}}}\right]^{2/5}\theta^{2/5}\frac{R_{\mathrm{p}}}{R_{\mathrm{b}}} \tag{2.21}$$

The average frequency of drug particle compressions a was estimated using Eq. (2.22) below as the product of this probability p and the frequency of single-bead oscillations ν

$$a = p\nu \tag{2.22}$$

The energy dissipation rate resulting from the deformation of the drug particles per unit volume Π characterizes the grinding intensity and is expressed as follows:

$$\Pi = 2.23\frac{c^{2}(2-c)}{(1-c)^{3}}\frac{1}{\pi^{5/2}\varepsilon\sigma_{\mathrm{y}}}\left(\frac{Y_{\mathrm{b}}}{1-\eta_{\mathrm{b}}^{2}}\right)^{18/15}\left(\frac{Y^{*}}{Y_{\mathrm{p}}}\right)^{\gamma}\rho_{\mathrm{b}}{}^{4/5}\frac{R_{\mathrm{p}}}{R_{\mathrm{b}}^{2}}\theta^{13/10} \tag{2.23}$$

where ε, Y^{*}, Y_{p}, η_{b}, σ_{y}, R_{p}, and R_{b} respectively denote volumetric drug loading in the milled suspension, reduced elastic modulus of the bead–drug particle contact, elastic modulus of the drug particles, Poisson's ratio of the beads, contact pressure in a drug particle captured when the fully plastic condition is obtained, radius of the drug particle, and radius of the bead.

To calculate Π using the expressions derived by Eskin et al. (2005b) (Eq. (2.23)), one must either find the mechanical properties of the drug particles (Y_p, η_p, σ_y) from the literature or measure them. First, it is difficult to find reliable mechanical properties of the drug particles or to measure them. Second, the objective of this dissertation is to gain fundamental insight into the impact of the process parameters on the breakage kinetics. While the potential influence of different bead materials and drugs are of interest, it is not considered here. Therefore, multiplicative decomposition or factorization of Π into a material-dependent factor λ and a process-dependent factor, F, which is referred to as the milling intensity factor, yields: $\Pi = \lambda F$, where functional forms of λ and F will be specifically introduced in Chapter 4 and Chapter 5.

CHAPTER 3

A COMBINED MICROHYDRODYNAMICS–POLYMER ADSORPTION ANALYSIS FOR ELUCIDATION OF THE ROLES OF STABILIZERS IN WET STIRRED MEDIA MILLING

3.1 Introduction

About 40% of active substances identified through combinatorial screening programs in pharmaceutical industry are poorly water-soluble (Lipinski, 2002). Size reduction of drug crystals increases the specific surface area, which can improve the dissolution rate of drugs according to the Noyes–Whitney equation (Noyes et al., 1897). Wet stirred media milling has found common use as a robust process to reduce micron-sized drug particles to nanoparticles, i.e., particles less than 1 μm (Bruno et al., 1996; Merisko-Liversidge et al., 2003). In this process, an aqueous suspension containing drug particles and dissolved stabilizers (polymer and/or surfactant) as well as hard beads is stirred at high speed by a rotor. Stabilizers are added to prevent the aggregation of milled drug particles and to inhibit particle growth (ripening) during milling/storage. An optimal stabilizer type/concentration, which ensures proper short- and long-term physical stability of a drug nanoparticle suspension, is usually obtained by stabilizer screening studies at the bench-scale (Kesisoglou et al., 2007; Van Eerdenbrugh et al., 2008), where milling dynamics, process cycle times, and scale-up effects are not of major concern. To this end, milling in a planetary mill (Van Eerdenbrugh et al., 2009) or in a ball mill (e.g. Lee and Cheng, 2006; Van Eerdenbrugh et al., 2007), both making use of vials containing drug suspensions with various stabilizers, has previously been described for their capability in obtaining nanoparticles. These mills are regarded as medium or low-energy mills; hence, suspension flow and microhydrodynamics are quite different in these mills than in the

wet *stirred media mills*. It is not surprising to see that the nanoparticles are produced after several hours to a few days of milling even at the bench scale with suspension quantities on the order of ~10 ml. In other screening studies, wet stirred media mills have been used: e.g. the Nanomill® System (e.g. Kesisoglou et al., 2007). However, the impact of stabilizers on the microhydrodynamics has not been reported. More importantly, as pointed out by Bhakay et al. (2011), most wet media milling work in pharmaceutical literature disregarded the breakage kinetics completely (e.g. Ain-Ai and Gupta, 2008; Tanaka et al., 2009). Other studies (Choi et al., 2008; Deng et al., 2008; Lee et al., 2008) did not characterize the breakage kinetics and its relationship to the stabilizers quantitatively.

While scant information is available regarding the impact of stabilizers on the breakage rate during wet stirred media milling, the microhydrodynamics, which is the study of the fluctuating motion of the beads in sheared suspensions, has not been investigated at all. The wet media milling has been largely treated as a "black-box" in pharmaceutical literature. It is known that high solids loading results in high suspension viscosity, which could dampen the collision of the milling beads, resulting in a reduced breakage rate (Knieke et al., 2010; Mende et al., 2003). Knieke et al. (2010) provided a semi-theoretical model based on the kinematic equations describing the relative motion of undeformed spheres (beads). However, their model does not allow calculation of the bead oscillation velocity and frequency, which fundamentally determine the breakage rate along with the material properties in a wet stirred media mill. Eskin et al. (2005a) developed a microhydrodynamic model to study the effects of stirring speed and bead size on the microhydrodynamics in a mixing tank with Rushton type paddles, which

provided significant insight into the experimentally observed impact of these process parameters on the breakage rate. However, this model has not been applied to the wet milling of drug suspensions with the goal of elucidating the impact of stabilizers such as viscous dampening of the polymers.

This chapter is a first attempt to develop a fundamental understanding of the roles of a cellulosic polymer (hydroxypropyl cellulose, HPC) on the apparent breakage rate of griseofulvin (GF), a model poorly water-soluble drug, in the presence–absence of an anionic surfactant (sodium dodecyl sulfate, SDS) during wet stirred media milling. The major novelty here is the use of a *combined microhydrodynamics–polymer adsorption analysis*. To this end, temporal evolution of the particle size during milling was investigated as a function of HPC concentration, in the presence and absence of SDS. The particle size data were analyzed via an empirical rate model to quantify the overall apparent breakage rate. Particle sizing via laser diffraction, scanning electron microscopy (SEM), and rheometry were used to characterize the milled suspensions. Another novelty is that unlike most wet media milling studies that solely relied on particle sizing. This chapter examined the aggregation state of the milled suspensions via *both* laser diffraction and rheometry. HPC adsorption on GF particles was determined using a thermo-gravimetric method. The viscosity of the milled suspensions was measured and used in the microhydrodynamic model. In the absence of SDS, an increase in HPC concentration reduced the extent/rate of particle aggregation leading to faster apparent breakage. On the other hand, due to a synergistic stabilizing action of HPC with SDS, lower HPC concentration was needed to stabilize the suspensions, and an optimum HPC concentration for the fastest apparent breakage was found. The microhydrodynamic

analysis quantified the viscous dampening effect of HPC, while only the combined analysis could explain the experimentally observed optimum.

3.2 Experimental

3.2.1 Materials

Griseofulvin (GF, Cat# 606440, US Pharmacopeia, Letco Medical, Livonia, MI, USA) was used as a model BCS Class II drug because of its low solubility in water: 7.7 µg/ml (Merisko-Liversidge and Liversidge, 2011). A non-ionic cellulosic polymer, hydroxypropyl cellulose (HPC, Klucel® SL, Lot# NOH-4811, Nisso America Inc, New York, NY, USA) and an anionic surfactant, sodium dodecyl sulfate (SDS, 99% ACS reagent, Cas# 436143-100G, Sigma Aldrich, Bellefonte, PA, USA) were acquired due to their common use in wet media milling (Kesisoglou et al., 2007). Wear-resistant yttrium stabilized zirconia beads (Zirmil Y, Saint Gobain ZirPro, Mountainside, NJ, USA) with a median size of 430 µm were used as the media in the milling.

3.2.2 Methods

3.2.2.1 Preparation of GF Suspensions. Table 3.1 presents the suspension formulations used in this chapter. Throughout the chapter, all percentages (%) refer to w/w with respect to de-ionized (DI) water; suspension refers to drug particles with the stabilizer solution; and slurry refers to a combination of the beads and the drug suspension. The drug (GF) loading was 20 g GF per 200 g DI water (10%). Feed GF suspensions were prepared using a shear mixer (Cat#. 14–503 Fisher Scientific Pittsburgh, PA, USA) running at a fixed speed of 300 rpm. The required amount of

stabilizer(s) was dissolved in DI water for 60 min followed by dispersion of the GF powder in the stabilizer(s) solution for 30 min (except Run 1). The GF powder was dispersed in DI water for 30 min in Run 1.

The wet stirred media mill used in this chapter was manufactured by Netzsch Fine Particle Technology, LLC. (Model: Microcer) (Exton, PA, USA). The schematic of the mill is shown in Figure 3.1. The milling chamber has a volume of 80 ml and is lined with zirconia. During the milling, a peristaltic pump recirculated the suspension between the holding tank and the milling chamber, while a 200 μm screen kept the zirconia beads in the milling chamber allowing the passage of the drug suspension. Process parameters were selected based on previous work on the wet media milling of GF (Bhakay et al., 2012). The feed suspensions prepared using the shear mixer were poured into the holding tank and milled under the same conditions: bead loading of 50 ml (bulk), suspension flow rate of 126 ml/min, and stirrer (rotor) speed of 3200 rpm corresponding to a tip speed of 11.7 m/s. Both the milling chamber and the holding tank were equipped with a cooling system (model number M1-.25A-11HFX, Advantage Engineering, Greenwood, IN, USA) to keep the suspension in the holding tank below 35 ^{o}C. Due to the relatively high HPC concentration, the heat dissipation rate in Runs 8, 9, 15, and 16 was high. To keep the temperature below 35 ^{o}C, the rotor was stopped twice in Runs 8 and 15 and several times in Runs 9 and 16 while the suspension continued to recirculate under cooling for few minutes. The experiments were resumed once the temperature in the holding tank reached ~25 ^{o}C.

Samples at several milling times were taken at the outlet of the milling chamber for particle sizing. The final suspensions (after 64 min milling) were tested for density

and shear viscosity, and they were refrigerated at 8 ^{o}C for a period of 7 days. Particle sizes right after milling and after 7 days of storage were compared to assess the physical stability of the suspensions.

Table 3.1 Formulation used in the Wet Stirred Media Milling Experiments

Run No.	Drug Loading (% w/w)[a]	HPC Concentration (% w/w)[a]	SDS Concentration (% w/w)[a]
1	10	—	—
2	10	—	0.5
3	10	0.1	—
4	10	0.5	—
5	10	1	—
6	10	2.5	—
7	10	5	—
8	10	10	—
9	10	15	—
10	10	0.1	0.5
11	10	0.5	0.5
12	10	1	0.5
13	10	2.5	0.5
14	10	5	0.5
15	10	7.5	0.5
16	10	10	0.5
17[b]	10	3	—
18[b]	10	3	0.5

[a] % w/w with respect to de-ionized water.
[b] Runs 17–18 were performed as part of the adsorption study.

3.2.2.2 Measurement of Power Input for the Microhydrodynamic Analysis. The power input per unit volume of the slurry, i.e., P_w, was measured during a milling experiment (Runs 5–9 and Runs 12–16), and an average value was reported. In the absence of the milling beads, the power input per unit volume of the suspension, i.e., ε_{ht}, was also measured while each stabilizer solution with 10% GF particles was stirred at 3200 rpm. In both cases, the no-load power value obtained from a dry run of the mill rotor at 3200 rpm was subtracted from the power values in the calculation of P_w and ε_{ht}.

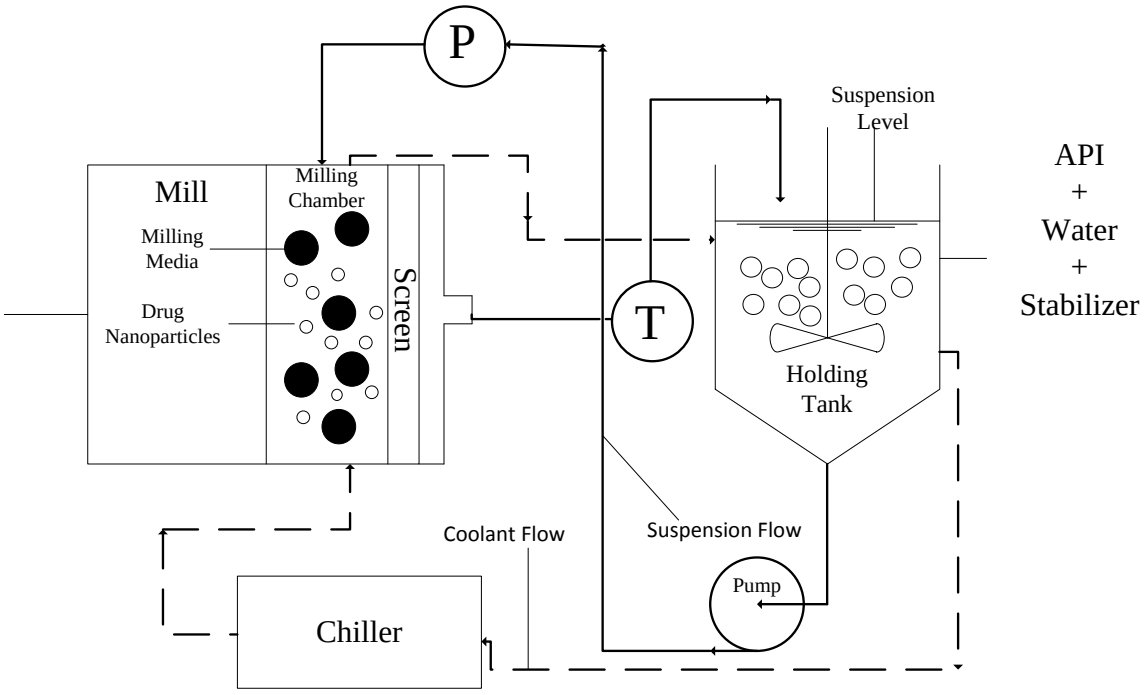

Figure 3.1 Schematic of the Netzsch stirred media mill (Model: Microcer) operating in the recirculation mode. P and T stand for pressure gauge and thermocouple, respectively.

3.2.2.3 Particle Sizing. Particle size distributions were measured with the laser diffraction device LS 13 320 (Coulter Beckman, Brea, CA). A polarized intensity differential scattering (PIDS) obscuration water optical model was employed. The PIDS was maintained between 40% and 50% while the obscuration was maintained below 8% for all particle size measurements. Particle size distribution was computed by the software using the Mie scattering theory. A refractive index (RI) value of 1.65 for the GF particles (Watanabe, 2002) and 1.33 for the measurement medium (DI water) were used. Prior to the size measurement, milled suspension samples (~2 ml) were diluted with 10 ml of DI water or solution of HPC, SDS, or HPC–SDS depending on the stabilizer(s) used in the milling experiment. The refrigerated suspension samples after 7-day storage were mixed with the shear mixer running at 300 rpm for 5 min. Then, ~2 ml samples

were taken and diluted for particle size measurement using the pertinent stabilizer solution.

3.2.2.4 Scanning Electron Microscopy (SEM). SEM imaging was used to examine the morphology of the as-received and milled particles and to determine the primary particle sizes of the GF nanoparticles. Suspension samples were mounted on a silicon chip (Ted Pella, Inc., Redding, CA, USA), placed on top of carbon specimen holders, and dried in a desiccator. The samples were then sputter coated with carbon and observed under a LEO 1530 SVMP (Carl Zeiss, Inc., Peabody, MA, USA).

3.2.2.5 Apparent Shear Viscosity and Density of the Milled Suspensions. The apparent shear viscosity of the milled suspensions (Runs 5–9 and Runs 12–16) and the stabilizer(s) solutions was measured using an R/S plus rheometer (Brookfield Engineering, Middleboro, MA, USA) with a water jacket assembly Lauda Eco (Lauda-Brinkmann LP, Delran, NJ, USA). A coaxial cylinder (CC40) was used to impart controlled shear rate on the samples from 0 to 1000 1/s in 60 s. The temperature of the jacket was kept constant at 25 ± 0.5 ^{o}C. The raw data were analyzed using the Rheo 3000 software (Brookfield Engineering, Middleboro, MA, USA) of the R/S plus rheometer to obtain the apparent shear viscosity as a function of the shear rate. The suspensions with very low HPC concentration (< 1%) (Runs 3–4; 10–11) could not be tested precisely by this rheometer set-up since the viscosity was very low (< 4 cP). The density of the milled suspensions (Runs 5–9; Runs 12–16) were experimentally determined using a 60 ml glass cylinder (Cat#. 08-559D Fisher Scientific, Pittsburgh, PA, USA) for volume measurements and a digital scale balance Adventurer-Pro (Ohaus Corporation, Parsippany, NJ, USA) to obtain the weights. The weight was divided by the volume to

obtain the density. Average value of three measurements on each suspension was reported.

3.2.2.6 Differential Scanning Calorimetry (DSC). The melting point and heat of fusion of the as-received GF powders and dried GF suspension (Run 1) were determined using a Mettler-Toledo POLYDSC (Mettler Toledo Inc., Columbus, OH, USA). A sample of 9–10 mg powder was placed in a sealed perforated aluminum pan. The samples were heated under nitrogen flow from 25 °C to 300 °C with a rate of 10 °C/min.

3.2.2.7 Determination of the Polymer Adsorption on Milled GF Particles. Fresh GF suspensions with 0.1–10% HPC concentration in the absence and presence of 0.5% SDS (Runs 3–8 and 10–16, respectively) were prepared by milling with similar conditions to those described in Section 3.2.1. A 10 min milling yielded Sauter-mean diameter values in the range of ~0.4–1.0 μm, which allowed easier separation of these particles from the suspensions during the centrifugation step. Two additional suspensions with 3% HPC were produced similarly: one without SDS and the other one with 0.5% SDS (Runs 17 and 18). The adsorption isotherms were determined using a thermo-gravimetric technique (Lee, 2003; Panmai and Deshpande, 2003). Each suspension was centrifuged (Sorvall RS-28S, DuPont Company, Wilmington, Delaware, USA) at 20,000 rpm for about 6 h. The supernatant solution was assayed for stabilizer content using a thermogravimetric analyzer (TGA): Mettler-Toledo TGA/DSC1/SF, Star^{e} system (Mettler Toledo Inc., Columbus, OH, USA). A sample (30–80 mg) taken from the supernatant solution was heated to 200 °C under nitrogen environment with a heating rate of 10 °C/min to remove the water and determine the residual weight. The stabilizer concentration in the supernatant solution was determined using the initial weight and the

residual weight. The amount of stabilizer adsorbed per mass of the GF particles was back-calculated by subtracting the stabilizer concentration in the supernatant solution from the total stabilizer concentration in the suspension sample. Assuming sphericity of the GF particles, the external specific surface area (S) was calculated from $S = 6/(\rho_p d_{sm})$, where ρ_p is the true density of GF (1.45 g/cm^3) and d_{sm} is the Sauter-mean diameter of the milled particles, which was obtained from the laser diffraction measurement. The S value was used to express the amount of HPC adsorbed per GF surface area.

3.3 Results and Discussion

3.3.1 Main Role of Polymers and Surfactants: Stabilization/Dispersion

Polymers and surfactants play a major role in two phenomena that determine the apparent breakage rate during wet media milling: stabilization/dispersion of the milled drug particles (Kim, 2004; Kissa, 1999) and microhydrodynamics of the milling beads (Eskin et al., 2005a) as affected by the suspension rheology. To elucidate the main role of the stabilizers, milling was performed in the absence (Run 1)/presence (Runs 2, 6, and 13) of stabilizers. Figure 3.2a shows the evolution of the GF particle size distribution (PSD) during milling as measured by the laser diffraction method when stabilizers were not used. The GF particles exhibited a bimodal PSD after milling; the shoulder in the 100–400 nm region suggests the existence of primary nanoparticles and some small aggregates of few primary particles. Although the fraction of particles in this region increased slightly upon prolonged milling, overall the PSD did not seem to change after 4 min milling.

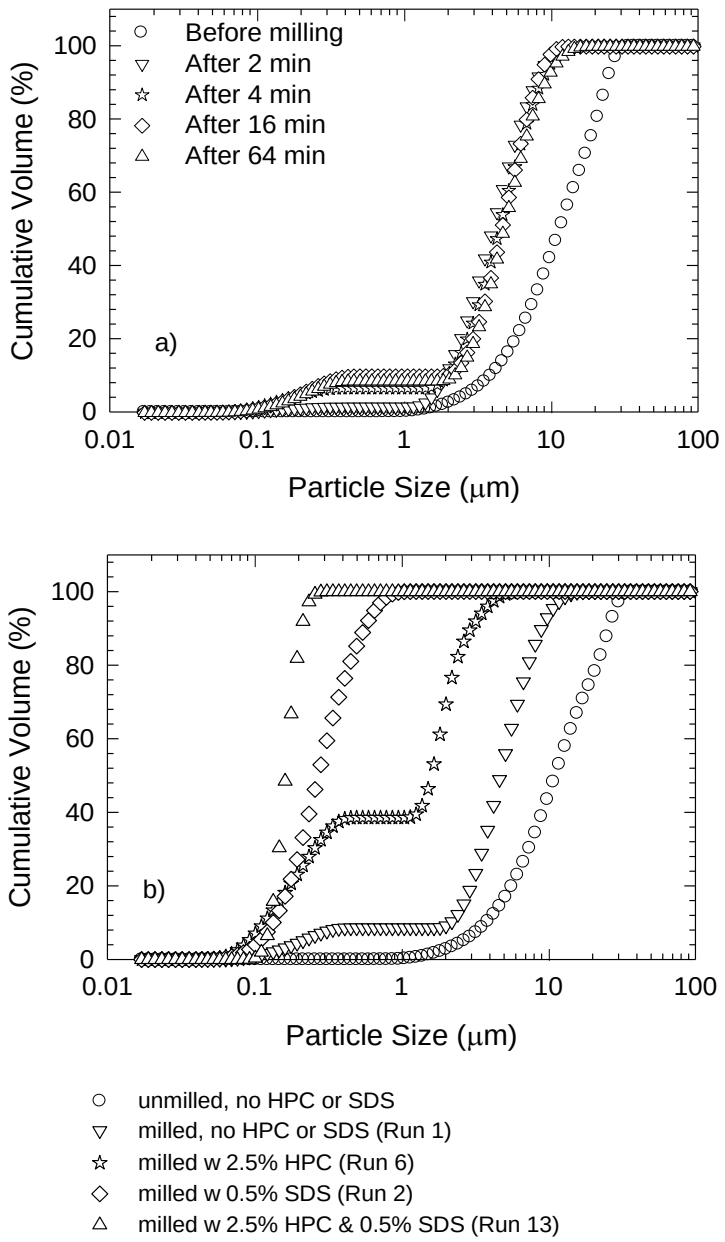

Figure 3.2 (a) Evolution of the cumulative particle size distribution of GF suspension milled in the absence of stabilizers (Run 1), (b) cumulative particle size distribution of the unmilled GF suspension without stabilizers and various 64 min milled suspensions: without HPC or SDS (Run 1), with 2.5% HPC (Run 6), with 0.5% SDS (Run 2), and with 2.5% HPC and 0.5% SDS (Run 13).

SEM images of the unmilled and milled GF particles in Figure 3.3a–c confirm the breakage of the GF particles and formation of 50–250 nm primary particles. A

comparison of LD results and SEM images suggests that GF nanoparticles were formed by breakage; however, they aggregated fast via attractive interparticle forces (van der Waals) in the absence of stabilizers. Hence, it can be noted that GF nanoparticles can form even in the absence of stabilizers; however, the so-produced nanoparticles cannot be preserved against aggregation.

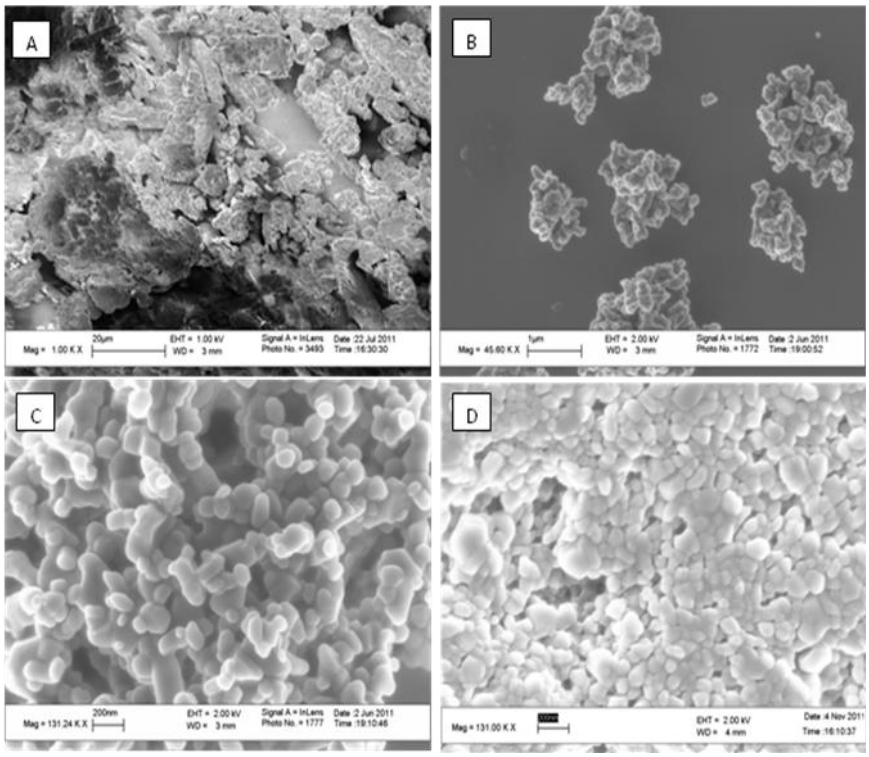

Figure 3.3 SEM image of (a) the as-received GF particles (marker size: 20 μm,1 kX magnification), (b) the GF particles milled for 64 min without stabilizers (Run 1, marker size: 1 μm, 46 kX magnification), (c) the GF particles milled for 64 min without stabilizers at a higher magnification (Run 1, marker size: 200 nm, 131 kX magnification) , (d) the GF particles milled for 64 min with 2.5% HPC and 0.5% SDS (Run 13, marker size: 200 nm, 131 kX magnification).

In general, polymers and surfactants adsorb on particle surfaces, providing a steric or electrostatic barrier (Merisko-Liversidge et al., 2003; Ploehn and Russel, 1990). In addition, they allow proper wetting of the hydrophobic drug surfaces, which can help to disperse aggregates formed during the milling process (Kissa, 1999). Various

concentrations of stabilizers (0.5% SDS (Run 2), 2.5% HPC (Run 6), and 2.5% HPC/0.5% SDS (Run 13)) were used to elucidate their stabilizing roles. Figure 3.2b illustrates that finer GF particles were obtained after 64 min milling when the stabilizers were used. In view of the median size of Run 1 suspension (4.725 μm), the addition of 2.5% HPC alone (Run 6) improved the dispersion of the nanoparticles, leading to a smaller median size (1.599 μm). HPC, an electrically neutral polymer, stabilizes particles by steric forces that are created by the long-tail interference of adsorbed protruding large chains onto the particle surfaces (Stuart, 1991). The median particle size of GF was reduced to 0.273 μm in the presence of SDS alone (Run 2). SDS (an anionic surfactant) appears to disperse the nanoparticles more effectively than HPC (a non-ionic cellulosic polymer). SDS has a smaller molecular weight than HPC and thus diffuses and adsorbs to the drug particle surfaces faster. In addition, being an anionic surfactant, SDS can make the GF particles negatively charged after adsorption and increase the electrostatic repulsion among the GF particles, thereby preventing the aggregation.

Figure 3.2b also shows that a combination of HPC–SDS (2.5% HPC and 0.5% SDS, Run 13) led to the narrowest PSD and smallest d_{50} and d_{90} values (0.163 and 0.211 μm). HPC–SDS mixtures are known to have synergistic effects in the stabilization of drug suspensions (Basa et al., 2008; Lee et al., 2008; Ryde and Ruddy, 2002). HPC and SDS interact, forming aggregates or micelle-like SDS clusters bound to HPC (Winnik and Winnik, 1990). These clusters can co-adsorb on surfaces (Berglund et al., 2003a, 2003b; Evertsson and Nilsson, 1997), potentially facilitating adsorption of HPC (Cerdeira et al., 2010) and enabling electrosteric stabilization. The SEM image (Figure 3.3d) shows the primary GF nanoparticles in the size range of 50–250 nm. Along with the LD results,

where the d_{50} and d_{90} sizes after 64 min milling were 0.163 and 0.211 μm (Figure 3.2b, Run 13), the SEM image suggests that the HPC–SDS stabilized suspension had relatively small extent of aggregation. GF primary particle sizes in the absence or presence of stabilizers was in the range of 50–250 nm, as seen in the SEM images (Figures 3.3c and 3.3d, respectively), which suggest that stabilizer(s) are needed to disperse the nanoparticle aggregates. A combination of stabilizers (HPC–SDS) can help to disperse the aggregated nanoparticles effectively. On the other hand, a slight reduction in the fraction of GF nanoparticles in the <100 nm size range when SDS was used at 0.5%, above the critical micelle concentration (CMC) of 0.23%, either alone or along with HPC is observed. The aqueous solubility of GF increases above the CMC of SDS (Rao et al., 1997), which may cause preferential loss of <100 nm particles due to enhanced dissolution or aggregation.

The reproducibility of the wet media milling process was checked by repeat experiments of Run 2 (0.5% SDS), Run 6 (2.5% HPC), and Run 13 (0.5% SDS/2.5% HPC). The d_{50} and d_{90} values of the repeat experiments were 0.289 and 0.532 μm, 1.765 and 3.182 μm, and 0.163 and 0.207 μm, respectively. The (absolute) percent deviations from the d_{50} and d_{90} values were all less than 10%: 5.86 and 5.51%, 10.4 and 6.89%, and 0.0 and 1.90%, respectively. Hence, the particle size statistics were fairly reproducible. In general, the reproducibility was better for the suspensions with a smaller extent of aggregation (Runs 2 and 13 vs. Run 6). Excellent reproducibility observed for the suspension with HPC–SDS combination and higher variability observed for the suspension with HPC alone agree with the recent work on the wet media milling of

griseofulvin, naproxen, and azodicarbonamide suspensions containing HPC or HPMC in the presence/absence of SDS (Bhakay et al., 2011, 2013; Monteiro et al., 2013).

The DSC thermograms of the as-received GF particles and milled GF particles exhibited a sharp endothermic peak associated with the melting of the crystalline GF (Figure 3.4). The peak melting temperature decreased slightly from 219.3 ^{o}C (as-received GF powder) to 217.5 ^{o}C after milling (Run 1), while the heat of fusion did not change much: 115 J/g to 113 J/g. These results indicate that a significant change to the crystallinity of GF did not occur during the wet milling. Readers are referred to Monteiro et al. (2013) for a more detailed characterization using powder-XRD and Raman spectroscopy on milled GF particles, which supported the above finding.

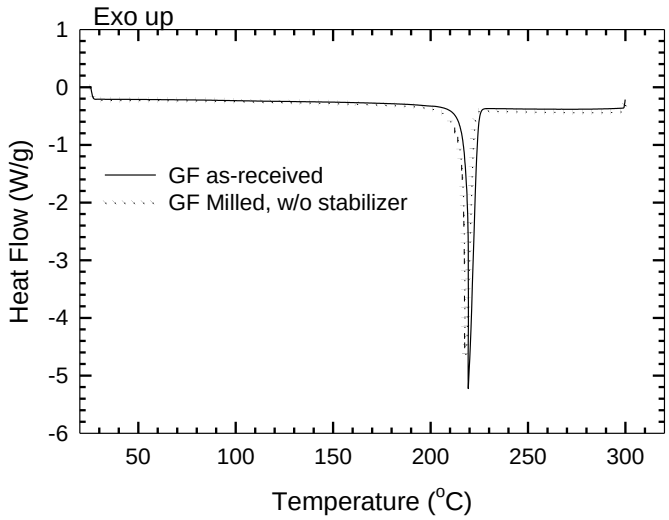

Figure 3.4 DSC thermograms of the as-received GF particles and 64 min milled GF particles in the absence of stabilizers (Run 1).

3.3.2 Analysis of the Apparent Breakage Kinetics

To investigate the role of HPC in the apparent breakage rate, a wide range of HPC concentrations was considered in the absence/presence of SDS. Figures 3.5a and 3.5b

illustrate the evolution of the median particle size (d_{50}) and the 90% passing size (d_{90}) as a function of HPC concentration: 0.1–2.5% (Runs 3–6) and 2.5–15% (Runs 6–9), respectively, in the absence of SDS. Figures 3.6a and 3.6b present the same information as a function of HPC concentration: 0.1–2.5% (Runs 10–13) and 2.5–10% (Runs 13–16), respectively, in the presence of 0.5% SDS. Table 3.2 presents the particle size statistics for the suspensions that were milled for 16 min and 64 min.

3.3.2.1 Effects of HPC in the Absence of SDS. Both d_{50} and d_{90} decreased fast within the first 4 min as the large micron-sized GF particles were easier to break (Figure 3.5). As milling continued, the apparent breakage rate decreased, and the particle size exhibited either a clear minimum followed by an increase or varied about a plateau size. This non-monotonic evolution of the particle size cannot be explained by pure breakage of the particles. The GF suspensions with HPC as the sole stabilizer, even after prolonged milling (64 min), did not have d_{90} less than 1 μm. Moreover, the suspensions with 0.1–2.5% HPC had median sizes greater than 1 μm. Both d_{50} and d_{90} after 16 min and 64 min milling were smaller at higher HPC concentration (Table 3.2, Runs 3–9), which suggests that the overall apparent breakage rate increased with an increase in the HPC concentration. Considering that 50–250 nm primary GF nanoparticles were produced even in the absence of stabilizers (Figure 3.3c), the findings here imply the significant impact of the particle aggregation in the apparent breakage rate and the particle size of the final milled suspension.

During wet stirred media milling, two particle change mechanisms act simultaneously: breakage of as-received particles, fragments of already broken particles as well as aggregates (also known as deaggregation) and aggregation of the particles

(Bilgili et al., 2004; Sommer et al., 2006). The particle size distribution at a given time reflects the net effect of the competing breakage and aggregation mechanisms (Monteiro et al., 2013). During the course of milling (Runs 3–9), the particle size decreased initially within the first 4 min and increased/decreased instantaneously thereafter and seemed to approach or varied around a large plateau size because the aggregation rate of the produced fine particles equaled or exceeded the rate at which the particles and aggregates broke upon prolonged milling. Initially, the breakage was faster than the aggregation due to the presence of relatively large (micron-sized), weaker GF particles.

As milling progressed, the aggregation rate increased upon production of finer (colloidal) drug particles because steric stabilization imparted by HPC alone was not sufficient to keep the freshly formed nanoparticles discrete. Moreover, as the drug particle size decreased, particle number concentration in the suspension increased and the interparticle distance decreased, leading to more frequent collisions and potentially higher aggregation rate (Sommer et al., 2006). An increase in HPC concentration reduced the extent and rate of the aggregation, which resulted in finer particles and a higher apparent breakage rate.

3.3.2.2 Effects of HPC in the Presence of SDS. Unlike the evolution of d_{50} and d_{90} in the absence of SDS (Figure 3.5), the evolution of both d_{50} and d_{90} exhibited a monotonic decrease in the presence of SDS (Figure 3.6). For the formulations with SDS (Runs 10–16), Table 3.2 shows that the suspensions with an HPC concentration greater than 0.5% reached identical particle size after 64 min (within experimental accuracy), and all suspensions reached ~160 nm median size after 64 min milling (except Run 10, with the

lowest HPC concentration). All of the suspensions had d_{50} and d_{90} values less than 1 μm after 64 min.

Table 3.2 Effects of the HPC Concentration on the Median Size (d_{50}) and 90% Passing Size (d_{90}) of the GF Suspensions for Runs 1–9 (without SDS) and Runs 10–16 (with 0.5% SDS) After 16 and 64 min Milling and After 7 Day Storage

Run No.	HPC Concentration (% w/w)	Milled (16 min) d_{50} (μm), d_{90} (μm)	Milled (64 min) d_{50} (μm), d_{90} (μm)	7 day storage d_{50} (μm), d_{90} (μm)
1	—	4.586, 7.995	4.725, 9.023	4.416, 7.568
2[a]	—	0.648, 1.723	0.273, 0.563	0.279, 0.543
3	0.1	2.976, 5.295	2.895, 5.173	2.318, 4.265
4	0.5	2.334, 4.855	2.189, 4.362	2.173, 4.127
5	1	2.001, 3.932	2.030, 3.721	NM[b]
6	2.5	1.588, 2.894	1.599, 2.977	1.684, 3.709
7	5	1.117, 2.176	0.473, 1.762	1.178, 2.327
8	10	0.559, 2.022	0.358, 1.425	0.390, 1.725
9	15	0.426, 1.460	0.300, 1.125	0.332, 1.176
10	0.1	0.419, 1.442	0.274, 0.469	0.257, 0.510
11	0.5	0.450, 1.470	0.165, 0.394	0.197, 0.442
12	1	0.441, 1.483	0.154, 0.238	0.158, 0.258
13	2.5	0.256, 0.476	0.163, 0.211	0.164, 0.214
14	5	0.315, 0.577	0.162, 0.221	0.161, 0.228
15	7.5	0.367, 0.670	0.165, 0.235	0.173, 0.250
16	10	0.399, 1.170	0.161, 0.237	0.190, 0.314

[a]This run has 0.5% SDS and included here for comparative purpose.
[b]NM: not measured.

In view of the 50–250 nm primary particles produced in Run 13 (Figure 3.3d) and the above information, the extent of aggregation in the 64 min milled suspensions was low, and the breakage mechanism dominated over the aggregation mechanism when SDS was used in combination with HPC. Moreover, the presence of SDS allowed a much lower concentration of HPC (as low as 1%) that can ensure the formation of a stable GF nanosuspension. This finding can be explained by the aforementioned synergistic stabilizing action of the HPC–SDS combination (Section 3.4.1).

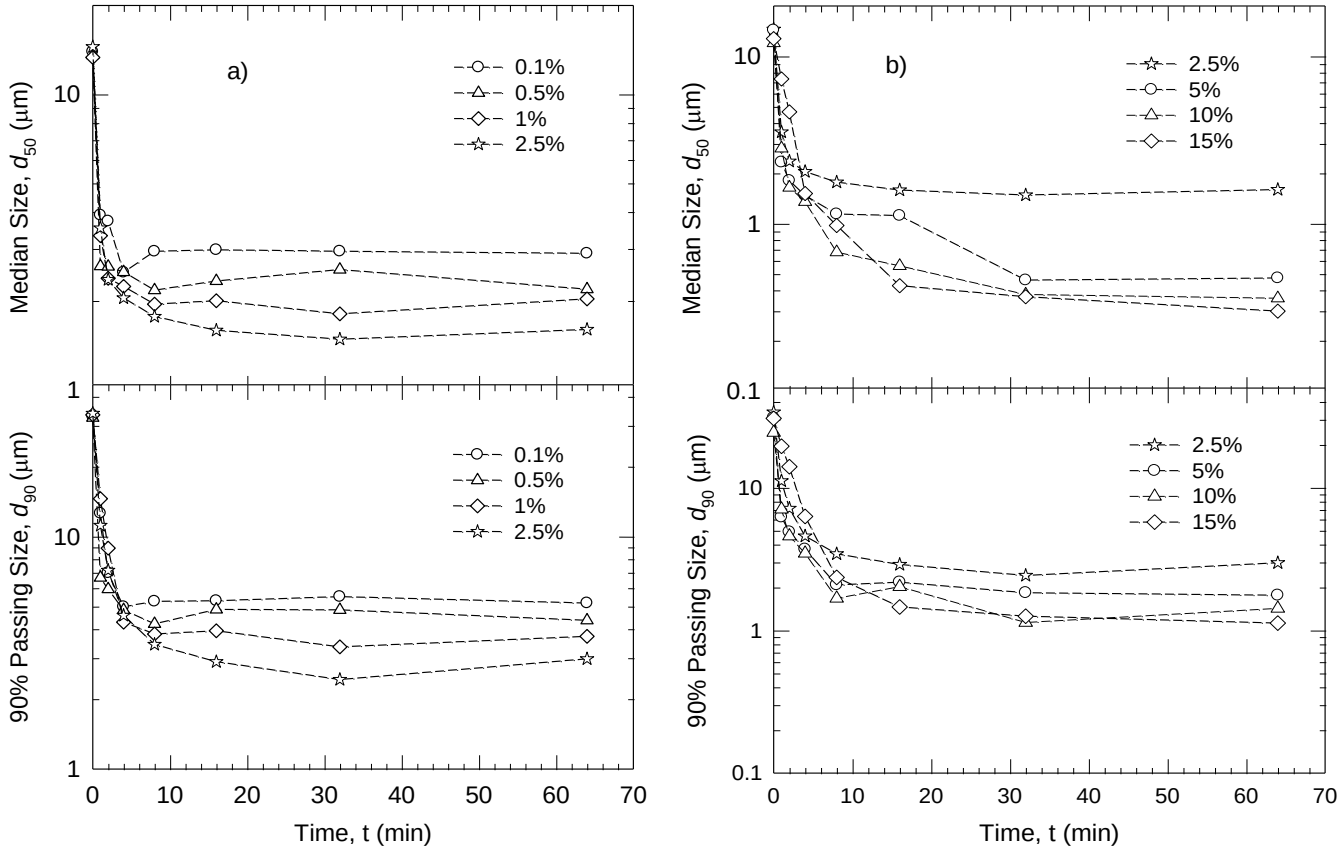

Figure 3.5 Effects of the HPC concentration on the evolution of d_{50} and d_{90} during the milling of the GF particles in the absence of SDS: (a) 0.1–2.5% HPC (Runs 3–6), (b) 2.5–15% HPC (Runs 6–9).

The particle size decreased fast within the first 8 min (Figure 3.6). The apparent breakage rate decreased with further milling and the particle size approached or reached a plateau size: d_{50} value of ~160 nm and d_{90} value of ~220 nm for HPC concentration greater than 0.5%. The monotonic decrease of the particle size and tendency toward a plateau size signify the dominance or higher extent of particle breakage over particle aggregation for these relatively stable suspensions. For prolonged milling, a plateau size is theoretically expected for two reasons: a dynamic equilibrium between the particle breakage and aggregation can be established (Bhakay et al., 2011) and the true breakage rate decreases upon generation of finer particles, especially nanoparticles, which are more difficult to break stemming from their high strength (Lee, 2003; Bilgili et al., 2006). Since a plateau size was approached after 64 min milling, the apparent breakage rate may be conveniently assessed considering the particle size at an earlier time point, e.g., 16 min of milling in Table 3.2 and Figure 3.6. Within the HPC range studied, an optimum HPC concentration of 2.5% was identified, which yielded the smallest d_{50} and d_{90} at 16 min. The larger values of d_{50} and d_{90} for the other HPC concentration values can be explained as follows: below 2.5% HPC, the particle aggregation might have occurred to a larger extent leading to slower apparent breakage, whereas the viscous dampening effect might have reduced the true breakage rate and led to the formation of coarser particles for the relatively more stable suspensions with an HPC concentration above 2.5%. These aspects will be elucidated in Section 3.4.7 using the combined microhydrodynamics–polymer adsorption analysis. The result suggests that 2.5% is the optimal HPC concentration in view of the HPC concentrations studied. Finding a more accurate and precise value of the

optimum polymer concentration entails additional milling experiments with many more HPC concentrations within the 1–5% range. However, since an emphasis is on the qualitative nature of this optimum, this aspect will not be studied.

To confirm the optimality of 2.5% HPC in the presence of SDS, a quantitative analysis of the breakage rate, which considers all milling time points including 16 min, was performed using the two-parameter empirical model (Section 3.1). The evolution of the median size in Runs 12–16 (1–10% HPC), excluding runs with 0.1 and 0.5% HPC, was fitted to minimize the confounding effect of the particle aggregation and to improve the goodness-of-fit and statistical significance of the parameters. Table 3.3 presents the values of the parameters d_{lim} and τ_p (see Chapter 2.3) and the coefficient of determination (R^2). For all fits, R^2 value was greater than 0.90 and the empirical model was statistically significant (p-value < 0.05). In addition, all p-values for the parameters estimated were found to be less than 0.005, proving the statistical significance of the parameter estimates. The process time constant τ_p correlates negatively with the overall apparent breakage rate: a larger τ_p indicates a slower apparent breakage during the milling.

Table 3.3 confirms the aforementioned result obtained from the analysis of 16 min milling data: 2.5% HPC concentration led to the fastest apparent breakage. The monotonic increase of τ_p with an increase in HPC concentration from 2.5% to 10% could be attributed to greater viscous dampening of the beads and resultant slower particle breakage. The estimated d_{lim} values were about 200 nm (Table 3.3) and slightly greater than the experimental d_{50} values obtained after 64 min milling (Table 3.2), suggesting a limitation of the simple empirical model expressed by Eq. (2.7).

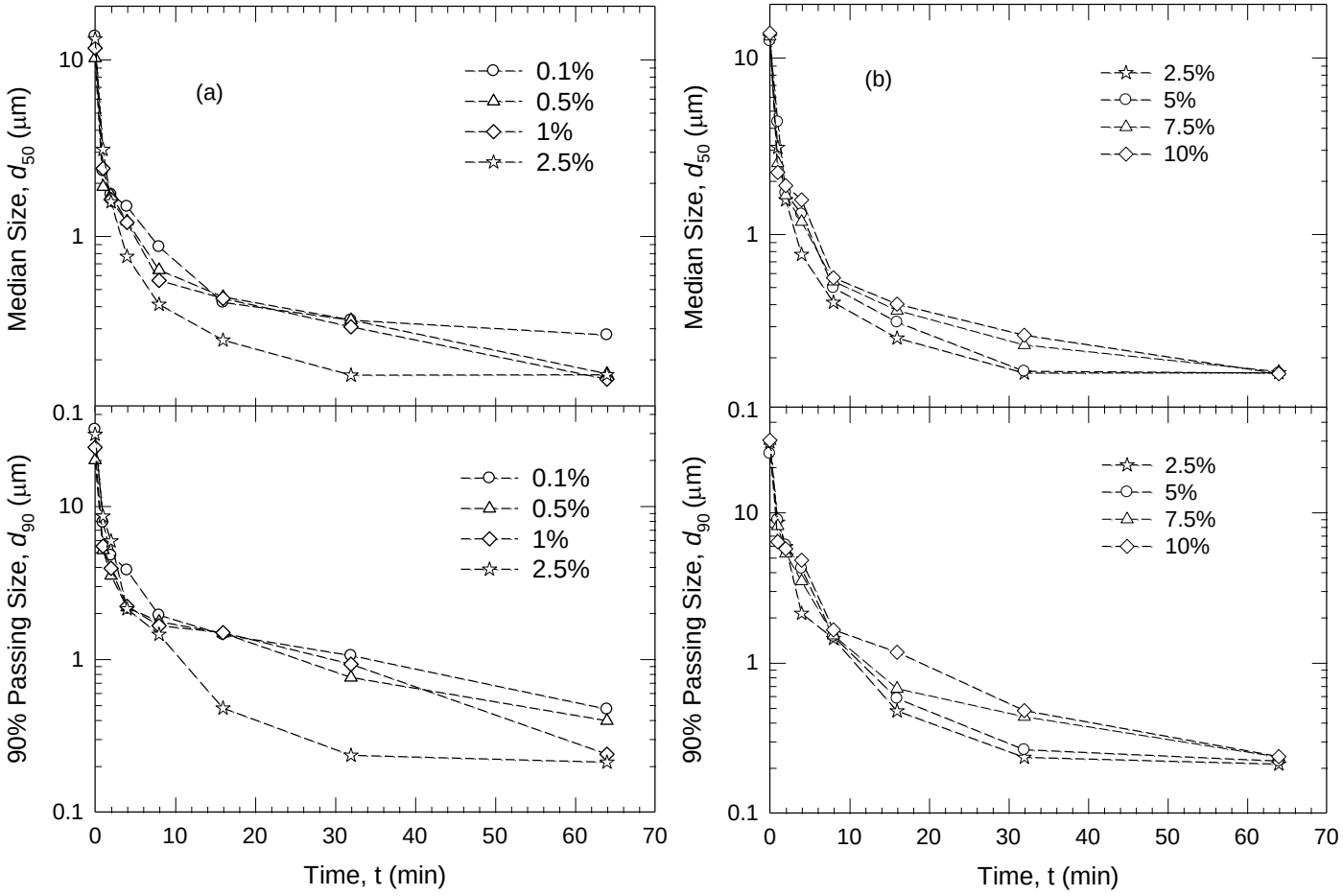

Figure 3.6 Effects of the HPC concentration on the evolution of d_{50} and d_{90} of the GF particles in the presence of 0.5% SDS: (a) 0.1–2.5% HPC (Runs 10–13), (b) 2.5–10% HPC (Runs 13–16).

This deviation is the largest for Run 12 (1% HPC) among Runs 12–16, which may suggest that the deviation can be partly explained by the presence of particle aggregation. Experimental errors may also partly explain the deviation: experimental d_{50} values (64 min) were still within ±2 standard deviations of the estimated d_{lim}, which were quantified by the coefficient of variation (COV) values.

Table 3.3 Fit of the Empirical Model (Eq. (2.7)) to the Evolution of the Median Particle Size in Runs 12–16 (with 0.5% SDS)

Run No.	HPC Concentration (% w/w)	d_{lim}, COV% (μm), (–)	τ_p, COV% (min), (–)	R^2 (–)
12	1	0.239 (20.7)	4.33 (23.6)	0.919
13	2.5	0.194 (14.4)	2.22 (15.7)	0.960
14	5	0.202 (20.0)	2.45 (18.4)	0.940
15	7.5	0.218 (14.5)	3.90 (15.9)	0.962
16	10	0.209 (16.4)	5.40 (16.6)	0.961

3.3.3 Physical Stability of the Milled Suspensions

Milled GF suspensions were refrigerated at 8 ^{o}C for a period of 7 days to examine the aging effects. In the absence of SDS, the size-dependence of the aged particles on the HPC concentration followed the same trend as that for 64 min milled suspensions: smaller particle size at higher HPC concentration (Table 3.2). Interestingly, upon storage, the particle size increased for the milled suspensions with an HPC concentration greater than 1% (Runs 6–9), while it decreased for the milled suspensions with 0%, 0.1%, and 0.5% HPC (Runs 1, 3, and 4). It must be noted that the latter group of suspensions had such a low viscosity (less than 4 cP) that could not be measured reliably with the current rheometer set-up. After refrigerated storage for 7 days, the suspensions were mixed using a shear mixer for 5 min at 300 rpm to obtain a homogeneous sample for particle sizing. Due to the very low viscosity and presence of a appreciable fraction of large and weak

aggregates (>3–4 μm after milling and storage), Runs 1, 3, and 4 suspensions were subjected to higher shear, leading to the breakage of the large aggregates and reduction in d_{50} and d_{90}. On the other hand, Runs 6–9 suspensions were more viscous and subjected to lower shear rate at the same rotation rate (300 rpm). Since they had a much smaller fraction of large aggregates after milling, the low shear did not lead to significant breakage; hence, an increase in d_{50} and d_{90} was observed possibly due to Brownian aggregation during the storage. It should be noted that this shear rate dependence of the particle size of 7-day stored GF suspensions was mainly a consequence of the high extent of aggregation in these relatively less stable suspensions with HPC as the sole stabilizer and the relatively high speed of the mixer.

In the presence of SDS, the particle size of the milled suspensions increased slightly after 7-day storage (Table 3.2) because of the synergistic stabilizing action of the HPC–SDS combination, except at the very low HPC concentrations (0.1% and 0.5%). The particle sizes (d_{50} and d_{90}) measured by the laser diffraction were similar to the primary nanoparticle size range of 50–250 nm observed in Figure 3.3d, suggesting minimal or limited extent of aggregation in these suspensions. It appears that Ostwald ripening was not a serious issue during the 7-day refrigerated storage of these suspensions. Long-term stability of these suspensions was not investigated here as they were intended to be dried shortly after the milling (Bhakay et al., 2013; Sievens-Figueroa et al., 2012).

3.3.4 Polymer Adsorption on Milled GF Particles

To gain a deeper understanding of the steric stabilization imparted by HPC, HPC adsorption on the milled GF particles was studied in the absence/presence of SDS. HPC concentration in the GF suspension determines the maximum amount of HPC that can possibly adsorb on the GF particles and the thickness of the HPC layer. A thicker layer of the adsorbed polymer and strong adsorption are desirable for good steric stability (Lee, 2003). In the absence of SDS, the amount of HPC adsorbed per surface area of the GF particles increased with an increase in the total HPC concentration from 0.1% to 0.5% (Figure 3.7). It continued to increase and appeared to reach a plateau at about 2.5–3% HPC. Beyond 3%, the adsorption resumed to increase. One explanation may be that mono-layer adsorption occurred up to 3% HPC (mono-layer saturation) followed by multilayer adsorption. Similar observations were made about the HPC adsorption onto ibuprofen particles (Law and Kayes, 1983). The monotonic increase in the amount of HPC adsorbed with an increase in HPC concentration means a monotonic increase in the adsorbed HPC layer thickness and thus better steric stability. This enhanced steric stability at higher HPC concentration reduced the aggregation probability of the colliding GF particles, leading to the monotonic decrease in d_{50} and d_{90} (Table 3.2). In addition, an increase in HPC concentration led to a higher suspension viscosity (Section 3.4.5), which can reduce the collision rate among the GF particles and thus the aggregation rate (Sommer et al., 2006). In spite of all the positive effects associated with the use of a higher HPC concentration, the particle aggregation was not completely suppressed with the use of HPC even at the highest concentration (15%). An insufficient layer thickness on the GF particle surfaces, slow adsorption of large HPC molecules during milling, and

small repulsive forces stemming from the non-ionic nature of HPC and small surface charge of GF particles in aqueous cellulosic suspensions (Meng et al., 2011) could explain the inadequacy of HPC.

Adsorption of HPC on GF particles *in the presence of 0.5% SDS* was also studied to explain the synergistic effects observed during the milling (Figure 3.7). The amount of stabilizers (mostly HPC) adsorbed on the hydrophobic surfaces of the GF particles monotonically increased with an increase in the HPC concentration. The amount adsorbed was much higher in the presence of SDS potentially due to the co-adsorption of SDS with HPC and the facilitation of HPC adsorption by SDS, which was suggested earlier by Cerdeira et al. (2010) for HPC adsorption on miconazole particles in the presence of SDS. The co-adsorbed layers can impart electrosteric stabilization to the GF particles. Strictly speaking, the amount of stabilizers adsorbed reflects the contributions from both HPC and SDS. On the other hand, since SDS concentration was kept constant at 0.5%, the dramatic increase of the amount adsorbed above 0.5% HPC can only be explained by the enhanced adsorption of HPC and the amount adsorbed is mainly contributed by HPC. Regardless of the underlying mechanisms for the observed enhancement in the adsorption, the presence of SDS could allow formation of a thicker HPC–SDS layer at higher HPC concentration, leading to enhanced electrosteric stabilization.

The adsorption isotherms presented in Figure 3.7 explain the synergistic effects of the HPC–SDS combination, the larger d_{50} and d_{90} values of the milled suspensions with HPC concentration less than 1% and the large τ_p value of Run 12 as well as the relatively good physical stability of the suspensions with >1% HPC. At higher HPC concentrations,

the shear viscosity of the suspensions were higher (see below), which could reduce the collision rate of the GF particles, leading to a reduced aggregation rate besides the lower aggregation probability (thicker HPC–SDS layer). Interestingly, since the adsorption isotherm is a monotonically increasing function of the HPC concentration when 0.5% SDS is present, the optimal HPC concentration (2.5%) cannot be explained by the isotherm alone.

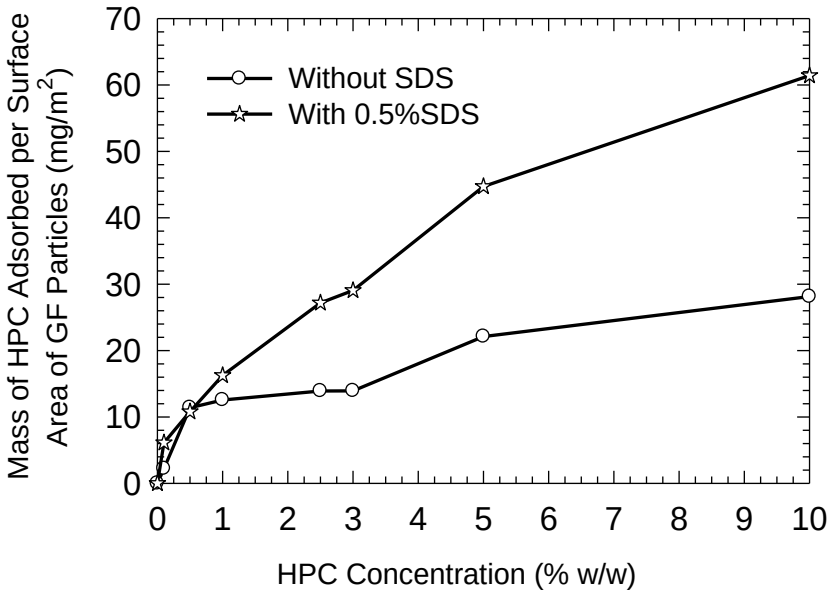

Figure 3.7 Adsorption of HPC on milled GF particles in the absence (Runs 3–8 and 17) and presence (Runs 10–16 and 18) of 0.5% SDS.

3.3.5 Suspension Rheology and Assessment of the Aggregation State

The apparent shear viscosities of aqueous HPC solutions (without GF) and 64 min milled GF suspensions (Runs 5–9) *without SDS* were measured as a function of shear rate at various HPC concentrations and presented in Figures 3.8a and 3.8b, respectively. An increase in HPC concentration significantly increased the viscosity in the absence or presence of the milled GF particles. In general, as the shear rate was increased, the viscosity of the HPC solutions decreased significantly (shear-thinning behavior) and

tended to an asymptotic value (Newtonian fluid behavior) above a shear rate of 500 1/s (Figure 3.8a). A slight increase in the viscosity was observed for the 1% HPC solution above 400 1/s shear rate. The milled suspensions had higher viscosity and exhibited stronger shear-thinning behavior that was prevalent up to 1000 1/s as compared with the HPC solutions. The approach to an asymptotic viscosity was delayed, and the decrease of viscosity above 500 1/s was still notable. These findings accord well with other studies in literature and could be attributed to the higher extent of aggregate breakage (deaggregation) at higher shear rates (Barthelmes et al., 2003; Bernhardt et al., 1999). Presence of aggregates, which can occlude liquid in their void space, increases the effective volume fraction of the solid in a suspension with fixed solids loading. Hence, in general, an aggregated suspension has a higher shear viscosity than a fully-dispersed suspension consisting of discrete primary particles. Since the GF aggregates broke more extensively at higher shear rates, the apparent shear viscosity decreased with an increase in the shear rate. As a crude measure of shear-thinning, the ratio of shear viscosity at a low shear rate (16 1/s) to that at a high shear rate (1000 1/s), i.e., μ_{L0}/μ_L, was calculated. The ratio decreased from 8.2 (1% HPC) to 1.6 (15% HPC) monotonically, which suggests a less pronounced shear-thinning behavior, thus signifying a less aggregated state of the GF suspensions at higher HPC concentrations. The same behavior can be seen from the absolute value of the slope of the viscosity curve on semi-log axes (Figure 3.8b): as the HPC concentration was increased, the absolute value of the slope decreased at a given shear rate (e.g. 250 1/s). The viscosity measurements independently confirmed the aggregation state of the milled suspensions, agreeing well with the laser diffraction data

(Table 3.2). Both methods suggest that the extent of aggregation decreased monotonically when the milled suspension had a higher HPC concentration.

In order to investigate the impact of HPC–SDS combination on the suspension rheology, the apparent shear viscosity was obtained as a function of shear rate in the absence (solution) and presence of GF (milled suspension) (see Figures 3.8c and 3.8d, respectively). An increase in HPC concentration increased the viscosity significantly in the absence or presence of the milled GF particles. A comparison of Figures 3.8a and 3.8c shows that addition of SDS to an HPC solution increased the viscosity significantly, which can be attributed to the formation of HPC–SDS aggregates or micelle-like SDS clusters bound to the polymer (Berglund et al., 2003a; Evertsson and Nilsson, 1997; Winnik and Winnik, 1990).

Unlike the viscosity profiles presented in Figures 3.8a and 3.8b (no SDS), the viscosity of a milled suspension was lower than that of the HPC–SDS solution (Figures 3.8c and 3.8d). This finding can be explained by the relatively well-dispersed nature of the GF suspensions with HPC–SDS (less number of smaller aggregates) and the reduced concentration of HPC–SDS in the bulk solution of the GF suspensions due to enhanced HPC adsorption, as mentioned above. Moreover, a comparison of the absolute value of the slope of the viscosity curves in Figures 3.8b and 3.8d suggests that at the same HPC concentration, the shear thinning behavior was weaker (flatter curves) in the presence of SDS. Figure 3.8d also illustrates that the apparent viscosity of the milled suspensions tends to plateau at low shear rates, exhibiting a near-Newtonian behavior. Similarly, the shear viscosity ratio (μ_{L0}/μ_L) was lower (0.9–1.8) in the presence of SDS than in its

absence (1.6–8.2). These results agree with the laser diffraction results in that the milled suspensions with HPC–SDS were better dispersed and more stable.

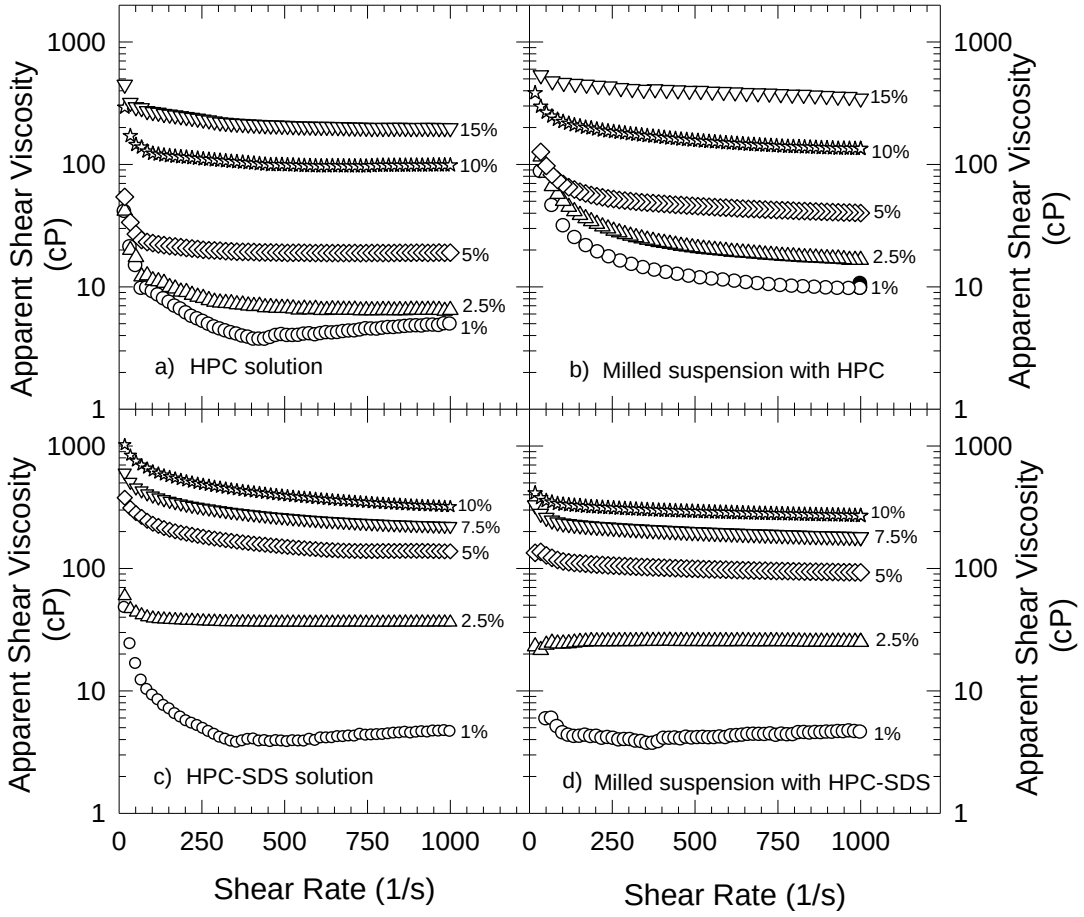

Figure 3.8 Effects of the HPC concentration on the apparent shear viscosity as a function of the shear rate for (a) the HPC solutions without SDS, (b) 64 min milled GF suspensions without SDS (Runs 5–9), (c) the HPC solutions with 0.5% SDS, (d) 64 min milled GF suspensions with 0.5% SDS (Runs 12–16).

3.3.6 Microhydrodynamic Analysis of the Wet Stirred Media Milling Process

A microhydrodynamic analysis was performed to further elucidate the impact of the HPC concentration and absence (Runs 5–9)/presence (Runs 12–16) of SDS. Table 3.4 presents the power input (P_w and ε_{ht}), density and shear viscosity of the milled suspensions (ρ_L and μ_L), and the microhydrodynamic parameters (θ, ν, and u_b) (see Chapter 2.4). The power

applied by the rotor in the presence of the beads (P_w) and in the absence of the beads (ε_{ht}) monotonically increased with an increase in the HPC concentration, which can be explained by a corresponding increase in the suspension viscosity. On the other hand, for the same reason, the granular temperature (θ), average bead oscillation velocity (u_b), and the single bead frequency (ν) monotonically decreased. Hence, the microhydrodynamic analysis has enabled the quantification of the viscous dampening effect of HPC during the wet media milling of drugs for the first time. The decrease in the values of θ, ν, and u_b at higher HPC concentration correlates to a reduction in the number and intensity of the bead–bead collisions, which implies a smaller number of less intense compression events during which the GF particles are deformed and/or broken by the colliding beads during milling. The general trends for the effects of HPC concentration on the power input and the microhydrodynamic parameters were similar regardless of the absence/presence of 0.5% SDS. However, the use of SDS in addition to HPC has a negative effect on the microhydrodynamic parameters, as suggested by the lower θ, ν, and u_b values (except at 1% HPC). The higher viscosity of the milled suspensions with HPC–SDS can explain this negative effect even though P_w values were also higher in the presence of SDS.

Although the decrease in θ, ν, and u_b values at higher HPC concentration (viscous dampening) suggests a decrease in the breakage rate of the GF particles, the overall apparent breakage rate presented in Table 3.2 and Figure 3.5 suggests otherwise (Section 3.3.2.1). Hence, in the absence of SDS, the apparent breakage kinetics and final particle size distribution of the milled GF suspensions, with HPC as the steric stabilizer,

are affected more by the rate–extent of the particle aggregation than the viscous dampening observed at the higher HPC concentration.

3.3.7 Combined Microhydrodynamics–Polymer Adsorption Analysis

Figure 3.9 summarizes the effects of HPC concentration, in the presence of SDS, on the median size after 16 min milling, the characteristic process time constant estimated by the empirical model, the adsorption isotherm, and the granular temperature. Both the median size and the process time constant showed a minimum at 2.5% HPC (most favorable condition from a processing and physical stability perspective). The same optimum, even more pronounced, could be identified if the 90% passing size instead of the median size was plotted in Figure 3.9. The granular temperature was a monotonically decreasing function of the HPC concentration (viscous dampening), whereas the adsorption isotherm was a monotonically increasing function. Therefore, neither the granular temperature nor the adsorption isotherm alone can explain the observed optimum at 2.5% HPC: both of these values should be sufficiently high to ensure the highest apparent breakage rate. Below 2.5% HPC, the particle aggregation was more pronounced due to the relatively small thickness of the adsorbed HPC layer and higher GF particle collision frequency at the low viscosity of the milled suspensions. Above 2.5%, the viscous dampening effect becomes pronounced for the stable suspensions with the lower extent of aggregation.

3.3.8 Correlating the Microhydrodynamics with Equipment-Scale Hydrodynamic Behavior

The stirrer (rotor) Reynolds number (Re) and the stirrer (rotor) Euler number (Eu), also known as the power number, are widely used to assess the overall flow behavior of the suspensions and to relate the power consumption to the operating parameters, equipment

parameters, and the fluid properties (Kawatra, 2006; Mannheim, 2011). In the absence or presence of SDS, Re decreased and Eu increased with an increase in the HPC concentration (Figure 3.10). For scale-up purposes, one can relate Eu to Re (Manneheim, 2011), which is beyond the scope of this work.

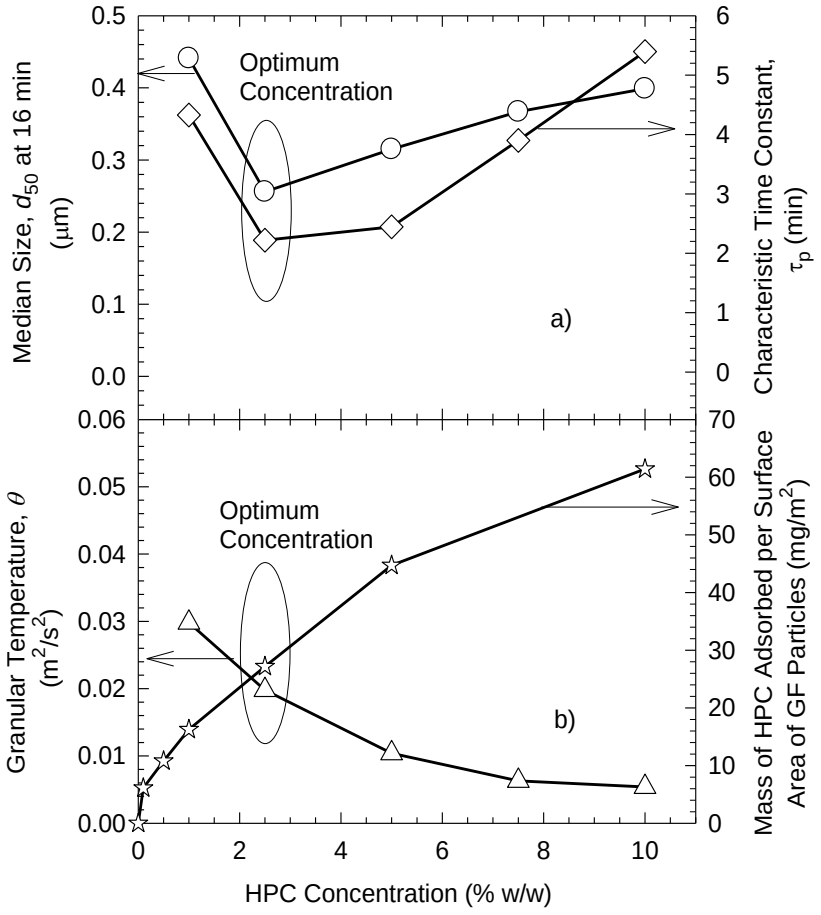

Figure 3.9 Effects of the HPC concentration, in the presence of 0.5% SDS, on (a) the median size of the GF particles after 16 min milling and the characteristic time constant (Runs 12–16), (b) the granular temperature (Runs 12–16) and the amount of HPC adsorbed on the GF particles (Runs 10–16).

Eu exhibited a continuous increase with HPC concentration in the presence of SDS (Figure 3.10b), whereas it had a smaller slope and tend to plateau at higher HPC concentration in the absence of SDS (Figure 3.10a). In both cases, the granular

temperature (θ) monotonically decreased and exhibited a profile similar to that of Re, suggesting a correlation.

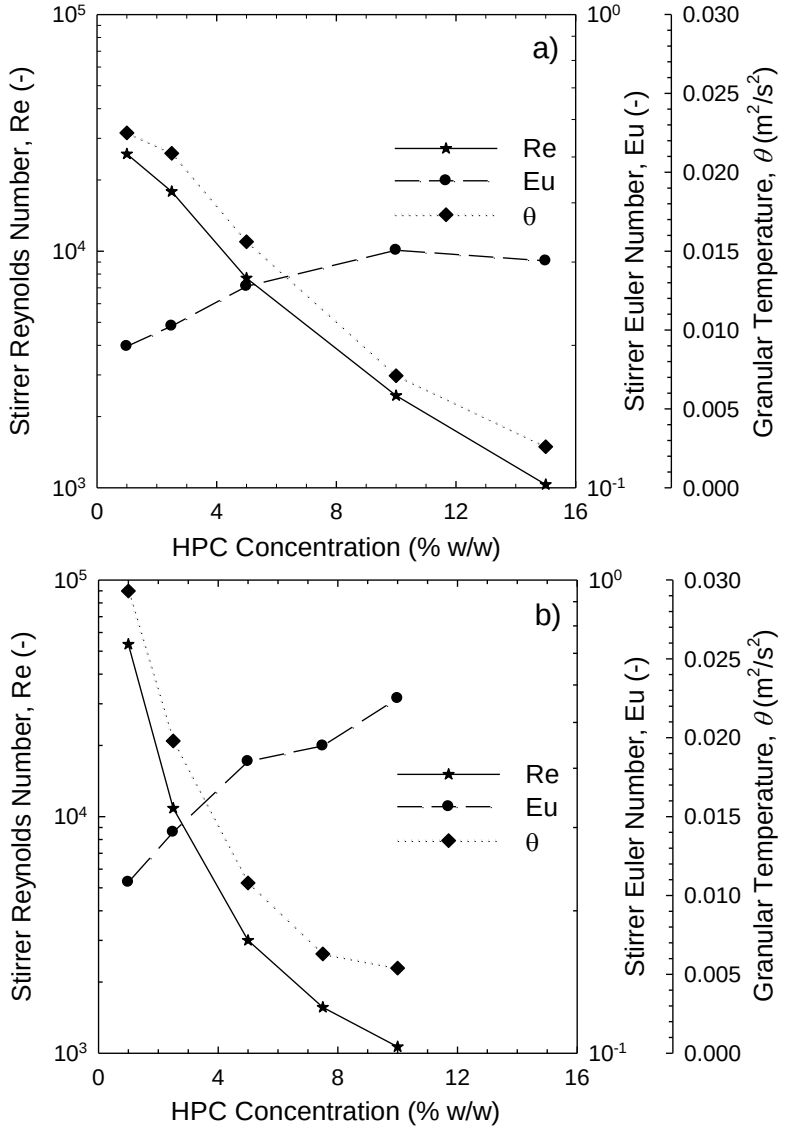

Figure 3.10 Effects of the HPC concentration on the stirrer Reynolds number, the stirrer Euler number, and the granular temperature: (a) in the absence of SDS (Runs 5–9), (b) in the presence of 0.5% SDS (Runs 12–16).

Figure 3.11 presents a statistically significant correlation between the fundamental microhydrodynamic parameter θ and macro-scale (equipment/stirrer scale) flow

parameter Re in the form of a simple logarithmic function, which was built on both HPC formulations and HPC–SDS formulations.

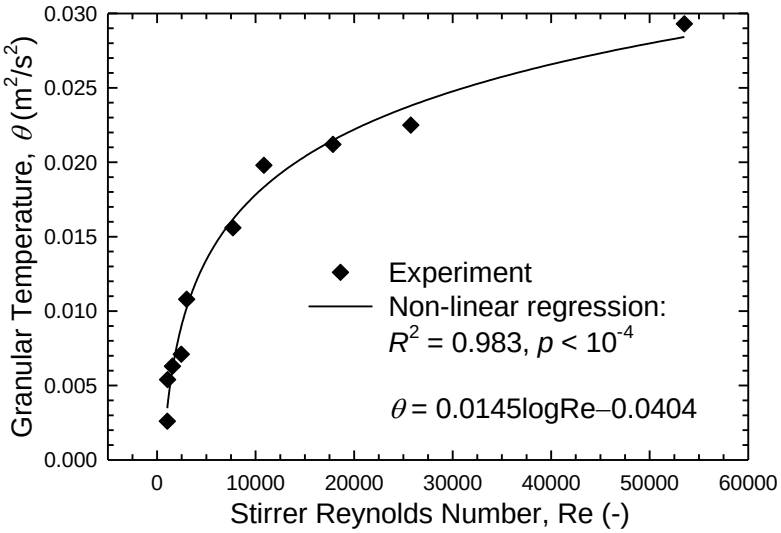

Figure 3.11 A correlation between the granular temperature and the stirrer Reynolds number for the formulations without SDS (Runs 5–9) and with 0.5% SDS (Runs 12–16).

3.4 Summary and Conclusions

Impact of polymers and surfactants on the wet stirred media milling of poorly water-soluble drugs is commonly examined within the context of their stabilizing action. Hence, a significant gap exists in terms of a fundamental engineering understanding of their roles in breakage kinetics, which determine the cycle times and production rate–volume for a desired fineness of the drug suspension. With the goal of developing such an understanding, for the first time, used a combined microhydrodynamics–adsorption analysis and elucidated the impact of a non-ionic cellulosic polymer (HPC), in the absence/presence of an anionic surfactant (SDS), on the apparent breakage kinetics of griseofulvin (GF) during wet stirred media milling. The aggregation state of the milled suspensions was examined by both particle sizing and rheometry.

Table 3.4 Effects of the HPC Concentration on the Parameters Measured (P_w, ε_{ht}, ρ_L, and μ_L) and the Microhydrodynamic Parameters (θ, ν, and u_b) for Runs 5–9 (without SDS) and Runs 12–16 (with 0.5% SDS)

Run No.	HPC Concentration (% w/w)	P_w (W/m^3)	ε_{ht} (W/m^3)	μ_L (cP)	ρ_L (kg/m^3)	θ (m^2/s^2)	u_b (m/s)	ν (1/s)
5	1	6.88×10^{5}	0[a]	11	1084	2.25×10^{-2}	2.39×10^{-1}	6.42×10^{3}
6	2.5	8.13×10^{5}	0[a]	17	1161	2.12×10^{-2}	2.32×10^{-1}	6.24×10^{3}
7	5	1.00×10^{6}	0[a]	40	1178	1.56×10^{-2}	2.00×10^{-1}	5.35×10^{3}
8	10	1.28×10^{6}	5.74×10^{4}	135	1266	7.10×10^{-3}	1.35×10^{-1}	3.61×10^{3}
9	15	1.31×10^{6}	2.11×10^{5}	346	1366	2.60×10^{-3}	8.18×10^{-2}	2.20×10^{3}
12	1	7.50×10^{5}	0[a]	5	1024	2.93×10^{-2}	2.73×10^{-1}	7.33×10^{3}
13	2.5	9.69×10^{5}	5.74×10^{4}	25	1037	1.98×10^{-2}	2.24×10^{-1}	6.02×10^{3}
14	5	1.41×10^{6}	7.66×10^{4}	93	1067	1.08×10^{-2}	1.66×10^{-1}	4.45×10^{3}
15	7.5	1.53×10^{6}	1.15×10^{5}	180	1077	6.30×10^{-3}	1.27×10^{-1}	3.41×10^{3}
16	10	1.97×10^{6}	1.91×10^{5}	270	1100	5.40×10^{-3}	1.17×10^{-1}	3.14×10^{3}

[a]Too small to be measured accurately.

Due to the non-ionic nature of the HPC and low inherent charge of GF in aqueous suspensions, HPC, even at high concentrations, was not able to fully stabilize the milled suspensions: the milled GF particles were highly aggregated in the absence of SDS, which was confirmed by laser diffraction and rheometry. The suspensions exhibited strong shear-thinning behavior that spanned the whole shear rate range investigated in this chapter. Although an increase in HPC concentration caused a reduction in the granular temperature (viscous dampening), the particle size decreased monotonically due to a decrease in the extent of particle aggregation, which was facilitated by the lower collision frequency (higher suspension viscosity) and lower aggregation probability (greater thickness of the adsorbed HPC layer). The inclusion of SDS during milling enhanced the HPC adsorption (thicker adsorption layer), allowing a synergistic electrosteric stabilizing action. Less HPC was needed to reduce the aggregation tendency in the presence of SDS. Similarly, these milled suspensions showed a weaker shear-thinning behavior and exhibited a lower extent of particle aggregation. Since they were physically more stable, the viscous dampening effect associated with high HPC concentration (above 1% HPC) was dominant in determining the apparent breakage kinetics. The combined microhydrodynamics–adsorption analysis aided the explaination of not only the viscous dampening effect of HPC, but also the optimum HPC concentration (2.5%) in the presence of SDS. The apparent breakage rate was the fastest at 2.5% HPC because both the granular temperature and the HPC adsorbed per unit surface area of the GF particles were relatively high. A simple logarithmic correlation between the granular temperature and the stirrer Reynolds number connected the intensity of the bead–bead collisions at the microscopic (bead) scale to the flow behavior

of the suspensions at the macroscopic (stirrer) scale. This correlation expresses the impact of suspension formulation parameters on the granular temperature for a given scale and operating conditions of the mill. The combined microhydrodynamics–polymer adsorption analysis has opened a new path to the work of the wet media milling process in terms of microhydrodynamic parameters as they are affected by formulation–design–operating parameters. It will potentially help formulators and engineers to design the nanosuspension formulations, to select the operating mill parameters, and to scale-up milling processes. Future work will involve the analysis of the impact of other commonly used polymers such as HPMC and PVP with/without SDS on the apparent breakage rate.

CHAPTER 4

IMPACT OF PROCESS PARAMETERS ON THE BREAKAGE KINETICS OF POORLY WATER-SOLUBLE DRUGS DURING WET STIRRED MEDIA MILLING: A MICROHYDRODYNAMIC VIEW

4.1 Introduction

Size reduction of drug crystals is known to be a feasible approach for improving the dissolution rate and bioavailability of poorly water-soluble drugs (Muller and Peters, 1998). Among all size reduction techniques, wet stirred media milling has proved to be a robust top-down process for producing drug nanoparticles (Bhakay et al., 2011; Bruno et al., 1996; Merisko-Liversidge et al., 2003). In this technique, micron-sized drug particles and media (beads) in an aqueous solution of stabilizers, usually polymers and/or surfactants are mixed by a stirrer at very high speeds. Repeated stressing of the micron-sized drug particles that are captured between the colliding beads causes size reduction down to the nanometer size range provided milling is continued for a sufficient time. Stabilizers are usually added to prevent the aggregation of the milled drug particles, while some polymeric stabilizers can also inhibit particle growth (ripening) during milling/storage (Ghosh et al., 2011; Kesisoglou et al., 2007).

Finding an optimal stabilizer type/concentration is an important aspect of drug nanoparticle formulation development because short or long-term physical stability of a drug nanoparticle suspension must be ensured for the intended end use of the suspension in a desired dosage form. Therefore, a great majority of the wet media milling studies have focused on the physical stability of the milled drug suspensions that are formulated with various stabilizers (Kesisoglou et al., 2007; Van Eerdenbrugh et al., 2008). For example, milling in a planetary mill (Van Eerdenbrugh et al., 2009) or in a ball mill (Lee

and Cheng, 2006; Van Eerdenbrugh et al., 2007), both making use of vials containing drug suspensions with various stabilizers, has previously been described for their capability in obtaining nanoparticles. These mills are regarded as medium or low-energy mills. Hence, the suspension flow and microhydrodynamics, which is the fluctuating motion of the beads in suspensions, are quite different in these mills than in the wet stirred media mills. It is not surprising to see that nanoparticles are produced after several hours to a few days of milling, even at the bench scale, for suspension quantities on the order of ~10 g. In other studies (e.g. Cerdeira et al., 2010; Merisko-Liversidge et al., 2003), wet stirred media mills have been used; however, the impact of process parameters on the breakage kinetics and microhydrodynamics has not been reported. It is clear that milling dynamics, breakage kinetics, process cycle times, and scale-up effects have not been of major concern in these formulation studies. Bhakay et al. (2011) points out that most wet media milling studies in pharmaceutical literature (e.g. Ain-Ai and Gupta, 2008; Tanaka et al., 2009) did not consider the breakage kinetics explicitly and focused mainly on the physical stability of the final milled suspensions, which were produced upon prolonged milling. Other studies (Choi et al., 2008; Deng et al., 2008; Lee et al., 2008) reported limited analysis of the effects of milling time, with little to no quantification of the breakage kinetics and its relation to the microhydrodynamics.

As wet media milling process is time-consuming, costly, and energy-intensive (Kawatra, 2006) and the breakage kinetics determines the cycle time and production rate for a desired fineness, milling process design and optimization entails a good understanding of the breakage kinetics and its controlling process parameters. Process parameters such as stirrer speed, bead loading, and drug loading can significantly affect

the breakage rate and milling time required in a wet stirred media milling process. In a recent review paper, Peltonen and Hirvonen (2010) summarized various process parameters and their ranges investigated in wet media milling processes. While Peltonen and Hirvonen (2010) and the references cited therein provide great understanding of the impact of stabilization and formulation, little fundamental understanding of the impact of process parameters is available at the beads scale (microhydrodynamics). In a more recent work, Ghosh et al. (2012) present the effects of stirrer speed, bead size, and drug content on the final milled suspension; however, the impact of these parameters on the breakage kinetics was not investigated. Singare et al. (2010) and Singh et al. (2011) used a statistical design of experiments with a response surface methodology (RSM) with the goal of optimizing the process parameters including milling speed and time. However, no information regarding the breakage kinetics was presented explicitly. In general, the statistically-based designs of experiments such as those in Singare et al. (2010) and Singh et al. (2011) may not provide significant physical insight at the beads scale as to how the process parameters affect the breakage kinetics.

While valuable and sizeable body of work exists in pharmaceutical literature regarding the impact of processing parameters on the particle size of milled suspensions, as mentioned above, the breakage kinetics and its relation to the microhydrodynamics has not been investigated. To a certain extent, wet media milling has been treated as a "black-box". In a separate field, Eskin et al. (2005a, 2005b) developed a model to study the microhydrodynamics in a mixing tank filled with beads that are stirred with a pair of Rushton type paddles. The impact of bead size, stirrer speed, and bead concentration was simulated for a mixing tank with water as the medium. Bilgili and Afolabi (2012) have

applied this model (see Chapter 3) to the wet media milling of drug suspensions with polymer–surfactant and elucidated/quantified the viscous dampening effect of the stabilizers. While the excellent work by Eskin et al. (2005a, 2005b) built the theoretical foundation for analysis of the microhydrodynamics, developing a fundamental understanding of the impact of milling process parameters on the breakage rate of drug nanoparticle suspensions entails a combined analysis of the microhydrodynamics and breakage kinetics.

The preceding chapter investigates the impact of formulation parameters; the key results suggest a minimum stabilizer-to-drug ratio, synergistic stabilizing effect of a hydrophilic polymer and surfactant, and a dampening effect of the polymer on the breakage kinetics above an optimum loading level. The major objective of this chapter is to elucidate the impact of stirrer speed, bead concentration, and drug loading on the breakage kinetics during the wet stirred media milling of griseofulvin (GF), a model poorly water-soluble drug, via a microhydrodynamic model of the milling process. GF particles were wet-milled in the presence of two stabilizers, hydroxypropyl cellulose (HPC) and sodium dodecyl sulfate (SDS), to prepare stable GF suspensions under various processing conditions. Laser diffraction, scanning electron microscopy, and rheometry were used to characterize the suspensions. The evolution of the median particle size was measured and fitted by a well-established empirical model (Strazisar and Runovc, 1996), yielding a characteristic time constant of the process as a measure of the breakage kinetics. The impact of the process parameters on the breakage kinetics was explained in terms of various microhydrodynamic parameters, including the newly defined milling intensity factor. Besides providing physical insight and guiding process optimization, the

theoretical analysis also rationalizes preparation of a single highly drug-loaded batch (20% or higher) instead of multiple dilute batches.

4.2 Experimental

4.2.1 Materials

Griseofulvin (GF, Cat# 606440, BP/EP micronized grade of GF was purchased from Letco Medical, Decatur, AL, USA) was used as a model BCS Class II drug. Hydroxypropyl cellulose (HPC) and sodium dodecyl sulfate (SDS) were used as stabilizers as reported in Chapter 3.

4.2.2 Methods

4.2.2.1 Preparation of GF Suspensions. Feed suspensions to be milled were prepared in a shear mixer (Cat#. 14–503 Fisher Scientific Pittsburgh, PA, USA). Based on a previous formulation study (see Chapter 3) with GF (Bilgili and Afolabi, 2012), a 2.5% HPC–0.5% SDS aqueous solution was prepared with 200 g deionized water so as to properly stabilize GF suspensions during milling and after storage. Note that all percentages (%) refer to w/w with respect to deionized water unless otherwise specified. SDS was added to deionized water in a beaker gradually for 15 min while the mixer ran at a fixed speed of 300 rpm. Then, HPC was added to the SDS solution gradually for 30 min. The final HPC–SDS solution was further mixed for 15 min to ensure proper dissolution of HPC and SDS particles. Desired amount of GF powder was weighed and added to this solution gradually for 30 min while mixing continued.

The feed suspensions were milled in a Microcer wet stirred media mill (Netzsch Fine Particle Technology, LLC. Exton, PA, USA), whose schematic is shown in Figure 3.1. Table 4.1 presents the process parameters examined in this chapter, while other parameters were kept constant. *Run 1 was regarded as the base-case* as its process parameters were selected based on prior formulation study (see Chapter 3) (Bilgili and Afolabi, 2012).

Table 4.1 Processing Parameters used in the Wet Milling Experiments

Run No.	Drug Loading (% w/w)[a]	Stirrer Speed (rpm, m/s)	Bead Load, Concentration (ml), (c)
1	10	3200, 11.7	50, 0.388
2	10	1600, 5.86	50, 0.388
3	10	2400, 8.80	50, 0.388
4	10	4000, 14.7	50, 0.388
5	10	3200, 11.7	14, 0.107
6	10	3200, 11.7	32, 0.244
7	10	3200, 11.7	75, 0.572
8	5	3200, 11.7	50, 0.388
9	20	3200, 11.7	50, 0.388
10	30	3200, 11.7	50, 0.388

[a] % w/w with respect to de-ionized water.

In Runs 2–10, stirrer speed, bead concentration, and drug loading were systematically studied by varying only one variable at a time and keeping the other variables constant. The suspensions were milled for 96 min, which allowed sufficient time for preparation of GF nanoparticles (d_{90} < 1000 nm) under all processing conditions. The maximum stirrer speed allowed per mill design is 4200 rpm; hence, 4000 rpm was studied as the highest value (Run 4). The milling chamber is lined with zirconia and has a volume V_m of 80 ml. To minimize potential pressure build-up and fast temperature rise,

the mill was loaded with a maximum of 75 ml of zirconia beads (bulk volume) in Run 7. Also, a maximum of 30% drug loading was used to conserve the drug (Run 10).

The milling procedure was followed as in section 3.2.2.1 at a constant volumetric flow rate Q of about 126 ml/min by a peristaltic pump (Figure 3.1). In Runs 4 and 7, the stirrer was stopped occasionally when the temperature reached 35 ^{o}C due to high heat generation rate. Samples were taken from the outlet of the milling chamber at several intervals of milling and the particle size distribution was measured. The final milled suspensions were stored in a refrigerator at 8 ^{o}C after density and shear viscosity measurements.

4.2.2.2 Measurement of Power Consumption for the Microhydrodynamic Analysis. The power applied by the mill motor P was measured during 96 min milling. The stirrer power per unit volume of the slurry in the milling chamber (shortly will be referred to as the stirrer power), i.e., $P_w = P/V_m$ was calculated and an average value was reported. The power input per unit volume of the milled suspension in the absence of the beads i.e., P_{ht}, was also measured. Its value was multiplied by the equivalent liquid (drug suspension) volume fraction to obtain ε_{ht}, which will be used in the microhydrodynamic analysis along with P_w (Section 2.4). The no-load power values obtained from dry runs of the mill stirrer running at 1600, 2400, 3200, and 4000 rpm were subtracted from the measured power values in the calculation of P_w and P_{ht}.

4.2.2.3 Particle Sizing and Scanning Electron Microscopy (SEM). Particle size analysis was followed as in section 3.2.2.3. Prior to the size measurement, milled suspension samples (~2 ml) were diluted in a vial with 10 ml of HPC–SDS solution by using a vortex mixer (Fisher Scientific Digital vortex mixer, Model No: 945415, NH,

USA), which rotated at 1500 rpm for 1 min. The PSD of the milled suspension samples was also measured after 7 day storage at 8 ^{o}C to assess the physical stability. SEM imaging was carried out as in section 3.2.2.3 to examine the morphology of the milled particles and to determine the primary particle size of the GF.

4.2.2.4 Apparent Shear Viscosity and Density of the Milled Suspensions. The apparent shear viscosity of the milled suspensions (Runs 1–10) was measured using an R/S plus rheometer (Brookfield Engineering, Middleboro, MA, USA) as reported in section 3.2.2.5. The suspension densities were determined by weighing the suspension filled in a 60 ml glass cylinder. The weight of the suspension was divided by the volume to obtain the density. Average value of three measurements on each suspension was reported in Table 4.4.

4.2.2.5 Milling Intensity Factor. Recall the energy dissipation rate Π can be decomposed into a material-dependent factor λ and a process-dependent factor, F, which is referred to as the milling intensity factor, as follows:

$$\lambda = 2.23 \frac{1}{\pi^{5/2}\sigma_{\mathrm{y}}} \left(\frac{Y_{\mathrm{b}}}{1-\eta_{\mathrm{b}}^2} \right)^{18/15} \left(\frac{Y^*}{Y_{\mathrm{p}}} \right)^{\gamma} \rho_{\mathrm{b}}{}^{4/5} \frac{R_{\mathrm{p}}}{R_{\mathrm{b}}^2} \tag{4.1}$$

$$F = \frac{c^2(2-c)}{(1-c)^3} \frac{1}{\varepsilon} \theta^{13/10} \tag{4.2}$$

Where F represents the milling intensity factor with the use of the same drug, same bead material, and the same bead size. Upon a change in each process parameter, a possible increase/decrease in F corresponds to a proportional increase/decrease in Π in some time- and space-averaged sense because well-mixedness and average power consumption during the milling are considered, and λ is taken as a constant for a given pair of drug–

bead materials. One can then refer to either F or Π while reporting the impact of the process parameters. All microhydrodynamic parameters calculated are presented in Table 4.4.

4.3 Results and Discussion

4.3.1 Preparation of Stable GF Suspensions

As the major objective of this chapter is to elucidate the impact of processing parameters on the breakage kinetics, potential confounding effects that may arise from particle aggregation should be minimized via proper stabilization of the GF nanoparticle suspensions. Based on a previous formulation study (Bilgili and Afolabi, 2012), a 2.5% HPC–0.5% SDS stabilizer combination was selected here for proper stabilization. Figure 4.1a shows the evolution of the GF particle size distribution (PSD) during milling (Run 1, base-case) as measured by the laser diffraction method. Upon further milling, the PSD shifted toward finer particles monotonically. At 96 min, GF particles had d_{50} and d_{90} values of 0.149 and 0.180 μm, respectively. The SEM image (Figure 4.1b) shows the primary GF nanoparticles in the size range of 50–200 nm, similar to the range observed in Figure 4.1a. Hence, both the laser diffraction and the SEM imaging suggest that the HPC–SDS stabilized suspension had relatively small extent of aggregation and the dominant mechanism during the milling was breakage and not aggregation. The combination of HPC and SDS is known to have a synergistic effect in the stabilization of drug suspensions (Basa et al., 2008; Lee et al., 2008). HPC and SDS interact, forming aggregates or micelle-like SDS clusters bound to HPC (Winnik and Winnik, 1990). These clusters can co-adsorb on surfaces (Berglund et al., 2003; Evertsson and Nilsson, 1997),

facilitating adsorption of HPC on drug particles (Cerdeira et al., 2010) and enabling electrosteric stabilization.

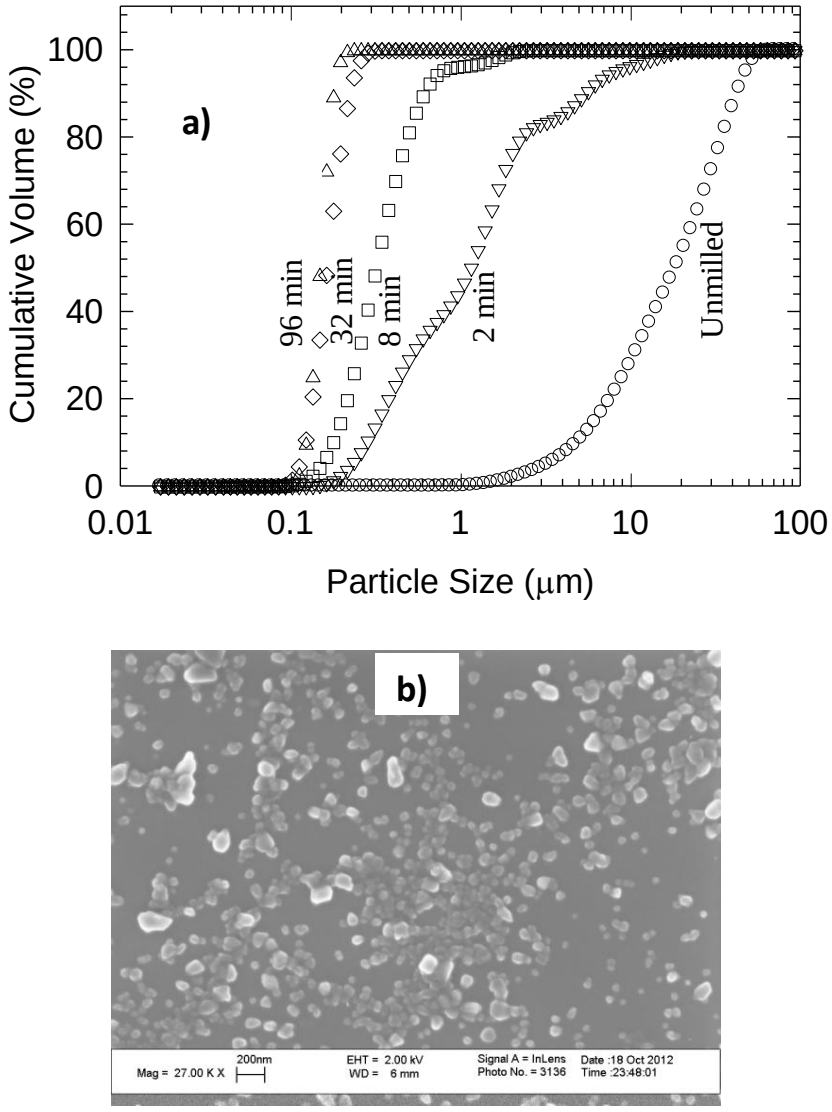

Figure 4.1 Wet media milling of GF particles in the presence of stabilizers (Run 1): (a) evolution of the cumulative particle size distribution, (b) SEM image of the GF particles milled for 96 min (marker size: 200 nm, 27 kX magnification).

To establish the reproducibility of the milling process, the milling experiment (Run 1) was repeated. The d_{50} and d_{90} values of the repeat experiment were 0.151 and 0.186 μm. The (absolute) percent deviations from the d_{50} and d_{90} values were negligibly

small: 1.34% and 3.33%, respectively. Hence, both the process and the particle size measurements were fairly reproducible. Good reproducibility has also been established in recent work on the wet stirred media milling of several poorly water-soluble drugs such as azodicarbonamide, fenofibrate, griseofulvin, and naproxen with HPC or HPMC (hydroxypropyl methyl cellulose) in the presence of SDS (Bhakay et al., 2013; Bilgili and Afolabi, 2012; Knieke et al., 2013; Monteiro et al., 2013).

Table 4.2 The Median Size d_{50} and 90% Passing Size d_{90} of the GF Suspensions After 96 min Milling and After 7 Day Storage

Run No.	Milled (96 min) d_{50} (μm), d_{90} (μm)	7 day storage d_{50} (μm), d_{90} (μm)
1	0.149, 0.180	0.152, 0.185
2	0.228, 0.393	0.230, 0.401
3	0.167, 0.212	0.164, 0.218
4	0.148, 0.178	0.152, 0.187
5	0.292, 0.497	0.311, 0.516
6	0.167, 0.218	0.165, 0.221
7	0.132, 0.160	0.140, 0.171
8	0.139, 0.170	0.139, 0.169
9	0.161, 0.208	0.161, 0.209
10	0.156, 0.220	0.158, 0.220

Short-term physical stability of the milled suspensions prepared in Runs 1–10 were assessed by comparing the particle size after milling and after 7 day storage (see Table 4.2). Long-term stability of these suspensions was not investigated here as they were intended to be dried shortly after the milling via various drying methods (as in Bhakay et al., 2013; Sievens-Figueroa et al., 2012). After 7 day storage, d_{50} and d_{90} of the milled suspensions did not change significantly; the suspensions were physically stable and remained colloidal mainly due to the synergistic stabilizing action of the HPC–SDS combination. In view of the effectiveness of the 2.5% HPC–0.5% SDS stabilizer combination and reproducibility of the milling process, the differences in d_{50} and d_{90}

values during 96 min milling can be mainly attributed to the changes in the process parameters.

4.3.2 Impact of Process Parameters on the Breakage Kinetics and Microhydrodynamics

The impact of stirrer tip speed, beads loading, and drug loading on the breakage kinetics was investigated and the effects were elucidated via the microhydrodynamic model in the present chapter. The overall apparent breakage rate or shortly the breakage rate was quantitatively assessed by two separate measures: the median size at 4 min and the characteristic time constant τ_p of the process, which was obtained by fitting Eq. (2.7) to the evolution of the median size. The breakage rate can be described mathematically by $1/\tau_p$. Albeit chosen somewhat arbitrarily, 4 min was long enough for the effects of different process parameters to develop, yet was still shorter than what a dynamic equilibrium would entail. Table 4.3 presents the values of the parameters d_{lim} and τ_p estimated (see Chapter 2.3), their coefficient of variation COV, and the coefficient of determination R^2. Considering the simplicity of the model, the fits were fairly good: R^2 values were greater than 0.90, COV values were less than about 20%, and the parameters were all statistically significant (p-value < 0.05). The estimated d_{lim} values were slightly greater than the experimental median particle sizes obtained after 96 min milling (Table 4.2), except for Runs 2 and 5, which entail further milling to approach a dynamic equilibrium. The differences are mostly small and within 1–2 standard deviation of the d_{lim} estimated and can be explained by experimental variability in d_{50} measured, insufficient number of time samples in the fitting, presence of low extent of aggregation that was not considered by the simple two-parameter model. Overall, the fit statistics

suggest that the use of τ_p to assess the impact of process parameters on the breakage kinetics.

Table 4.3 Parameters and Their Statistics Estimated From the Empirical Model (Eq. (2.7)) Fit to the Evolution of the Median Particle Size

Run No.	d_{lim}, COV% (μm), (–)	τ_p, COV% (min), (–)	R^2 (–)
1	0.160 (3.78)	2.56 (7.07)	0.99
2	0.269 (8.94)	9.77 (8.95)	0.98
3	0.184 (8.18)	3.57 (12.7)	0.97
4	0.165 (8.62)	1.97 (20.8)	0.91
5	0.404 (13.6)	7.06 (12.5)	0.95
6	0.190 (7.97)	3.78 (13.0)	0.97
7	0.144 (2.60)	1.91 (11.6)	0.97
8	0.163 (7.56)	1.50 (17.2)	0.94
9	0.171 (7.10)	3.14 (13.0)	0.97
10	0.173 (8.17)	4.46 (1.31)	0.96

4.3.2.1 Impact of Stirrer (Rotor) Tip Speed. Figure 4.2a shows the temporal evolution of d_{50} and d_{90} for angular speeds of 1600–4000 rpm or equivalent tip speeds of 5.86–14.7 m/s (Runs 1–4). For proper scaling and good discrimination of the impact of various tip speeds, the median size was plotted in log-scale and the initial size was not shown (d_{50} = 19.65 ± 1.17 μm and d_{90} = 50.88 ± 6.33 μm at t = 0 min). Both d_{50} and d_{90} decreased monotonically upon an increase in milling time, and no size increase was observed. This finding suggests that breakage was the dominant mechanism and aggregation of the particles probably occurred at a much smaller rate than the breakage in the presence of HPC–SDS. In general, the rate of decrease in d_{50} and d_{90} decreased with time, suggesting a slowing-down of the breakage. Hence, a dynamic equilibrium (plateau) in d_{50} was approached or practically attained, except at the tip speed of 5.86 m/s, for which the overall breakage rate appeared to be the lowest and d_{50} continued to decrease for the whole 96 min. In general, the dynamic equilibrium was approached or

attained earlier with an increase in the tip speed. Since d_{90} heavily weighs the contribution from the coarser particles, whose breakage into smaller particles of desired fineness will take more time, d_{90} continued to decrease up to 96 min. The slowing-down of the breakage and approach to a dynamic equilibrium can be explained as follows: while milling progressed, finer particles were produced, which are more difficult to capture between the beads and are harder to break. Finer particles, especially nanoparticles, are mechanically stronger and have a much smaller breakage probability than coarser particles (Bilgili et al., 2006). Theoretical work from Bilgili's research group using population balance models, even without any aggregation terms, were able to capture the sharp decrease in the breakage rate (Bilgili et al., 2006; Bilgili and Capece, 2011).

The particle breakage appears to get faster with an increase in the stirrer speed, as shown by the smaller median size at any given time point (Figure 4.2a). At the lowest speed of 5.86 m/s (Run 2), the breakage rate was so low that d_{50} and d_{90} continued to decrease significantly up to and including 96 min; much more time would be needed to reach a dynamic equilibrium. The breakage rate increased monotonically with an increase in the stirrer speed as indicated by the monotonic decrease in both d_{50} at 4 min and τ_p (Figure 4.2b), while d_{lim} decreased with an increase in the tip speed (Table 4.3). These effects got weaker at higher speeds (especially >11.7 m/s).

To explain the aforementioned effects of the stirrer speed at the beads scale, the microhydrodynamic parameters (see Chapter 2.4) granular temperature θ, the average bead oscillation velocity u_b, the frequency of single-bead oscillations ν, the maximum

contact pressure compressions σ_b^{max}, the milling intensity factor F, and the average frequency of drug particle a were calculated (Figures 4.3a and 4.3b).

Experimentally, upon an increase in the tip speed, the stirrer power increased and the viscosity of the milled suspension decreased due to the presence of finer particles (both reported in Table 4.4). Since more mechanical energy was imparted on the slurry and the beads, all microhydrodynamic parameters increased monotonically, as one would expect intuitively. Upon an increase in the stirrer speed, the fluctuating motion of the beads became more vigorous (higher θ). There were more frequent bead oscillations (higher ν), which led to a more frequent compression of the drug particles (higher a), i.e., a greater number of stressing events.

The beads had higher fluctuating velocity (higher u_b) and fluctuating momentum, which led to more impactful bead collisions and development of higher compressive stresses (higher σ_b^{max}), i.e., a greater stress intensity. For the griseofulvin (drug)–zirconia beads (milling media) pair, the energy dissipation rate attributed to the deformation of the drug particles per unit volume can be expressed in terms of a milling intensity factor F, which captures all of the above effects of the stirrer speed on the number/intensity of the stressing events through a lumped microhydrodynamic parameter. The increase in the overall breakage rate upon an increase in the stirrer speed (Figure 4.2b) can be simply explained by more bead collisions with greater stressing intensity (Figures 4.3a and 4.3b). In summary, a decrease in τ_p resulted from an increase in the stirrer speed through an increase in F. Despite the rapid rise of F especially above 11.7 m/s, τ_p decreased more gradually, implying that the impact of the milling intensity factor on the breakage rate begins to saturate above a certain value.

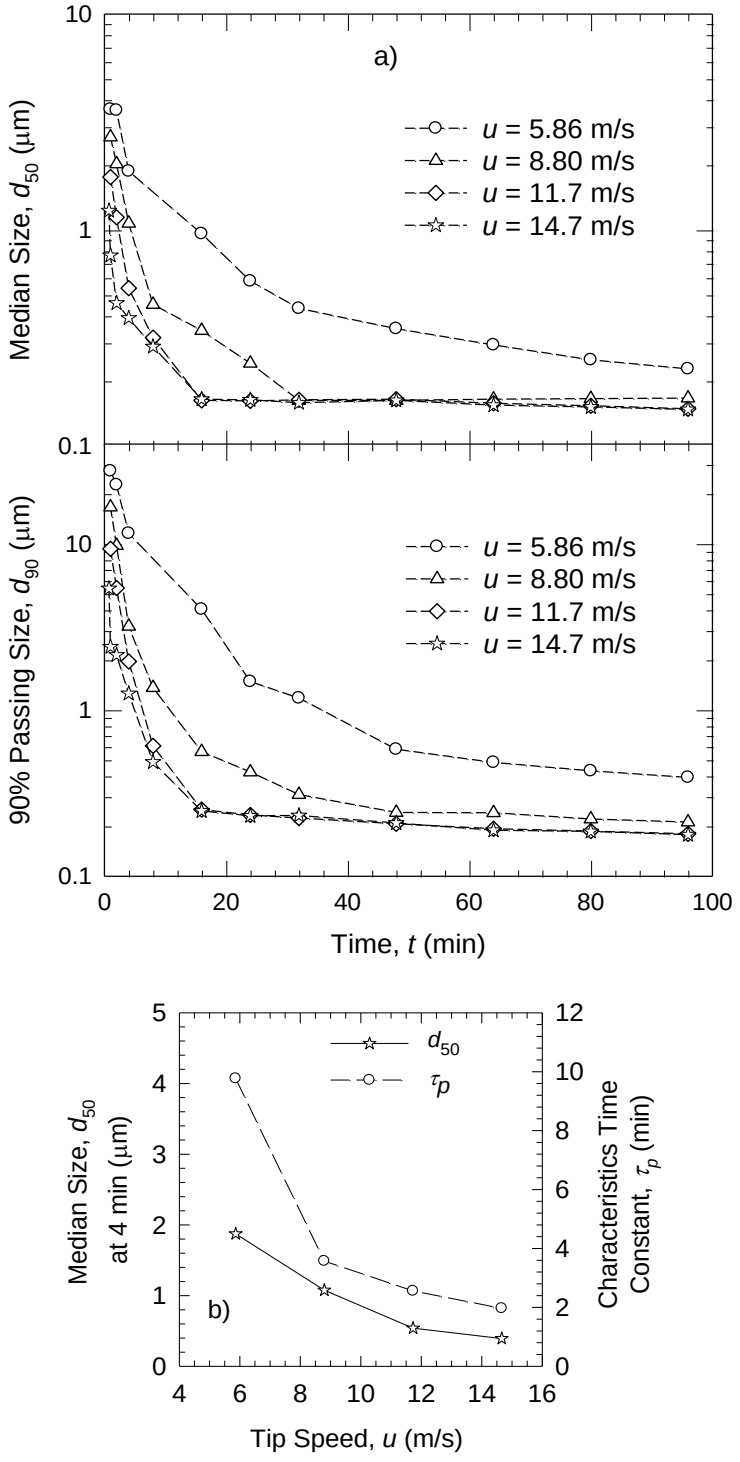

Figure 4.2 Effects of the stirrer speed on (a) the time-wise variation of the characteristic sizes of GF particles, (b) the median size of GF particles after milling for 4 min and the characteristic time constant (Runs 1–4). At t = 0 min, the GF particles have d_{50} = 19.65 ± 1.17 μm and d_{90} = 50.88 ± 6.33 μm.

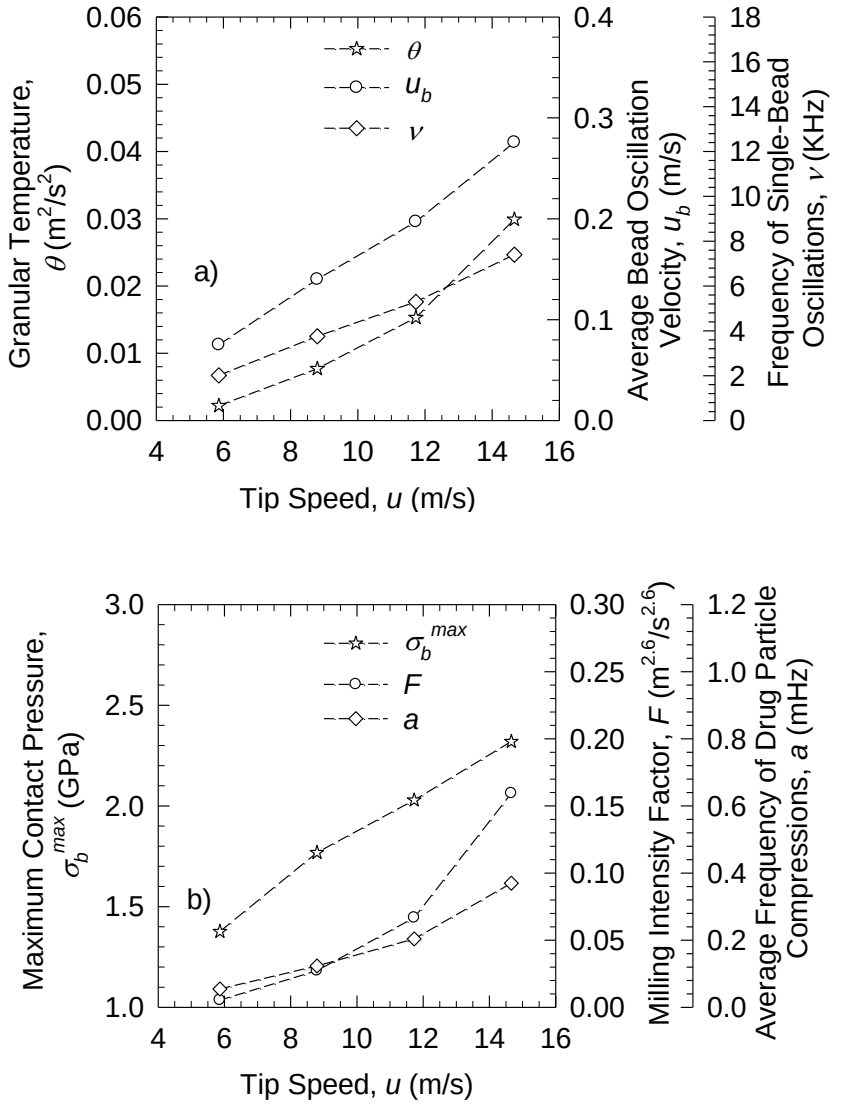

Figure 4.3 Effects of the stirrer speed on (a) the granular temperature, the average bead oscillation velocity, and the frequency of single-bead oscillations, (b) the maximum contact pressure, the milling intensity factor, and the average frequency of drug particle compressions (Runs 1–4).

4.3.2.2 Impact of Bead Concentration. The temporal evolution of d_{50} and d_{90} is illustrated in Figure 4.4a for bead concentrations of 0.107–0.572, which were described in terms of volume fraction c (Runs 5–7 and 1). In general, the evolution of d_{50} and d_{90} followed similar patterns as discussed in Section 4.2.1: both d_{50} and d_{90} decreased

monotonically with milling time. The absolute value of the slope of the d_{50} and d_{90} profiles decreased with time, suggesting a decrease in the breakage rate as milling progressed. Although d_{90} was evolving very slowly even up to 96 min of milling; a dynamic equilibrium (plateau) in d_{50} was approached or attained, except at a bead volume fraction of 0.107, for which the overall breakage rate was the lowest. The dynamic equilibrium was approached or attained earlier with an increase in the beads loading. The breakage rate appears to increase with an increase in the bead concentration, as shown by the smaller median particle size at a given time (Figure 4.4a). This finding was further reflected by the monotonic decrease in τ_p (Figure 4.4b) and decrease in d_{lim} (Table 4.3) upon an increase in the bead concentration. Interestingly, Figures 4.5a and 4.5b exhibit two counteracting effects of an increase in the bead concentration: θ, u_b, and σ_b^{max} decreased while ν, a, and F increased. In other words, the number of stressing events dramatically increased, but their intensity decreased (less impactful collisions and particle compressions). The increase in ν, a, and F seems to be more drastic than the decrease in θ, u_b, and σ_b^{max} in relative terms. Upon an increase in the bead concentration, the number of the beads increased and the clearance between the beads decreased, leading to a dramatic increase in the bead–bead collisions and the average number of drug particle compressions per unit time (ν and a).

On the other hand, despite the increase in the stirrer power and the decrease in the suspension viscosity at the higher bead loading (Table 4.4), higher number of inelastic bead–bead collisions and liquid-film squeezing events coupled with an increase in the effective drag coefficient R_{diss} led to greater energy dissipation.

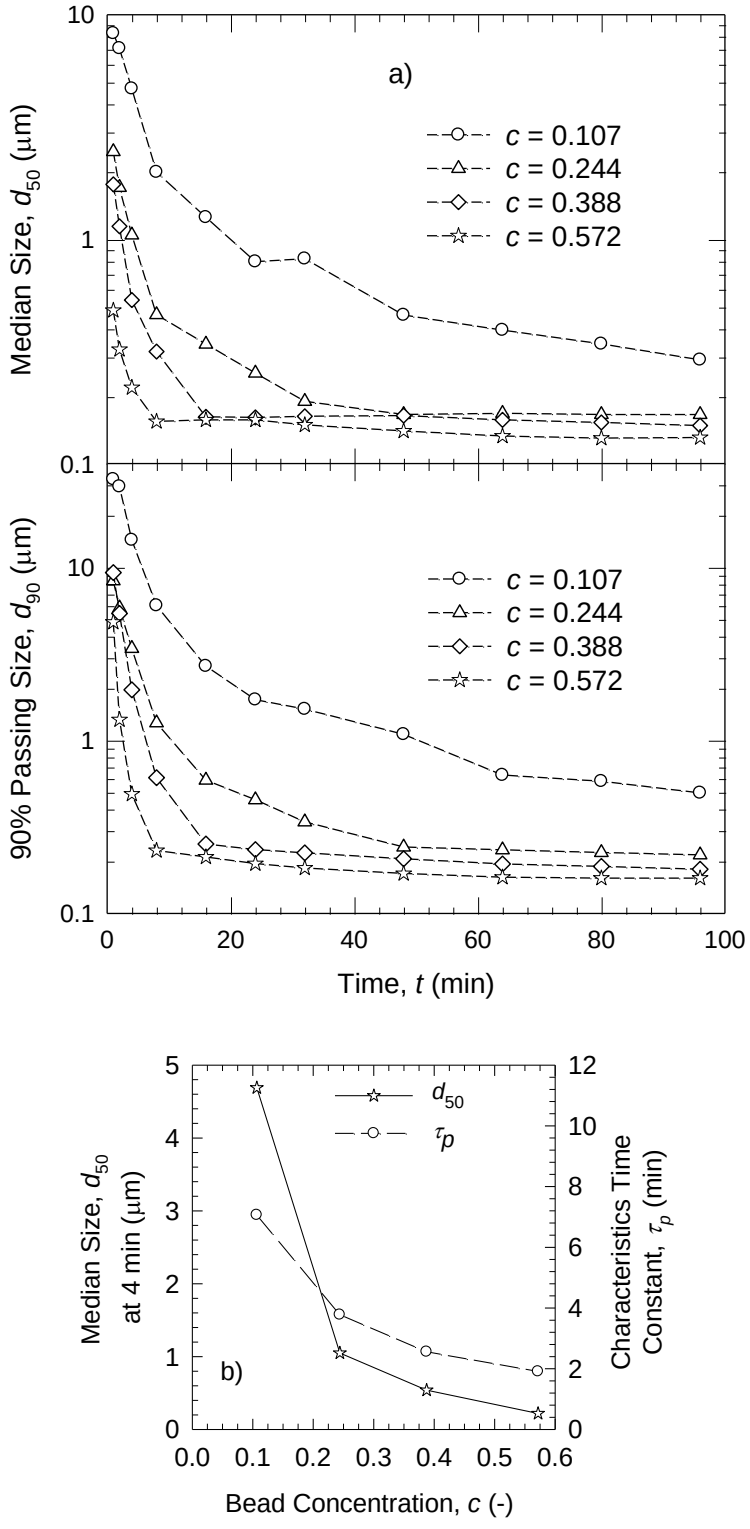

Figure 4.4 Effects of the bead concentration on (a) the time-wise variation of the characteristic sizes of GF particles, (b) the median size of GF particles after milling for 4 min and the characteristic time constant (Runs 5–7 and Run 1). At t = 0 min, the GF particles have d_{50} = 19.65 ± 1.17 μm and d_{90} = 50.88 ± 6.33 μm.

Table 4.4 Power Values (P_w and ε_{ht}) and Properties of the Milled Drug Suspensions (μ_L and ρ_L) Measured as Well as the Microhydrodynamic Parameters (θ, u_b, ν, σ_b^{max}, a, and F) Calculated

Run No.	P_w (W/m^3)	ε_{ht} (W/m^3)	μ_L (cP)	ρ_L (kg/m^3)	θ (m^2/s^2)	u_b (m/s)	ν (KHz)	σ_b^{max} (GPa)	a (mHz)	F (m$^{2.6}$/s$^{2.6}$)
1	5.23×10^{5}	0	17	1029	1.53×10^{-2}	1.97×10^{-1}	5.29	2.03	2.04×10^{-1}	6.67×10^{-2}
2	1.70×10^{5}	7.66×10^{4}	31	1024	2.20×10^{-3}	7.50×10^{-2}	2.01	1.38	5.46×10^{-2}	5.36×10^{-3}
3	2.95×10^{5}	0	24	1022	7.70×10^{-3}	1.40×10^{-1}	3.76	1.77	1.23×10^{-1}	2.73×10^{-2}
4	9.55×10^{5}	0	10	1023	2.99×10^{-2}	2.76×10^{-1}	7.40	2.32	3.70×10^{-1}	1.59×10^{-1}
5	2.50×10^{5}	2.03×10^{4}	37	1021	5.33×10^{-2}	3.68×10^{-1}	1.03	2.60	2.42×10^{-2}	9.71×10^{-3}
6	3.64×10^{5}	0	22	1024	2.84×10^{-2}	2.69×10^{-1}	2.63	2.30	7.41×10^{-2}	3.42×10^{-2}
7	1.32×10^{6}	0	6	1028	1.11×10^{-2}	1.68×10^{-1}	17.3	1.90	1.09	2.48×10^{-1}
8	5.00×10^{5}	0	13	1006	1.67×10^{-2}	2.06×10^{-1}	5.53	2.06	2.06×10^{-1}	1.50×10^{-1}
9	6.02×10^{5}	0	26	1039	1.36×10^{-2}	1.86×10^{-1}	5.00	1.98	1.98×10^{-1}	2.86×10^{-2}
10	6.20×10^{5}	0	34	1070	1.17×10^{-2}	1.73×10^{-1}	4.63	1.92	1.68×10^{-1}	1.57×10^{-2}

Consequently, the fluctuating motion of the beads was less vigorous (smaller θ and u_b), which in turn led to smaller bead compression stresses (smaller σ_b^{max}). It is worth-mentioning that even a decrease in θ could not prevent the drastic increase in ν and a because the impact of more beads and reduced clearance between them upon an increase in the bead loading was stronger.

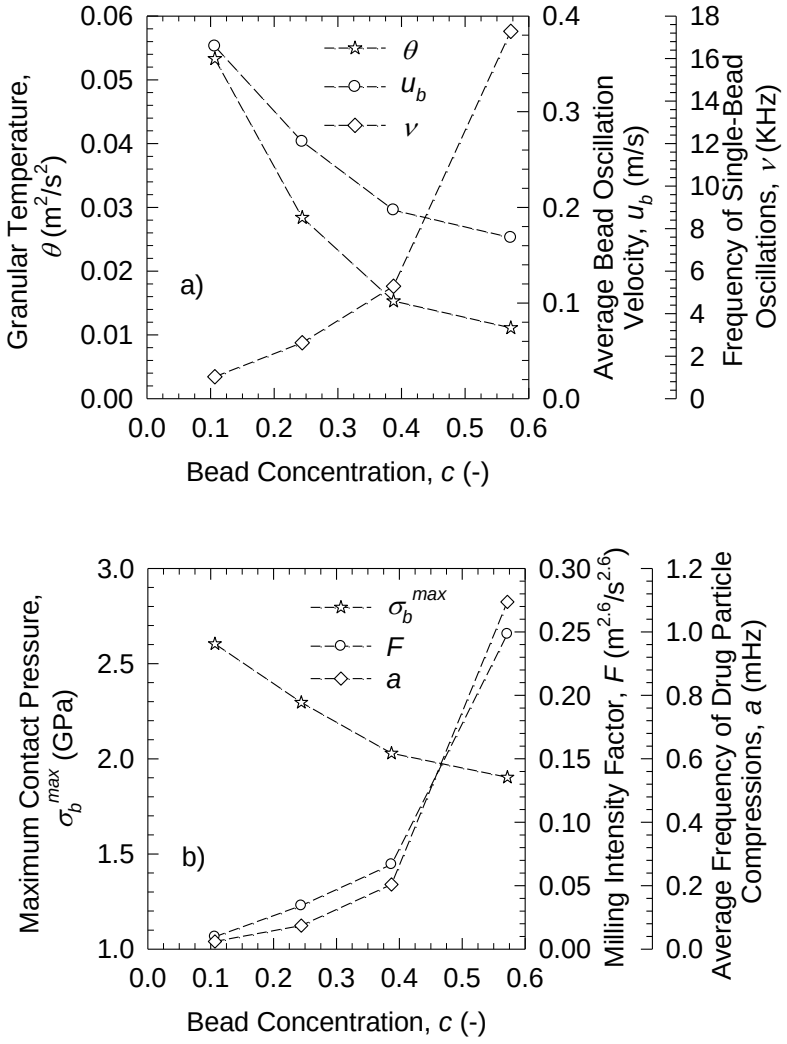

Figure 4.5 Effects of the bead concentration on (a) the granular temperature, the average bead oscillation velocity, and the frequency of single-bead oscillations, (b) the maximum contact pressure, the milling intensity factor, and the average frequency of drug particle compressions (Runs 5–7 and Run 1).

It is of fundamental importance to determine which of the aforementioned two effects will be dominant in explaining the observed increase in the breakage rate upon an increase in the bead concentration. A comparison of the trends in Figure 4.4b and Figures 4.5a and 4.5b suggests that upon an increase in the bead loading, the dramatic rise in a was more prevalent than the decrease in σ_b^{max}, leading to an increase in the milling intensity factor F, which explains the decrease in τ_p. Despite the rapid rise of F especially above a bead concentration of 0.388 in Figure 4.5b, the breakage rate did not change significantly (Figure 4.4b), implying that the impact of the milling intensity factor on the breakage rate begins to saturate above a certain value (similar to the impact of the tip speed).

4.3.2.3 Impact of Drug Loading. The temporal evolution of d_{50} and d_{90} is illustrated in Figure 4.6a for 5%, 10%, 20%, and 30% drug loadings (Runs 8–10, and Run 1). The evolution of d_{50} and d_{90} followed similar patterns as discussed in the previous sections; hence, this aspect will not be elaborated. In comparison with the impact of the stirrer speed and the beads loading, the impact of the drug loading appears to be weaker, within the parameter space investigated. A slight difference worth mentioning is the attainment of similar median size values after 96 min for all drug loadings. Figure 4.6 suggests that the overall breakage rate slightly decreased with an increase in the drug loading. Table 4.3 presents d_{lim} values that are slightly greater than the median size values at 96 min (Table 4.2).

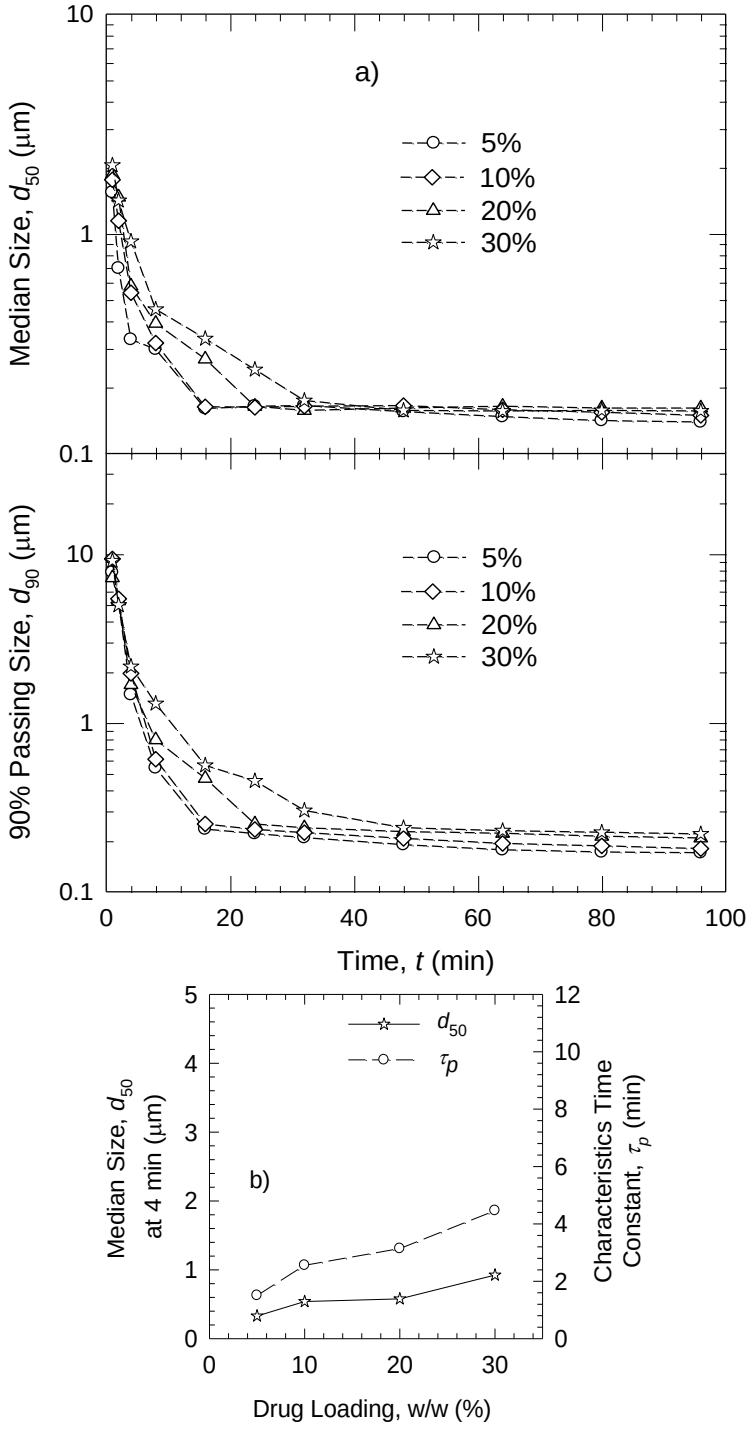

Figure 4.6 Effects of the drug loading on a) the time-wise variation of the characteristic sizes of GF particles and b) the median size of GF particles after milling for 4 min and the characteristic time constant (Runs 8–10 and Run 1). At t = 0 min, the GF particles have d_{50} = 19.65 ± 1.17 μm and d_{90} = 50.88 ± 6.33 μm.

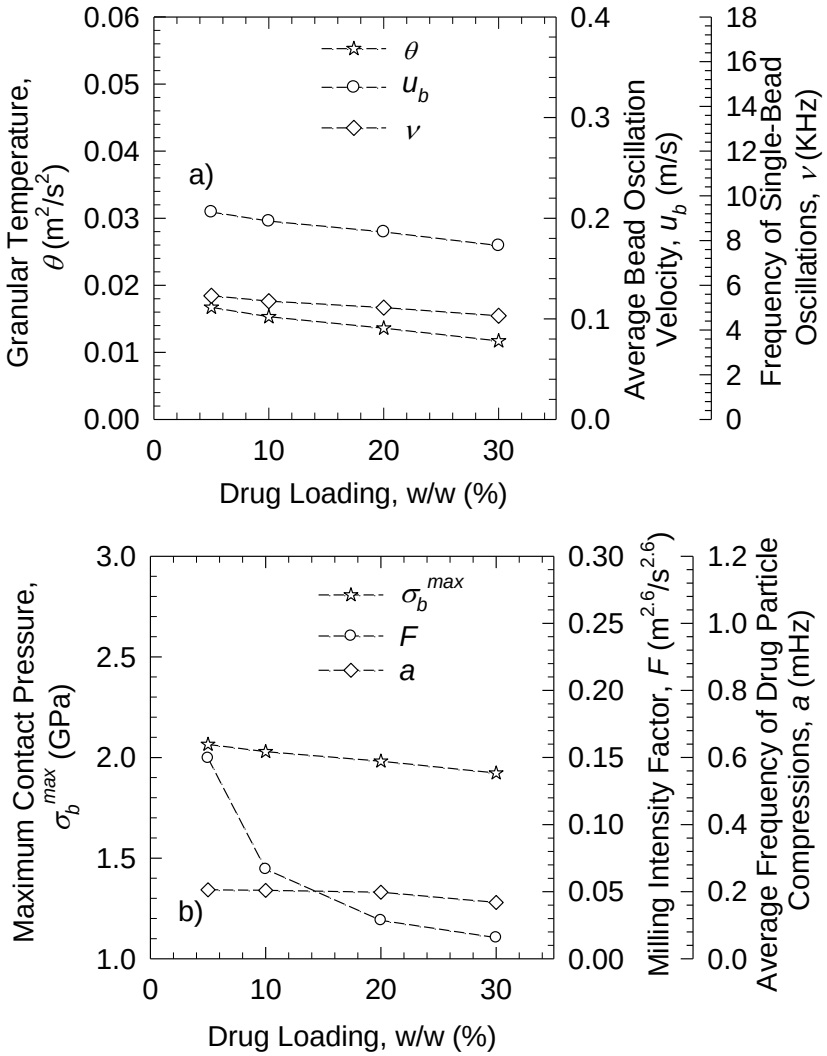

Figure 4.7 Effects of the drug loading on (a) the granular temperature, the average bead oscillation velocity, and the frequency of single-bead oscillations, (b) the maximum contact pressure, the milling intensity factor, and the average frequency of drug particle compressions (Runs 8–10 and Run 1).

An increase in the drug loading from 5% to 30% led to a slight, almost linear decrease in all microhydrodynamic parameters except the milling intensity factor F (see Figure 4.7), which exhibited a sharper decrease. While σ_b^{max} did not decrease significantly upon an increase in drug loading, the increase in the number of drug particles that are captured by the colliding beads caused a decrease in the compressive force applied on each drug particle, which in turn led to a stronger decrease in F. It is

worth noting that both the stirrer power and the suspension viscosity increased (Table 4.4), due to the presence of larger number of drug particles in the milled suspension. However, these changes counteracted each other and led only to a slight reduction in most hydrodynamic parameters except the milling intensity factor.

4.3.3 A Unified Correlation for the Breakage Kinetics–Microhydrodynamics

It is important to determine if a single microhydrodynamic parameter can explain the impact of all process parameters on the overall breakage rate, which is quantified by the characteristic time constant τ_p. The specific energy P_s is defined as the mechanical energy spent per unit mass of the drug particles and used in the milling literature for process design and scale-up purposes (Kawatra, 2006):

$$P_s = P_w V_m / Q \rho_p \tag{4.3}$$

As a fundamental microhydrodynamic parameter, the milling intensity factor F appears to explain the impact of individual process parameters on the breakage rate directly. In addition, P_w was considered to determine if the stirrer power plays a direct role in the breakage kinetics.

Figure 4.8 exhibits considerable scatter when τ_p is plotted against P_s and especially P_w. As a result, it was not possible to correlate τ_p to P_s or P_w using any of the linear or nonlinear regression models in SigmaPlot's (Version 11) comprehensive library of models. To be precise, a statistically significant model with statistically significant parameters could not be generated; R^2 was less than 0.80 and p-values were greater than 0.05 in all cases. On the other hand, the plot of τ_p vs. F showed relatively small scatter and the three-parameter exponential decay model

$$\tau_p = A_1 + A_2 \exp(-A_3 F) \tag{4.4}$$

fitted the data very well, as indicated by R^2 = 0.96, SSR = 2.387 min^2, and a standard error of the estimate of 0.584 min.

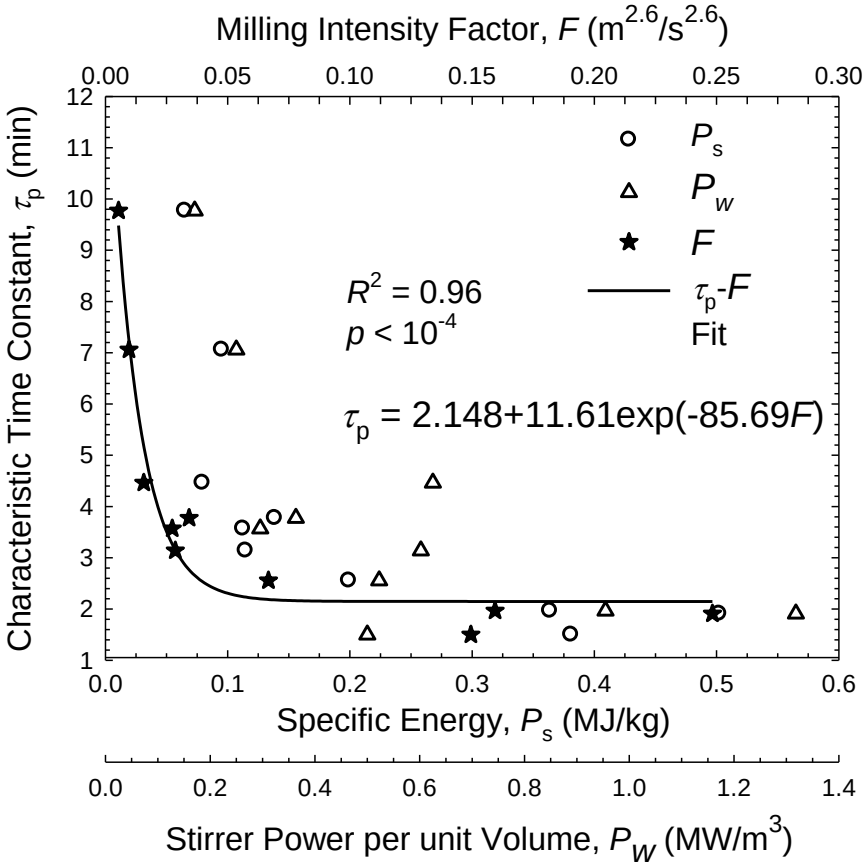

Figure 4.8 Scatter plots for the characteristic time constant versus the specific energy, the milling intensity factor, and the stirrer power per unit volume. Fit: an exponential decay correlation.

Both the model and its parameters were statistically significant with p-values < 0.05; the model parameters exhibited acceptably low COV values: 13.2%, 12.2%, and 18.1% for A_1, A_2, and A_3, respectively. The empirical model approaches a plateau above an F value of about 0.07 m$^{2.6}$/s$^{2.6}$, confirming that above a certain milling intensity, the breakage rate will not be affected significantly by F, which has already been elaborated in Sections 4.3.2.1 and 4.3.2.2. A caveat to the correlation in Figure 4.8 is strictly valid for

griseofulvin particles milled with 430 μm zirconia beads, signifying its descriptive nature.

Nonetheless, to the best knowledge of the author, no such simple three-parameter correlation, which connects breakage kinetics to a single microhydrodynamic parameter (F here) lumping three different process parameters, exists in the literature. It is expected that use of different drugs and beads could lead to a similar type of correlation with different A_1, A_2, and A_3. To develop relationships between the breakage kinetics of different drugs and their mechanical properties, it would be best to work with Π instead of F in Eq. (4.4). These aspects will be considered in a future study.

4.3.4 Implications for Process Design and Optimization

The effects of the process parameters on the specific energy P_s, the milling intensity factor F, and the stirrer power per unit volume P_w were illustrated in Figure 4.9. An increase in either the stirrer tip speed or the bead concentration led to an increase in P_s, F, and P_w, whereas an increase in the drug loading led to a decrease in P_s and F but an increase in P_w. The analysis of the data illustrated in Figures 4.9 and 4.10 suggests that a wet media milling process should operate at the highest F, which will increase the breakage rate and minimize the milling time required for desired product fineness (d_{50} or d_{90}). For the range of processing parameters considered, the mill should be operated at the highest possible stirrer tip speed (14.7 m/s) and the highest beads loading (0.572 or 93.8 vol.% of the milling chamber) provided that the product contamination due to bead wear is acceptably low (not studied here) and the heat dissipation can be controlled via effective cooling. Owing to the plateau observed for the region $F \geq 0.07$ in Figure 4.8, the mill could be operated at a lower tip speed (11.7 m/s) and bead loading (0.388) than the

above-mentioned values to minimize potential media contamination and to control the temperature rise reliably, while still ensuring fast particle breakage.

For a given batch size and desired end point particle size, selecting a drug loading level that minimizes the overall process cycle time seems to be a complex task. On one hand, Figure 4.6b suggests that the mill should be loaded with 5% drug to ensure the highest breakage rate (lowest τ_p) and shortest milling time as compared with 10%, 20%, and 30% drug loading cases. On the other hand, engineers/formulators must consider the fact that the negative effect of an increase in τ_p can be compensated by the positive impact of having more drug processed per batch at higher drug loadings: e.g. twice at 10% as compared with 5%. Note that τ_p increased with an in drug loading: 1.50 min, 2.56 min, 3.14 min, and 4.46 min for the 5%, 10%, 20%, and 30% drug loadings, respectively. Similarly, the times to produce suspensions with a median size of 400 nm and 300 nm, which are some potential end points in industrial scale milling operations, were calculated by Hermite interpolation of the data in Figure 4.6a. They were 3.19 min and 7.74 min, 5.98 min and 8.41 min, 7.70 min and 13.7 min, and 10.6 min and 18.7 min for the 5%, 10%, 20%, and 30% drug loadings, respectively.

A conjecture from these three different measures can be made that although the breakage kinetics slowed down or τ_p increased upon an increase in the drug loading, the time it takes to mill per mass of the drug for a desired median size decreased even more significantly, signifying enhanced operational efficiency and a decrease in the overall process cycle time. Hence, for a given mass of drug particles to be milled, engineers should prefer a single milling batch with 20% or 30% drug loading as opposed to two or three batches at 10% drug loading.

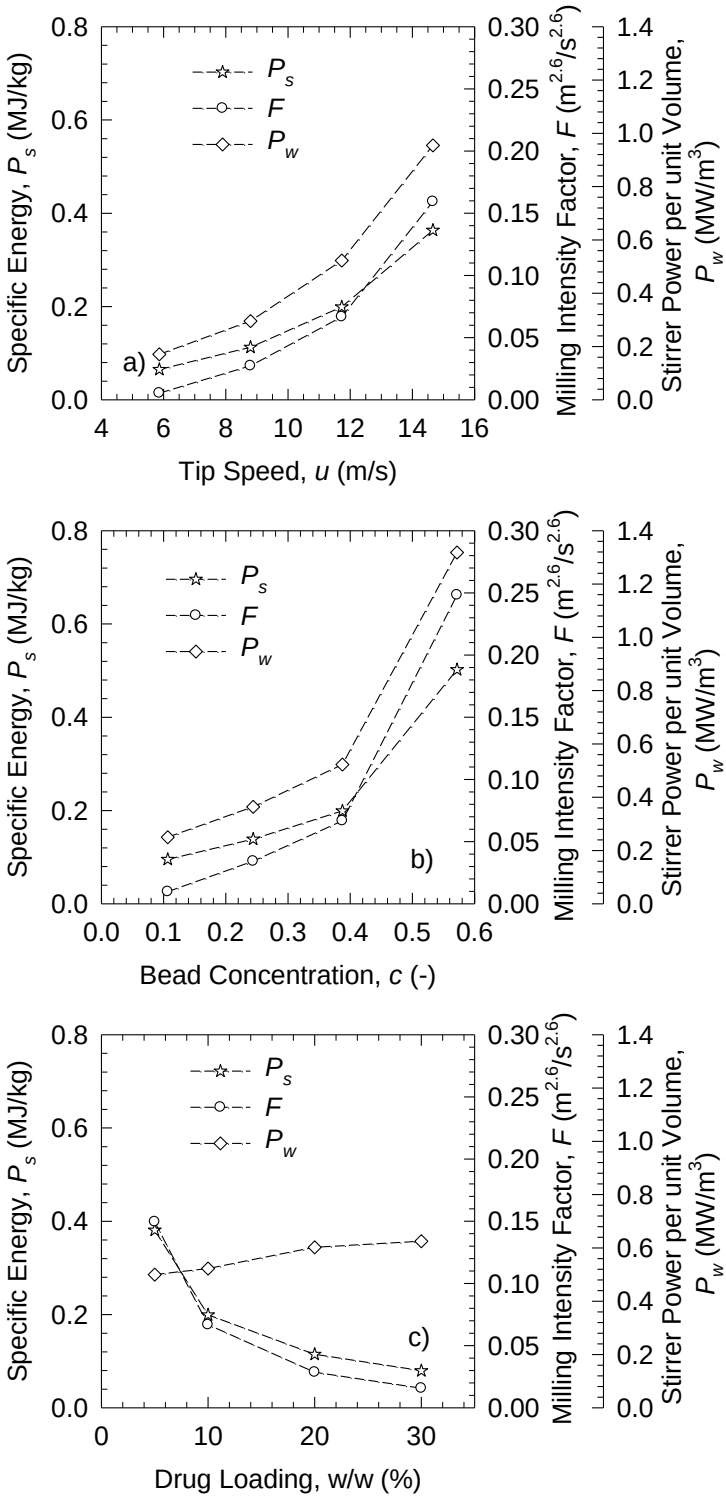

Figure 4.9 The specific energy, the milling intensity factor, and the stirrer power per unit volume at various (a) stirrer speeds (Runs 1–4), (b) bead concentrations (Runs 5–7 and Run 1), (c) drug loadings (Runs 8–10 and Run 1).

Considering the suspension preparation/unloading/cleaning times in-between the multiple batches with 10% drug loading along with the above breakage kinetics arguments, milling at a higher drug loading appears to be operationally more efficient, with appreciable reduction in the overall process cycle time. Depending on the final application of the milled suspension and its properties (viscosity, physical stability, etc.), the high drug-loaded suspensions may either be diluted or used as-is.

It is important to investigate if the milling intensity factor can be correlated to the energy consumption. Figure 4.10 presents scatter plots for the milling intensity factor versus the specific energy, and the stirrer power per unit volume. A statistically significant correlation between the milling intensity factor F and specific energy P_s in the form of a linear function is found. Considerable scatter is also seen when F is plotted against P_w. Therefore, it was not possible to correlate F to P_w using any of the linear or nonlinear regression models in SigmaPlot's (Version 11) comprehensive library of models. Despite the correlation between F and P_w, P_s was not able to predict the breakage rate (Figure 4.8) due to scatter in both the time constant and specific energy measurements. Moreover, F is a fundamental microhydrodynamic parameter which accounts for the physics of bead-bead collisions, whereas P_s cannot yield such fundamental information.

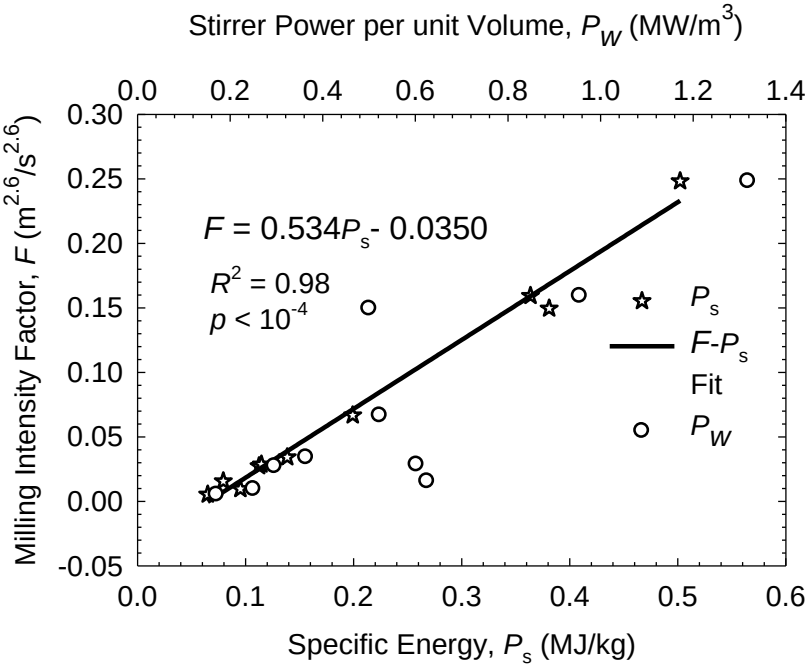

Figure 4.10 Scatter plots for the milling intensity factor versus the specific energy, and the stirrer power per unit volume. Fit: a linear correlation.

4.4 Summary and Conclusions

Significant advances have been made, for about two decades, in preparation and stabilization of drug nanoparticle suspensions via wet stirred media milling. Nevertheless, a fundamental understanding of the impact of process parameters on the breakage kinetics in terms of the underlying microhydrodynamics in the mills has not been developed. Considering the importance of nanoparticle production for the enhancement of dissolution rate/bioavailability and the relatively expensive and energy-intensive nature of the wet stirred media milling, it is of utmost importance to study the breakage kinetics, which determines the process cycle time and production rates for a desired fineness of the drug product. With the goal of developing a fundamental understanding and gaining physical insight, in this chapter, an elucidation of the impact of the stirrer

speed, the bead concentration, and the drug loading on the breakage rate of griseofulvin (GF) via a combined microhydrodynamics–breakage kinetics analysis was performed.

The experiments have shown that an increase in either the stirrer speed or the bead concentration led to an increase in the specific energy and the milling intensity factor, consequently faster breakage; whereas an increase in the drug loading led to a decrease in these parameters and consequently slower breakage. All microhydrodynamic parameters provided significant physical insight while only the milling intensity factor was capable of explaining the influence of all parameters uniquely through its strong correlation with the process time constant. Besides guiding process optimization and providing fundamental physical insight, the theoretical analysis has also rationalized the use of a single highly drug-loaded batch (20% or higher) over multiple dilute batches. This study has opened a new path to the investigation/design/optimization of the wet media milling process in terms of microhydrodynamic parameters as they are affected by the formulation–design–operating parameters. It will help formulators/engineers to streamline the development of nanosuspension formulations and to select the operating mill parameters in the context of a theoretical framework. Future studies will focus on the influence of bead size/type, suspension flow rate, batch size, and mechanical properties of different drugs and beads on the breakage kinetics and microhydrodynamics.

CHAPTER 5

FAST PRODUCTION OF DENSE, STABLE DRUG SUSPENSIONS WITH SUB - 100 NM PARTICLES AND MININMAL MEDIA CONTAMINATION VIA INTENSIFIED WET STIRRED MEDIA MILLING

5.1 Introduction

In recent years, wet stirred media milling (WSMM) technique has received much attention in producing fine drug particles in suspension form, because of its capability in producing a narrow particle size distribution, high drug loading, organic solvent-free processing, batch and continuous operation capability, and ease of scale up (Bilgili and Afolabi, 2012; Bruno et al., 1996; Merisko-Liversidge et al., 2003). In this method of preparing the drug nanoparticles, micron-sized drug particles and media (beads) in an aqueous solution of stabilizers is fed into the mill at a control flow rate, mixed by a rotor (mill stirrer) at very high speeds. Repeated stressing of the micron-sized drug particles that are captured between the colliding beads causes size reduction down to the nanometer size range provided milling is continued for a sufficient time (Ghosh et al., 2011; Verma et al., 2009).

Although several commercial nanoparticulate oral and parenteral drug products are being produced via WSSM, the technique is generally considered as time-consuming, costly, and energy-intensive (Kawatra, 2006). Even at the bench scale milling operations, drug nanoparticle suspension quantities in the order of ~10 g are produced after several hours to a few days of milling, leading to increased energy consumption. Perhaps the lack of fundamental understanding of the impact of process parameters and/or heavy reliance on purely empirical approaches make the process energy intensive and time consuming (Afolabi et al., 2013). In fact, the majority of the wet media milling studies have focused

mainly on optimization of various stabilizers, and physical stability of the milled drug suspensions (Kesisoglou et al., 2007; Lee et al., 2008; Peltonen and Hirvonen, 2008; Van Eerdenbrugh, 2008), and no explicit information on reducing the mill time, energy consumption, and bead wear is given. It is known that faster particle breakage rate leads to reduction in both milling time and energy consumption, and can be achieved by right selection of mill operating parameters such as bead size, bead load, rotor speed, and suspension flow rate. Influence of these parameters on final drug particle size has been studied previously through experiments (Cerdeira et al., 2011a; Ghosh et al., 2011, 2013) and statistical based approach (Singare et al., 2010; Singh et al., 2011). However, the influence of these parameters at intense conditions on breakage kinetics leading to the faster preparation of fine drug nanoparticles is not addressed. Therefore, a detailed strategy or methodology for combining different mill process parameters has to be developed which could lead to an intensified process for the faster production of fine drug nanoparticles with reduced specific energy consumption and bead wear.

In pharmaceutical applications, the demand for using drug nanoparticles with size as low as possible is increasing steadily, as fine drug nanoparticles offers a much faster dissolution rate due to their high surface area to volume ratio, and also result in rapid onset of therapeutic action (Merisko-Liversidge et al., 2011; Müller and Peters, 1998; Shegokar and Müller, 2008). Most importantly, drug nanoparticles with size < 100 nm renders feasible and efficient sterile filtration of aqueous drug nanosuspensions, and allows higher loading for reduced injection volume in parenteral dosage forms (Baert et al., 2009; Xiong et al., 2008). In addition to the nanosuspension dosage form, nanocomposite microparticles made of very small size drug nanoparticles offer rapid

redispersion of particles at an increase drug loading in a given mass of dosage (Bhakay et al., 2013). Therefore, it is important to prepare drug nanosuspensions with size as small as possible (< 100 nm) to achieve enhanced efficacy in various pharmaceutical applications. By varying the process parameters, several researchers have prepared inorganic nanoparticles in the size range of 10–100 nm using WSSM technique (Patel et al., 2012; Stenger et al., 2005; Wang and Forssberg et al., 2006). However, an investigation on the effect of process parameters for the preparation of drug nanoparticles having sub-100 nm has not been attempted so far. Table 1 shows the list of drugs milled in WSMM with their initial drug load, initial particle size, batch volume and the final particle size. To the best of our knowledge, only using smaller initial drug particle size and at low batch volume, the drug nanoparticles with a typical median size of 136 nm and above have been produced via WSMM. It is to be noted that the preparation of drug particles with < 100 nm size is a challenging task, especially if the mill is desired to operate with the large initial drug particle size, high batch volume (> 200 ml at the bench scale), and high drug load > 10 % (w/w).

Although the preparation sub-100 nm drug particle at a shorter milling time with reduced energy consumption is of great interest, the drug product contamination introduced by bead wear at intense process conditions is also not known. All of these aspects can be understood by investigating the impact of mill operating parameters on particle breakage rate and the energy dissipation rate during the deformation of the particles. This can be elucidated by studying the fluctuating motion of beads in sheared suspensions i.e., microhydrodynamics. Eskin et al., (2005a,b) developed a comprehensive microhydrodynamic model describing the dynamics of the milling beads and their

interactions with the particles in a dense slurry flow. Recently, Bilgili and Afolabi (2012) modified this model to understand the viscous dampening effect caused by the use of polymeric stabilizers in WSMM. The model consists of several intrinsic bead parameters and the magnitude of change in parameter values at different mill operating conditions enable us to select right process parameters.

The preceding Chapters 3 and 4 sheds more light on the impact of formulation and processing parameters on drug nanoparticle suspension produced via WSMM. A minimum stabilizer-to-drug ratio was attained and individual process parameter was optimized. The major objective of this chapter is to elucidate a combined experimental and theoretical approach to achieve faster production of sub-100 nm BCS class II drugs having reduced specific energy consumption with minimal bead wear contamination. In the experiments, the effects of media (bead) size on the energy consumption, bear wear and breakage kinetics of two model poorly water-soluble drugs, griseofulvin (GF) and naproxen (NAP) were studied. Then, this baseline process conditions with the optimal bead size was intensified by increasing the rotor tip speed, bead load, and suspension flow rate systematically, as guided by a microhydrodynamic model of the process. The intensified process led to the production of sub-100 nm particles within 30 min of milling with significant reduction in bead wear. Similarly, milling of NAP also led to sub-100 nm particles within 30 min. The use of small beads has enabled us to intensify the process, increase the particle breakage rate (shorter cycle time), and reduce the energy consumption with minimal bead wear contamination.

5.2 Experimental

5.2.1 Materials

GF, (EP/BP grade) was purchased from Letco Medical (Decatur, AL, USA). Naproxen, NAP, (USP grade, solubility in water: 15.9 mg/l) was purchased from Medisca (Plattsburgh, NY, USA). The d_{10} (10% passing size), d_{50} (median or 50% passing size) and d_{90} (90% passing size) values of as-received GF and NAP particles measured by laser diffraction device (LS 13-320, Coulter Beckman, Brea, CA) were 5.0 µm, 21.85 µm, 57.77 µm, and 6.93 µm, 16.60 µm, 77.12 µm respectively. Hydroxypropyl methyl cellulose (HPMC, Methocel- E3), a neutral polymeric stabilizer, was purchased from Dow Chemical (Midland, MI, USA). Sodium dodecyl sulfate (SDS), an anionic stabilizer, and nitric acid was purchased from Sigma Aldrich (Bellefonte, PA, USA). Wear resistant yttrium- stabilized zirconia milling media (YSZ) with a nominal size of 100, 200, 400 and 800 µm was purchased from Saint Gobain ZirPro (Zirmil Y, Mountainside, NJ, USA), were used as milling media. The reported density of milling media was 6000 kg/m^3, consists of 93 % ZrO_2 and 5 % Y_2O_3 . De-ionized water was used in all experiments.

Table 5.1 Literature Summary of Drug Particles Prepared via Wet Stirred Media Milling with Median Particle Size < 200 nm

Drug	Initial median particle size (μm)	Drug loading (% w/w)	Batch volume (ml)	Process time	Final median drug particle size (nm)	Reference
Etravirine	11	20	300	60 min	140	Cerdeira et al., 2011
Fenofibrate	16	10	200	120 min	150	Knieke et al., 2013
Griseofulvin	22	10	200	64 min	161	Bhakay et. al. 2013
Itraconazole	20	20	300	60 min	136	Cerdeira et al., 2013
Miconazole	20	20	300	60 min	140	Cerdeira et al., 2013
Naproxen	13	10	490	64 min	143	Monteiro et al., 2013
Undisclosed	15-20	5	NM	6 h	200	Bose et al., 2012

NM: not mentioned

5.2.2 Methods

5.2.2.1 Wet Stirred Media Milling. The milling procedure followed in the present work is the same as reported in Chapter 3 and Chapter 4. The schematic of the mill can be seen in Figure 3.1. The mill chamber has a volume (V_m) of 80 ml lined with zirconia, connected to a rotating shaft (diameter, D = 7 cm). A stainless steel screen (Netzsch, Exton, PA, USA) was used to restrict the flow of milling media (beads) out of the chamber. Screens having different opening (pore) size was used for varying bead size, and a ratio of 1:2 screen opening size to bead size was maintained in all experiments. 200 ml of aqueous suspension containing 10 % w/w (with respect to water) drug along with stabilizers was initially added to the holding tank (500 ml) of mill, and the recirculation of suspension between holding tank and milling chamber was achieved at a controlled flow rate with use of peristaltic pump. A paddle mixer connected to the holding tank was operated continuously at 800 RPM to ensure the suspension homogeneity in the holding tank. The suspensions at several milling time points (4, 8, 16, 32, 64, 120, 180, 240, 300 and 360 min) were collected from the outlet of milling chamber, and used for particle size and morphology analysis. The final milled suspensions were stored in a refrigerator at 8 ^{o}C. Table 5.2 shows different milling conditions (Runs 1–9) followed in the present work, with respect to change in mill operating parameters such as bead size d_b, mill tip speed u, bead volumetric concentration c, and suspension flow rate Q.

Prior to milling, the as received drugs were prepared in the form of suspensions along with stabilizers with use of low shear laboratory stirrer [Fisher Scientific (Catalog no. 14–503), Pittsburgh, PA, USA]. The procedure was followed as reported in Chapter 3

and Chapter 4. Stabilizer solution was prepared by initially adding 0.4 g of SDS to 200 ml de-ionized water, followed by gradual addition of 5 g of HPMC-E3 within 30 min under stirring (300 rpm).

Table 5.2 Processing Conditions used in the Wet Milling Experiments (Runs 1–9) at Drug Load: 10%[a], Batch Size: 200 Ml[b] and HPMC/SDS Concentration: 2.5%/0.2%

Run No.	Drug	Bead Size (μm)	Stirrer Speed (rpm, m/s)	Bead Load, Concentration (gm), (*c*)	Suspension Flow rate (mL/min)
1	GF	800	3200, 11.7	195.7, 0.408	126
2	GF	400	3200, 11.7	195.7, 0.408	126
3	GF	200	3200, 11.7	195.7, 0.408	126
4	GF	100	3200, 11.7	195.7, 0.408	126
5	GF	100	4000, 14.7	195.7, 0.408	126
6	GF	100	4000, 14.7	260.7, 0.543	126
7	GF	100	4000, 14.7	260.7, 0.543	343
8	NAP	100	3200, 11.7	195.7, 0.408	126
9	NAP	100	4000, 14.7	260.7, 0.543	343

[a] % w/w with respect to de-ionized water.
[b] de-ionized water.

The resultant solution was further stirred for 10 min and left at rest until a clear solution was obtained. To this stabilizer solution, 20 g of as received drug particles was added gradually within 30 min of stirring, and kept in refrigerator (8 ^{o}C) for 90 min. The prepared final suspension has 10 % w/w drug, 2.5% w/w HPMC, and 0.2% w/w SDS (all with respect to water). The particle size of drug in pre-suspension form was measured, and referred as 0^{th} minute particle size. At the end of milling process, the cumulative energy consumption (E) of the slurry (beads, drug, stabilizer and solvent) was directly recorded from the mill control panel. From this, the average stirrer power applied per unit volume of slurry P_w was calculated as

$$P_w = E/\Delta t V_m \quad (5.1)$$

where, Δt is the cumulative milling time i.e., final time point of milling process. The specific energy consumption, E^*, which is the energy spent per unit mass of drug in mill chamber was also calculated from E, and is given as

$$E^* = E/m_s \tag{5.2}$$

where m_s is the mass of the drug in the mill chamber.

Recall the energy dissipation rate Π (see Chapter 2.4) can be decompose into a material-dependent factor λ and a process-dependent factor, F, which is referred to as the milling intensity factor, defined as follows:

$$\lambda = 2.23 \frac{\rho_b^{4/5} R_p}{\pi^{5/2} \sigma_y} \left(\frac{Y_b}{1-\eta_b^2} \right)^{18/15} \left(\frac{Y^*}{Y_p} \right)^{\gamma} \tag{5.3}$$

$$F = \frac{c^2(2-c)}{(1-c)^3} \frac{1}{\varepsilon R_b^{\,2}} \theta^{13/10} \tag{5.4}$$

Where F represent the milling intensity factor with the use of the same drug, same bead material, but different bead sizes. Upon a change in each process parameter, a possible increase/decrease in F corresponds to a proportional increase/decrease in Π in some time- and space-averaged sense because well-mixedness and average power consumption during the milling are considered, and λ is taken as a constant for a given pair of drug–bead materials. One can then refer to either F or Π while reporting the impact of the process parameters. All microhydrodynamic parameters calculated are presented in Table 5.3.

5.2.2.2 Characterization Techniques. Laser diffraction (LD) was used to determine the particle size of milled suspensions with median particle size d_{50} above 200 nm. The measurements were performed in LS 13-320 Beckman Coulter instrument (Brea,

CA) as reported in Chapter 3 and Chapter 4. A refractive index (RI) of 1.65, 1.41 and 1.33 were used for GF, NAP and water (measurement medium) respectively. All the measurements were performed at 25 °C, and the particle size was measured at least thrice and the average values were reported. Milled suspensions with d_{50} less than 200 nm were investigated by dynamic light scattering (DLS) using Delsa Nano C Particle analyzer (Beckman coulter, Brea, CA). The milled suspension was diluted with de-ionized water, and the median particle size, d_{50} based on intensity weighted distribution was recorded along with polydispersity index (PI). All the measurements were performed at 25 °C, and the particle size was measured at least thrice and the average values were reported. The combined use of LD and DLS to analyze the particle size data have been previously reported by Knieke et al. (2009) and Schubert et al. (2006) and similar procedure is followed.

Particle size and morphology of the as-received and milled drug particles were examined using LEO 1530 SVMP (Carl Zeiss, Inc., Peabody, MA, USA) scanning electron microscopy (SEM). For this analysis, 0.5 ml of the milled suspension was diluted with 30 ml de-ionized water, and a drop was placed on a silicon chip (Ted Pella, Inc., Redding, CA, USA). The chip was mounted on a carbon specimen holder, followed by drying in dessicator for 2 h. All the samples were then sputter coated with carbon and observed in SEM. X-ray Powder Diffraction (P-XRD) technique was used to analyze the crystallinity of the as-received and milled GF particles. The suspension sample was dried at 40 ºC for overnight in a convective drier (Gallenkamp, Netherlands), and the particles were finely grounded with the help of a mortar and pestle. As-received drug powder was directly used for analysis. The dry powder was packed in an aluminum holder and

mounted on a Empyrean series 2 X-ray diffractometer (PANalytical, Westborough, MA, USA), provided with Cu K_α radiation (λ = 1.5406 Å). The samples were scanned for 2θ ranging from 5^o to 40^o at a scan rate of 0.165 s^{-1}.

The apparent shear viscosities μ_L of the milled suspensions were measured at 25 ± 0.5 ^{o}C using R/S plus Brookfield rheometer (Brookfield Engineering, Middleboro, MA, USA) as reported in Chapter 3 and Chapter 4. The density of the milled suspension was performed as reported in Chapter 3 and Chapter 4. Bead wear contaminants (zirconium and yttrium) levels in the final milled suspensions were analyzed by inductive coupled plasma mass spectrometry (ICP-MS) according to European Pharmacopeia 6.0 §2.2.58 with a limit of quantification of 0.1 µg/g. For this, the milled suspension sample was dried at 40 ºC for 24 h in a convective drier, and the dried particles were finely grounded with the help of a mortar and pestle. Then, 1 g of dried powder was added to 40 ml of water, followed by addition of 40 ml of 65 % nitric acid. The mixture was then heated up until a clear solution was observed. The resultant clear solution was cooled down to room temperature and diluted further with water for ICP-MS analysis. The measurements were performed thrice and the average value was reported.

5.3 Results and Discussion

5.3.1 Effect of Bead Size on the Temporal Evolution of GF Particles

Proper selection of bead size can help to improve the efficiency of wet media milling operation by producing fine size nanoparticles with low energy consumption. In this chapter, the effect of bead size on the preparation of GF particles was first studied by milling the as-received GF particles with varying bead size of 800, 400, 200 and 100 µm

(refer Table 5.2, Runs 1–4). Yttrium stabilized zirconia (YSZ) bead were selected for this study as they tend to exhibit low level contamination of the final drug product due to its high hardness of 19 GPa and a reduced modulus of about 218 GPa (Lian et al., 2007). The mill tip speed u, bead volumetric concentration c, and suspension flow rate Q were kept constant at 11.7 m/s, 0.4 and 126 ml/min, respectively (baseline process condition). Figure 5.1 shows the temporal evolution of the median size d_{50} of the GF particles. The median size d_{50} decreased exponentially and slowly approached an asymptote near 360 min of milling, illustrating that the size reduction slowed down during milling monotonically. After 360 min milling, the median sizes attained with 800, 400, 200 and 100 μm beads were 176, 140, 124 and 98 nm, respectively. The corresponding d_{10} and d_{90} values are given in Table 5.3. The poly dispersity index, PI of all the measured particles was less than 0.2. Thus, the use of smallest beads (100 μm) resulted in 98 nm median size, implying that sub-100 nm particles can be produced with use of small beads in wet stirred media milling provided the process can be intensified (see Section 5.3.2).

To establish the reproducibility of the milling process, repeat experiments of Runs 1–4 were performed. The d_{50} and d_{90} sizes attained with 800, 400, 200 and 100 μm beads were 174 and 295 nm, 144 and 261 nm, 121 and 245 nm, and 99 and 210 nm, respectively. The (absolute) percent deviations from the d_{50} and d_{90} values were negligibly small: 1.14 and 0.34%, 2.86 and 1.56%, 2.42 and 0.81%, and 1.02 and 1.87%, respectively. Hence, milling process and the particle size measurements were fairly reproducible. Good reproducibility has also been established in our recent work on wet stirred media milling of several other poorly water-soluble drugs such as azodicarbonamide, fenofibrate, griseofulvin, and naproxen with HPC (hydroxypropyl

cellulose) or HPMC in the presence of SDS (Bhakay et al., 2013; Bilgili and Afolabi, 2012; Knieke et al., 2013; Monteiro et al., 2013; Sievens-Figueroa et al., 2012).

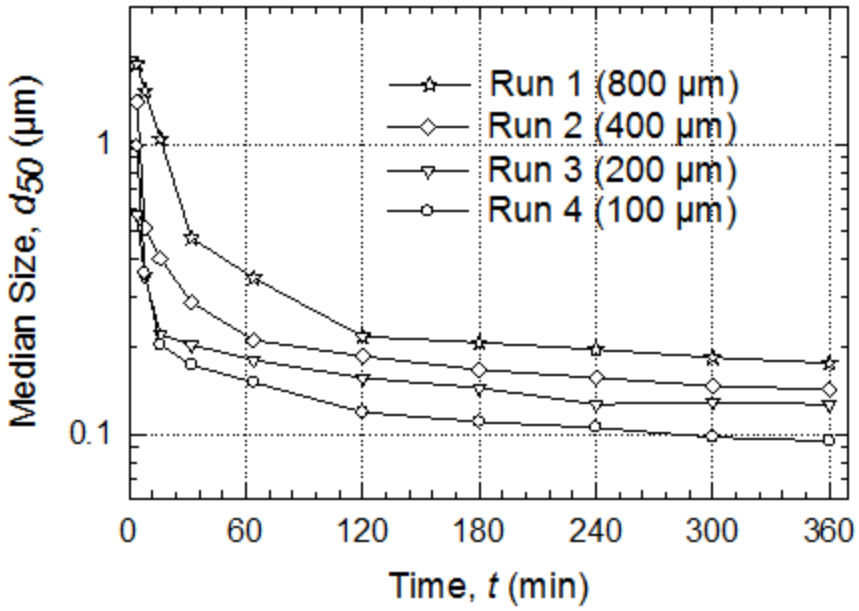

Figure 5.1 Temporal evolution of the median size d_{50} of GF particles for Runs 1–4. Runs 1, 2, 3 and 4 refer to milling of GF with 800, 400, 200 and 100 μm YSZ beads respectively, at baseline mill conditions of mill tip speed u = 11.7 m/s, bead volumetric concentration c = 0.4 and suspension flow rate Q = 126 ml/min. At t = 0 min, the GF particles have d_{50} = 21.85 ± 1.25 μm and d_{90} = 57.77 ± 4.35 μm.

Table 5.3 Particle Size Statistics of the Suspensions for Runs 1–9 after Milling and After 7 Day Storage

Run No.	Milling Time (min)	After Milling d_{10} (nm), d_{50} (nm), d_{90} (nm)	7 day storage d_{10} (μm), d_{50} (nm), d_{90} (nm)
1	360	110, 176, 294	NM[a]
2	360	84, 140, 257	NM[a]
3	360	72, 124, 247	NM[a]
4	360	57, 98, 214	60, 101, 298
5	120	57, 95, 209	NM[a]
6	120	41, 85, 180	NM[a]
7	120	38, 83, 164	41, 90, 214
8	360	35, 87, 154	NM[a]
9	120	26, 82, 139	32, 95, 165

[a]NM: not measured.

Before delving into analyzing the results presented above, it is of utmost importance to establish the aggregation state of the milled suspension. In the present work, HPMC and SDS stabilizer combination was used for stabilization of GF particles based on a previous formulation optimization study, which showed an excellent stabilization for several BCS II drugs such as fenofibrate, naproxen, ibuprofen etc (Bilgili and Afolabi, 2012; Knieke et al., 2013; Monteiro, et al., 2013). Figure 5.2 shows the SEM images of 4, 32, 120, 240, and 360 min milled GF particles with 100 µm beads (Run 4), capturing the evolution of the particle size and morphology. GF particles got smaller and more spherical as milling progressed. The calculated average size for the 360 min milled particles (Figure 5.2f) from SEM was 90 nm, which is very close to the median particle size obtained from light scattering measurements technique. Image J software was used to count and compute the particle size from SEM image, and a total of 1450 particles were used for the particle size analysis. These findings suggest that even the suspension with the smallest particles (Run 4) is not significantly aggregated at the time scale of the milling process, and the electrosteric stabilization mechanism imparted by the HPMC–SDS combination was quite effective (Run 4).

Short term physical stability of Run 4, Run 7 and Run 9 milled suspensions were performed for a period of 7 days at 8 °C. Table 5.3 shows the particle size statistics of 7 day storage of the milled suspension. After 7 day storage, d_{50} and d_{90} of the milled suspensions did not change significantly; the suspensions were physically stable and remained colloidal mainly due to the synergistic stabilizing action of the HPMC–SDS combination. Long term physical stability of these suspensions was not investigated in the present study.

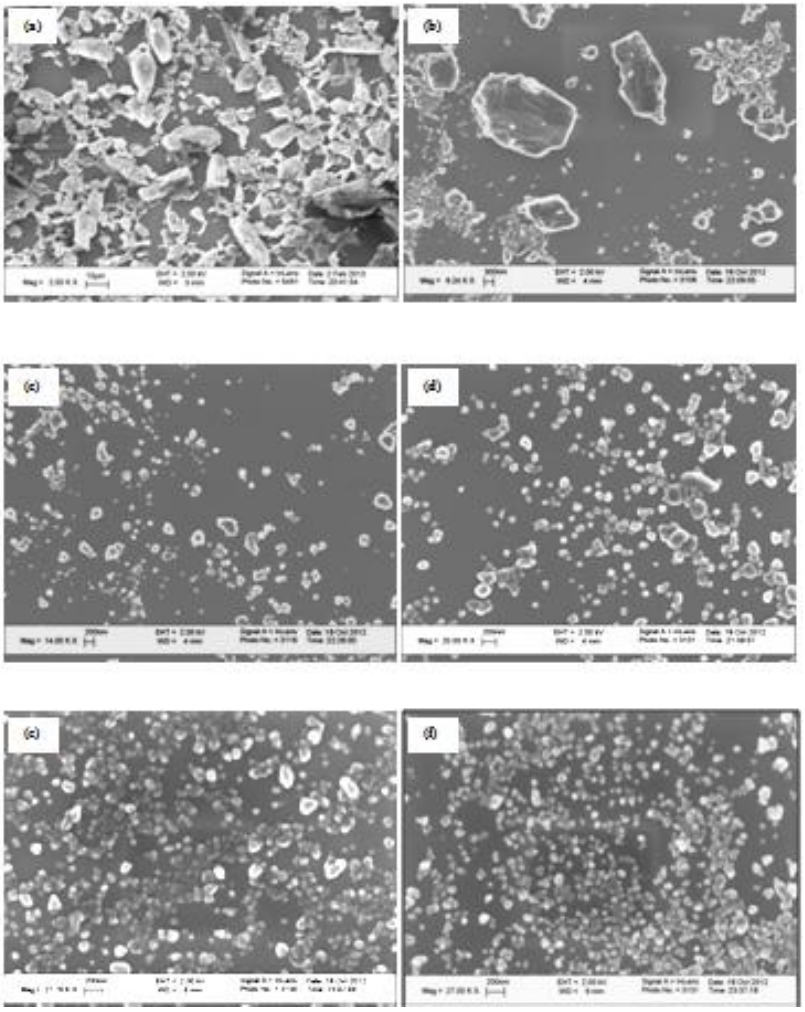

Figure 5.2 SEM images showing the evolution of GF particle size for Run 4: (a) as received, (b) 4 min, (c) 32 min, (d) 120 min, (e) 240 min, (f) 360 min of milling. Run 4 refers to the use of 100 μm YSZ beads at the baseline mill conditions (u = 11.7 m/s, c = 0.4 and Q = 126 ml/min). At t = 0 min, the GF particles have d_{50} = 21.85 ± 1.25 μm and d_{90} = 57.77 ± 4.35 μm.

In general, the observed slow-down of the size reduction during the milling (see Figure 5.1) may be explained mainly by particle breakage and aggregation mechanisms. Of course, as milling progressed long enough, aggregation rate may have increased upon production of finer (colloidal) drug particles, which could be a reason for the equilibrium (plateau), approached near 360 min. As the drug particle size decreases, number concentration in the suspension increases and the interparticle distance decreases, leading

to more frequent collisions and potentially higher aggregation rate (Bhakay et al., 2011; Sommer et al., 2006). The similarity of the primary particle sizes from the SEM image and the particle size measured by DLS suggests that particle breakage was the dominant mechanism and aggregation of the particles occurred at a smaller rate than the breakage in the presence of stabilizers during most of the milling process.

On the other hand, as milling progressed, finer particles were produced, which have a much lower specific breakage rate (breakage probability) than the coarser particles and thus are harder to break (Bilgili et al., 2004, 2006, 2008). In addition, smaller particles are more difficult to capture between the beads during the bead–bead collisions, further reducing the specific breakage rate. In fact, population balance models without any aggregation terms (Bilgili et al., 2007; Bilgili and Capece, 2011) were able to capture the sharp decrease in breakage rate even during the breakage of large microparticles. Considering that nanoparticles are even less likely to break than microparticles (Bilgili et al., 2004, 2006) a claim can be made that the approach to or attainment of a plateau size observed in Figure 5.1 is mainly explained by extremely the low breakage probability of nanoparticles and the lower capture efficiency of such particles, and, to a minor extent, by the aggregation of the produced nanoparticles in the presence of HPMC-SDS.

Figure 5.3 shows the XRD patterns of as-received and 360 min milled GF (Run 4). The peak positions of both patterns are identical, which confirms that the crystallinity of GF was not altered even after long hours of milling.

5.3.1.1 Quantification of Wear from Different Size Beads. Generation of wear from beads during milling leads to undesirable contamination of the milled drug product. To investigate the effect of bead size on bead wear contaminants levels [zirconium (Zr)

and yttrium (Y)], GF particles milled with use of 800 and 100 µm beads were analyzed using ICP-MS.

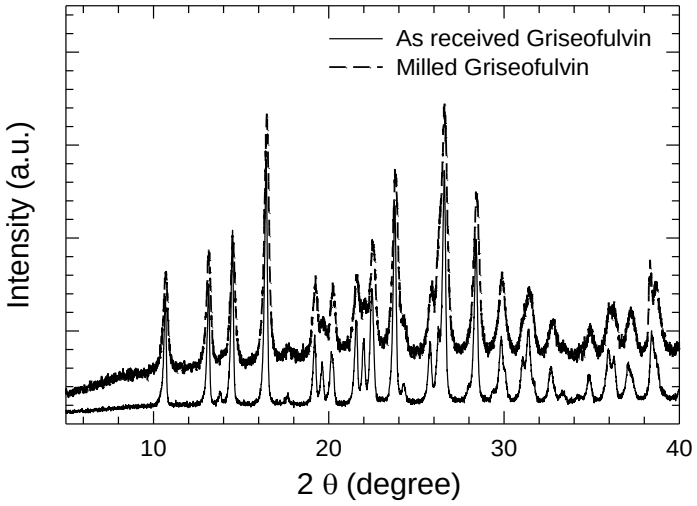

Figure 5.3 XRD patterns of as-received and 6 h milled GF particles (Run 4). Run 4 refers to the use of 100 µm YSZ beads at the baseline mill conditions (u = 11.7 m/s, c = 0.4 and Q = 126 ml/min).

As-received GF and stabilizers (HPMC and SDS) showed no elemental levels of Zr and Y. The elemental Zr and Y levels [mass of contaminant/mass of milled drug in dry form] of 6 h milled GF with 800 µm beads (Run1) and 100 µm beads (Run 4) were 607 ± 35 µg/g Zr, 32 ± 2 µg/g Y and 357 ± 7 µg/g Zr, 20 µg/g Y respectively. Approximately, 1.7 times reduction in both Zr and Y were observed by using 100 µm beads. Similarly, Juhnke et al., (2012) also observed reduced contaminant levels with use of smaller size beads. Hence, the use of smallest beads (100 µm) helps in achieving final drug product with low level contamination compared to the use of larger bead sizes.

5.3.1.2 Effects of Bead Size on Specific Energy Consumption and Applied Power.

Figure 5.4 shows the specific energy consumption E^* and the average power applied per unit volume of slurry P_w for varying bead sizes up to 360 min of milling. Both E^* and P_w were low for 100 µm beads and increases with increasing bead sizes. With this low

specific energy consumption, 100 µm beads were effective in producing the smallest GF particle size (refer to Figure 5.1), suggesting high grinding efficiency from an energetic perspective. From literature, it is understood that the specific energy consumption is proportional to the particle fineness (Breitung-Faes and Kwade, 2013). However, the particle size observed at higher specific energies is large (for 800 µm beads) as compared to small size particles obtained using 100 µm beads, accounting only low specific energy. Hence, a conclusion can be made that specific energy consumption is not a direct measure of particle fineness during wet media milling because only a small fraction of the specific energy is actually spent on deforming/breaking the drug particles, which is largely controlled by the microhydrodynamics.

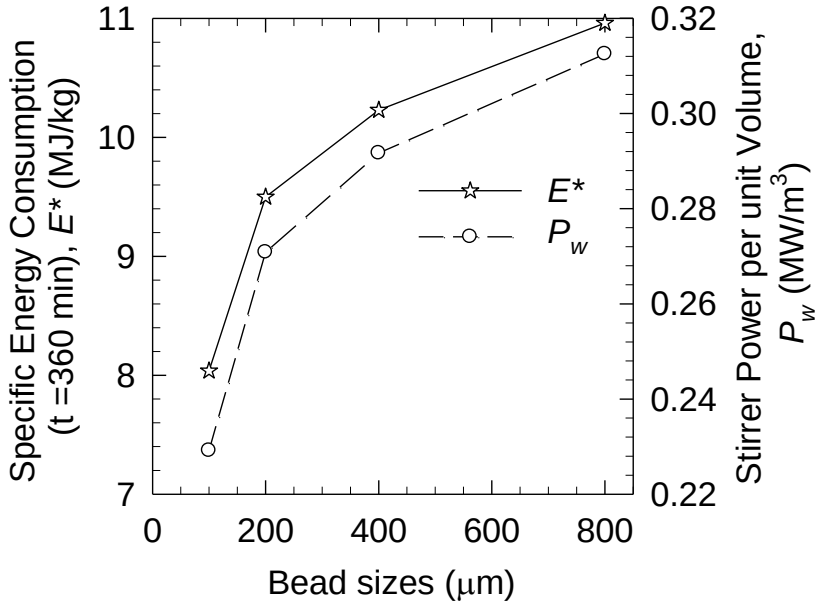

Figure 5.4 Specific energy consumption (E^*) and power applied by the mill stirrer per unit volume (P_w) for various bead sizes during 360 min of milling at the baseline mill conditions (u = 11.7 m/s, c = 0.4 and Q = 126 ml/min).

5.3.1.3 Microhydrodynamic Analysis of Beads. To develop a fundamental understanding of the bead size effect on the observed smallest GF particle size, reduced

energy consumption and reduced contaminant levels (bead wear), the microhydrodynamic parameters θ, ν, u_b, σ_b^{max}, F, and a were calculated and plotted as a function of bead size (see Figures 5.5a and 5.b). At constant mill tip speed, bead load and suspension flow rate, the fluctuating motion of beads (θ) becomes less vigorous with a decrease in bead size. This low fluctuating velocity led to low impact force and low compressive stresses (σ_b^{max}) i.e., a low stress intensity, for smaller beads (refer Figure 5.5b). On the other hand, the frequency of bead oscillations, ν (number of stressing events) and the average frequency of drug particle compression, a is seen higher with a decreasing bead size (Figure 5.5b). Smaller size beads constitute more in number causing a dramatic increase in the bead–bead collisions (increasing ν) which also allowed capturing of more drug particles (increasing a) due to less inter-bead distances. Thus, increase in ν led to faster breakage rate and increase in a helped in achieving sub-100 nm particles with the use of 100 µm smallest bead size. Also, a decrease in P_w is observed (see Figure 5.5b and Table 5.3) with decreasing bead size which is due to low u_b and θ. This resulted in reduced specific energy consumption for decreasing bead sizes. The observed reduced contaminants levels with the use smallest bead size (100 µm) can be explained in terms of compressive stresses (σ_b^{max}). Smaller beads undergo less impactful collision (lower σ_b^{max}) and results in less bead wear. On comparing the σ_b^{max} for 800 µm (Run 1) and 100 µm (Run 4) beads (Table 5.3), a 1.6 times reduction in σ_b^{max} was observed with use of 100 µm beads, yielding low levels of contamination. To better understand the impact of particle breakage rate of different size beads, the milling intensity factor F, which is proportional to the energy spent during the deformation of the drug particles per unit volume, was calculated using Eq.5.4. The milling intensity factor

F captures all of the above effects on the number and intensity of stressing events in a single parameter (Afolabi et al., 2013).

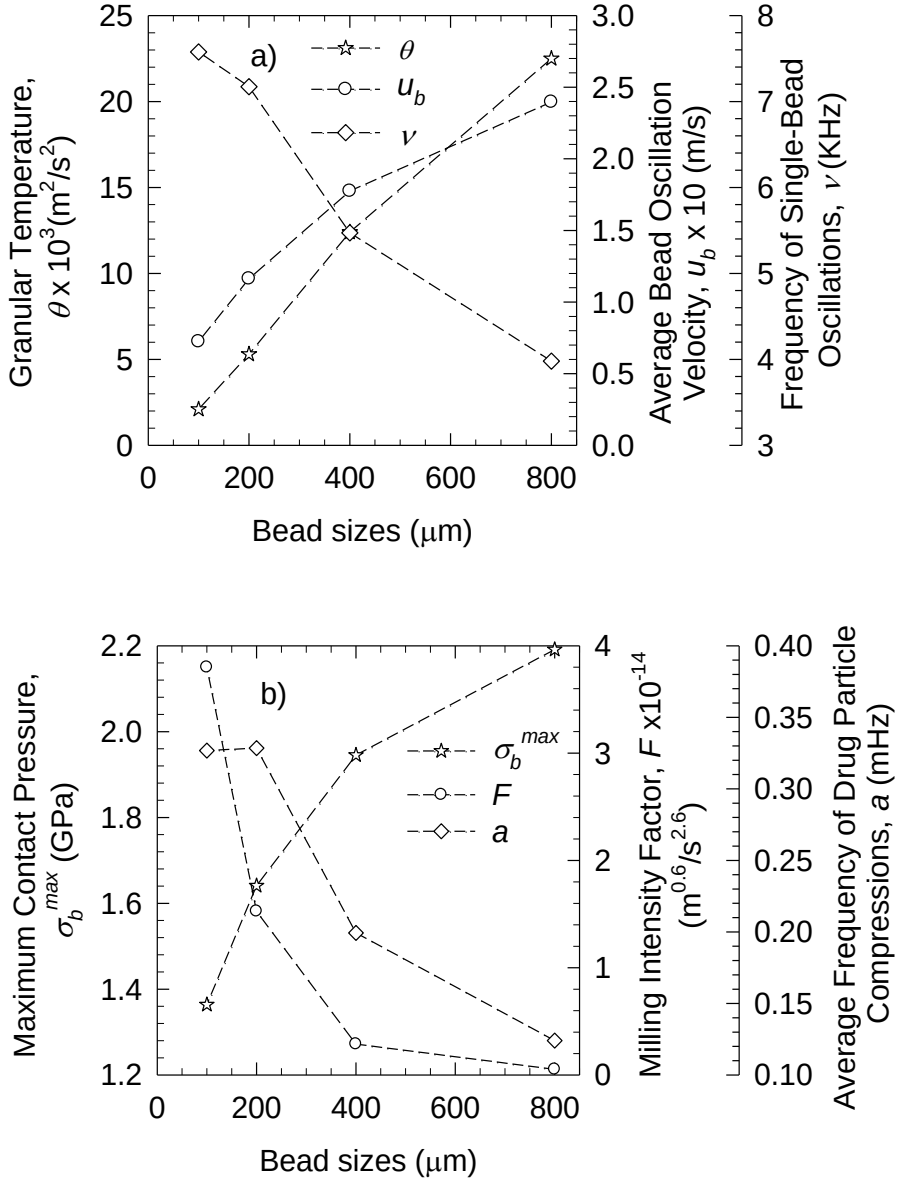

Figure 5.5 Effect of bead size on microhydrodynamic parameters: (a) granular temperature θ, average bead oscillation velocity u_b and frequency of single bead oscillation ν. (b) Maximum contact pressure σ_b^{max}, milling intensity factor F, and average frequency of drug particle compressions a. Milling conditions: u = 11.7 m/s, c = 0.4 and Q = 126 ml/min.

In Figure 5.5b, an increase in F is seen for decreasing bead sizes which implicates that smaller bead size possess faster breakage rate due to more number of stressing events. Thus, microhydrodynamic analysis justifies or rationalizes the use of smaller beads for finer particle preparation, and so 100 µm beads were further used in experiments.

In the planned experiments, an attempt to use less than 100 µm bead size resulted in inefficient operation of the mill. For example, when 50 µm beads were used for milling by having screen with pore size of 25 µm (recommended), the presence of large initial GF particle size (d_{90} = 57.77 µm) resulted in clogging of screen pores and the suspension was not even allowed to flow out of the milling chamber. Very small size beads are generally not employed for milling due to their difficulty in handling, high cost, and problems associated with separation of beads from the suspension (Haskell, 2003). Hence, due to practical limitation of the mill, 100 µm beads were used as the least size in this study.

5.3.2 An Intensified Process with 100 µm Beads

From the bead optimization study, it can be seen that 100 µm beads are effective in producing < 100 nm particles. However, the mill operating conditions employed in the bead optimization study took almost 360 min (6 h) to obtain GF particles with a median size of 98 nm (Run 4). The microhydrodynamics analysis suggests that the breakage rate of the GF particles was higher resulting in faster production of fine nanoparticles, when the milling intensity factor F was higher. Equation (5.4) suggests that F depends on parameters θ and c besides R_b, which can be directly increased by increasing the rotor (mill stirrer) tip speed and bead load, respectively (Afolabi et al., 2013). In addition to the above, it is also reported that an increase in suspension flow rate also leads to increased

breakage rate as high suspension flow rate results in tighter residence time distribution (RTD) (no back-mixing) of suspension in mill chamber (Monteiro, et al., 2013; Stehr, 1984). Hence, the combination of higher mill tip speed, higher bead load, and higher suspension flow rate may allow for the development of an intensified process.

Developing such an intensified process is important as it helps to increase the particle breakage rate, thereby achieving faster production of fine nanoparticles with reduced bead wear contamination level. Figure 5.6 shows the schematic of the methodology followed in development of an intensified process with 100 µm beads to produce sub-100 nm particles, with the objective of reducing the milling time and bear wear contamination level.

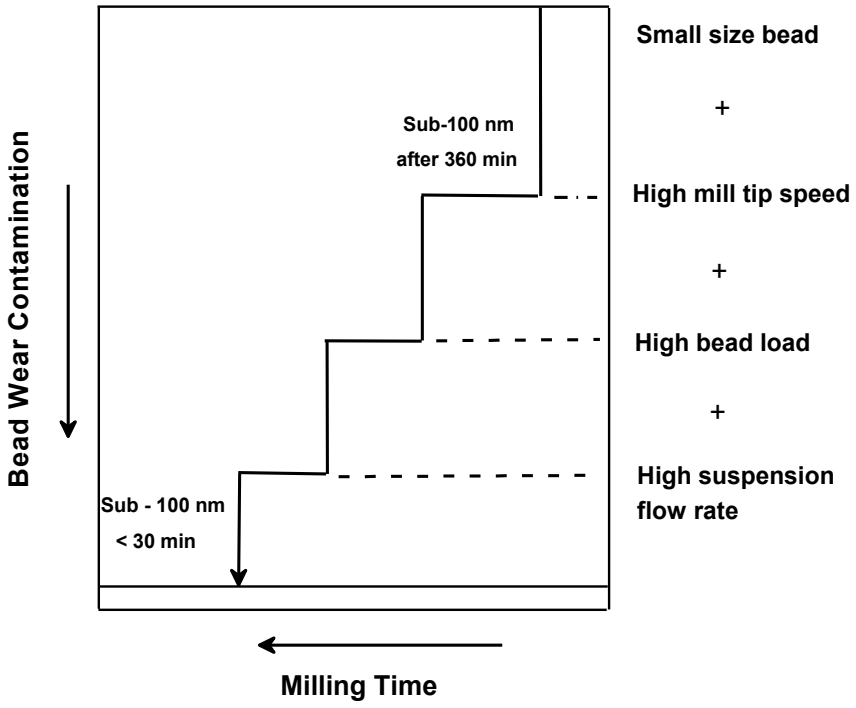

Figure 5.6 Schematic of the methodology followed for the development of an intensified wet stirred media milling process with the use of 100 µm YSZ beads for the faster production of sub-100 nm drug particles.

The effect of each process parameter on the reduction of milling time and particle size was studied by varying one process parameter at a time. From a specific parameter variation study, the intensified mill parameter was selected and subsequently used for other parameter intensification studies.

5.3.2.1 Effect of High Mill Tip Speed. To investigate the effect of mill tip speed on reduction in particle size and milling time, the mill tip speed u was increased to 14.7 m/s. It is to be noted that the maximum tip speed allowed per mill design is 15.4 m/s, and to avoid reaching the limitation of the mill, a mill tip speed of 14.7 m/s was used as maximum in this study. Figure 5.7a shows the temporal evolution of GF median particle size, milled at u = 14.7 m/s at c = 0.4, and Q = 126 ml/min (Table 5.2, Run 5). For the sake of comparison, experimental result of lower mill tip speed (Run 4, u = 11.7 m/s) is also plotted in Figure 5.7a. With an increase in mill tip speed (Run 5), a faster particle breakage rate is observed and a dynamic equilibrium was achieved from 120 min of milling (plateau not shown). The d_{50} particle size obtained at 120 min was 95 nm, and further size reduction was not observed even up to 6 h of milling (refer to Table 5.3 for the particle size statistics). Reduction in only milling time by increasing the mill tip speed was also observed by Afolabi et al., 2013; Fadhel and Frances, (2001). Therefore, a higher mill tip speed of 14.7 m/s was used in the further process intensification experiments.

5.3.2.2 Effect of High Bead Load at High Mill Tip Speed. Increasing the bead load (amount of grinding beads) reduces the volume of empty spaces between the colliding beads, and helps to increase the frequency of particle capture during bead-bead collisions. Better grinding performances were achieved especially at higher media fillings

as in Afolabi et al., (2013), Persson and Forssberg (1994), and Sadler et al. (1975). Therefore, the effect of bead load on reduction in particle size and milling time was investigated by increasing the bead load to c = 0.543, which corresponds to 90% of the total mill volume.

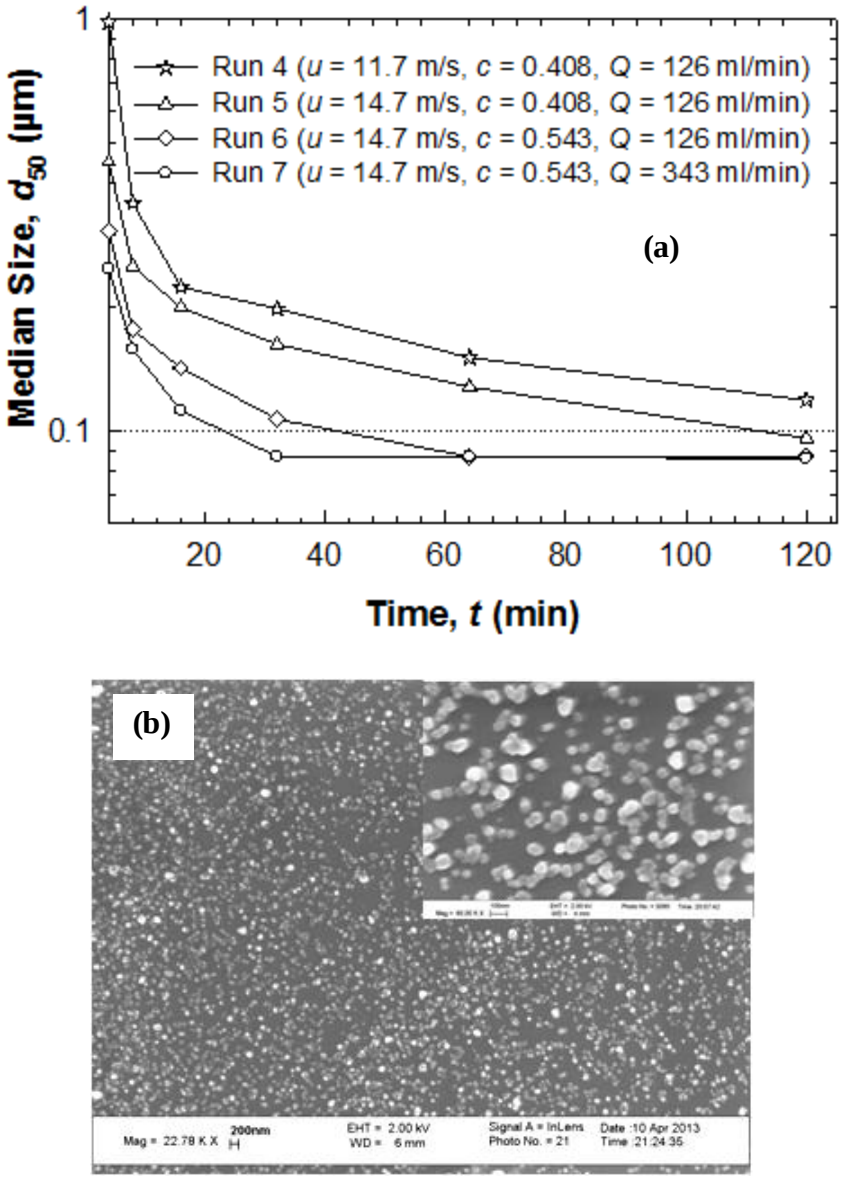

Figure 5.7 (a) Temporal evolution of the median size d_{50} of GF particles for the Runs 4–7 with the use of 100 µm YSZ beads, (b) SEM of GF nanoparticles prepared using intensified process conditions (Run 7: u = 14.7 m/s, c = 0.543 and Q = 343 ml/min). Inset SEM shows magnified GF nanoparticles. At t = 0 min, the GF particles have d_{50} = 21.85 ± 1.25 µm and d_{90} = 57.77 ± 4.35 µm.

Bead load above 90 % resulted in pressure build-up, and hence a maximum bead load of c = 0.543 was used in this study. Other operating process parameters, mill tip speed and suspension flow rate were kept at u = 14.7 m/s and Q = 126 ml/min (Table 5.2, Run 6) respectively. In Figure 5.7a, Run 6 shows a much faster breakage rate compared to Run 5 and a least size of 85 nm were produced within 60 min of milling (Table 5.3 shows the particle size statistics).. Hence, the intensified process with combined effect of higher bead load and higher mill tip speed was used in further studies.

5.3.2.3 Effect of High Suspension Flow Rate at High Bead Load and Tip Speed.

In an attempt to further reduce the milling time, the suspension flow rate Q was increased from 126 ml/min to a maximum of 343 ml/min at c = 0.543, u = 14.7 m/s (Table 5.2, Run 7). From Figure 5.7a, higher suspension flow rate (Run 7) resulted in much faster breakage rate compared to lower suspension flow rate (Run 6), and a particle size of 83 nm was achieved within 32 min of milling (Table 5.3 shows the particle size statistics). Further reduction in particle size was not observed even after prolong milling. SEM of the GF particles prepared with this condition (Figure 5.7b) shows the primary GF particles (refer inset of Figure 5.7b), with an average particle size of 74 nm. Higher suspension flow rate leads to reduction in cycle time (i.e., faster breakage rate) due to plug flow like behavior of the suspension in mill chamber resulting in tighter RTD (no back-mixing). Detailed study on the reduction in cycle time by increasing the suspension flow rate in terms of increasing Péclet number is given in Monteiro, et al. (2013) and Stehr (1984). Hence, the milling process was further intensified which resulted in a final GF nanoparticle size of 83 nm attained within 32 min of milling.

5.3.2.4 Reduction in Cycle Time, Specific Energy Consumption, and Bead Wear.

Considering some potential end points in industrial scale milling operations, the milling time required to produce GF median particle size of 100 nm was predicted by interpolating (Hermite interpolation) the experimental data of Runs 4–7. The predicted cycle time to achieve 100 nm GF particles for the Runs 4–7 were 300 min, 98 min, 41 min, and 22 min respectively. The cycle time was greatly reduced upon intensifying the mill process, and a comparative analysis of cycle time of the intensified process having high rotor speed at high bead load and suspension flow rate (Run 7) with the base line process (Run 4) show a 13.6 times reduction in cycle time. Thus the cycle time was largely reduced with the help of intensified process conditions compared to the baseline process conditions to get median GF size of 100 nm. Similarly, the specific energy consumption E^* up to the predicted time for all the Runs was also calculated. The E^* values for Runs 4–7 were 6.69 MJ/kg, 6.56 MJ/kg, 6.47 MJ/kg, and 3.81 MJ/kg respectively. It is to be noted that upon intensifying the process conditions, the power (P_w) spent on the slurry (Table 5.3) was higher. However, a steady decrease in specific energy consumption values was seen due to the reduction in cycle time. On comparing the Run 7 and Run 4, for a 13.6 time reduction in cycle time, the specific energy consumption was reduced to 1.6 times and is proportional to 43 % energy savings.

Scant information is available on the bead wear contaminant level in terms of cycle time, and varying process conditions (Hennart et al., 2010; Juhnke et al., 2012; Stein, et al., 2010). Figure 5.8 shows elemental level of zirconium and yttrium for Runs 4–7, milled with the use of 100 µm beads up to the predicted time to achieve GF median particle size of 100 nm. Recall that the predicted cycle time to achieve 100 nm GF

particles for Runs 4–7 were 300 min, 98 min, 41 min, and 22 min respectively. In Figure 5.8, the elemental zirconium (Zr) and yttrium (Y) levels contaminations for Runs 4–7 were 298 ± 4 µg/g Zr, 20 µg/g Y, 132 ± 6 µg/g Zr, 12 µg/g Y, 71 ± 4 µg/g Zr, 5 µg/g Y, and 40 ± 2.3 µg/g Zr, 3 µg/g Y respectively. From Figure 5.8, about 86.5% reduction in Zirconium level can be observed with the use of the intensified process (Run 7) compared to the baseline process condition (Run 4). Decrease in contaminants levels (from Runs 4–7) with respect to decrease in the cycle time to reach 100 nm GF particles, suggests that contaminant level is proportional to the milling time irrespective of the process conditions. It is also to be noted that if the milling time is kept constant for both baseline and intensified process conditions; an increase in contaminant levels with the intensified process conditions can be observed.

To prove this, we have also milled GF with the baseline process condition (u = 14.7 m/s at c = 0.53, and Q = 343 ml/min) and the intensified process condition (u = 14.7 m/s at c = 0.53, and Q = 343 ml/min) for a constant mill time up to 2 h with the use of 100 µm beads. The contaminants levels for baseline and intensified process conditions were 33 ± 5 µg/g Zr, 8 µg/g Y and 147 ± 18 µg/g Zr, 10 µg/g Y respectively. Compared to the baseline process, an increase in contaminant levels up to 4.5 times was observed with the intense process conditions for a constant mill time of 2 h. However, it is not required to run the intensified process for a long time, as the process leads to fine particle size at a much shorter time with reduced contamination levels. Hence, the assessment on cycle time and specific energy consumption suggests that one can use the intensified process conditions to achieve faster production of small size drug nanoparticles with significant energy savings and reduced product contamination by the beads. It is to be

mentioned that shortening of cycle time with reduced energy consumption and bead wear with the intensified process is mainly due to faster breakage rate of particles which is a resultant of increased bead-bead collisions (see Section 5.3.2.5).

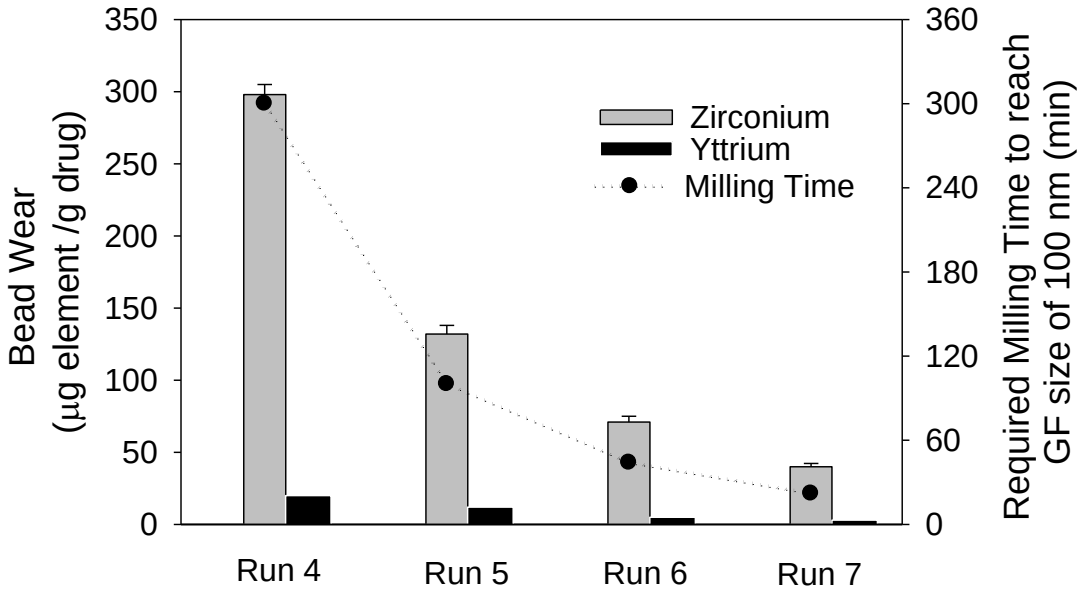

Figure 5.8 Elemental level (µg/g) of zirconium and yttrium from YSZ beads determined by induced couple plasma mass spectroscopy (ICP-MS) along with the time required to reach a median size of 100 nm at different mill process conditions for Runs 4–7. Run 4 at the baseline conditions (u = 11.7 m/s, c = 0.4 and Q = 126 ml/min); Run 5 (u = 14.7 m/s, c = 0.4 and Q = 126 ml/min); Run 6 (u = 14.7 m/s, c = 0.543 and Q = 126 ml/min); Run 7 (u = 14.7 m/s, c = 0.543 and Q = 343 ml/min). 100 µm YSZ beads were used for all the Runs from 4–7.

5.3.2.5 Microhydrodynamic Analysis of the Intensified Process. Table 5.4 shows the calculated MHD parameters for the baseline and intensified process conditions (see Runs 4–7). At higher tip speed (Run 5), all calculated MHD parameters (θ, ν, u_b, σ_b^{max}, F, and a) show higher values as compared to Run 4, and especially one order of magnitude increase in the milling intensity factor F is seen. At higher rotor tip speed, more mechanical energy was imparted on the slurry, which led to more impactful bead collisions (higher θ) and higher compressive stresses (higher σ_b^{max}), i.e., a greater stress

intensity. This effect led to a reduction in milling time (i.e., reduced bead wear) and reduced specific energy consumption. At combined conditions of both high tip speed and high bead load, a counteracting effect was observed: θ, $u_{b,}$, σ_b^{max} were smaller, whereas ν, a, and F were greater (Run 6, Table 5.4) as compared to Run 5. In other words, the amount of stress intensity decreased, but the number of stressing events dramatically increased due to higher bead load. This led to small clearance between the beads causing a dramatic increase in the bead–bead collisions and the average number of drug particle compressions per unit time (ν and a), i.e. higher particle capture efficiency than Run 5. The increase in the capture efficiency led to a further reduction in cycle time, specific energy consumption, and bead wear. Finally with the above intensified process, when the suspension flow (Run 7) rate was increased, the overall breakage rate was further increased due to tighter RTD and plug-flow like behavior of the suspension in the mill chamber. The increase in the suspension flow rate influenced the input MHD parameters: an increase in the rotor power and the decrease in the suspension viscosity (Table 5.4). This was due to the higher number of inelastic bead–bead collisions and liquid-film squeezing events coupled with an increase in the effective drag coefficient R_{diss} which led to greater energy dissipation. It is worth-mentioning that the increase in the energy dissipation further led to an increase in both MHD parameters and the overall breakage of the drug particles. Overall, 8.7 times increase in F can be observed with intensified condition (Run 7) compared to the baseline condition (Run 4) which led to a 13.6 times reduction in cycle time as compared to the predicted baseline mill time of 300 min with energy savings up to 43%, and 86.5% less zirconium wear from the beads. It is to be noted that the use of 100 μm beads enabled us to reduce the cycle and particle size due to

relatively higher particle capture frequency compared to other larger size beads. Though the compressive stresses (σ_b^{max}) of 800, 400, 200 μm beads are higher compared to 100 μm beads, the mill intensity factor (grinding efficiency) is higher for 100 μm beads. Therefore, an effective intensification of the mill process can be achieved only by using smaller size beads.

5.3.3 Milling of Naproxen with Intensified Process

It is important to demonstrate our intensified process with other drug, so as to confirm that the methodology developed results in fine nanoparticles at a shorter milling time. For this, we have selected naproxen (NAP), milled with baseline (Table 5.2, Run 8) and intensified process Table 2, Run 9) conditions. Naproxen loading of 10 % (w/w) and a combined stabilizer having 2.5% (w/w) HPMC, and 0.2% (w/w) SDS were used. Figure 10 shows the temporal evolution of Naproxen median particle size, milled with use 100 μm beads at the baseline conditions (Run8: u = 11.7 m/s, c = 0.408, and Q = 126 ml/min) and intensified process conditions (Run 9: u = 14.7 m/s, c = 0.543, and Q = 343 ml/min). Similar to GF milling, NAP also resulted in sub-100 nm range for both Run 8 and Run 9. In this case too, the baseline process condition (Run 8) took almost 6 h (data shown till mill time of 120 min) to reach 87 nm whereas, intensified condition (Run 9) resulted in 82 nm within 32 min of milling. XRD analysis also confirmed that crystallinity of milled NAP was not altered (Figure not shown).

Upon assessing the cycle time, specific energy consumption, and bead wear between Runs 8 and 9, the predicted cycle time to achieve 100 nm NAP particles were 194 min and 18 min respectively. Reduction in cycle time about 10.7 times was achieved upon intensifying the process, and the calculated energy savings and reduced zirconium

bead wear at this reduced cycle time were up to 21% and 76%, respectively. This observation is similar to the milling of GF particles as shown in Section 5.3.2.4, thus proving that the methodology followed in the intensified process works well for other drugs. Table 5.4 shows the calculated MHD parameters for Runs 8 and 9. Similar to GF, the intensified process conditions (Run 9) shows 8 times high F compared to the baseline process condition (Run 8). Overall most of the MHD parameters values were high for the intensified process which led to an increase in F (i.e. faster breakage of NAP particles).

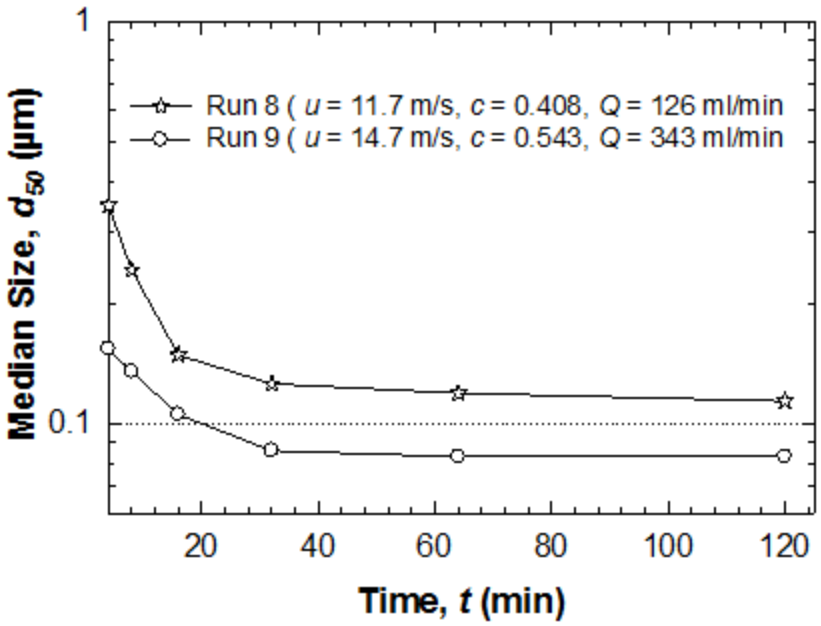

Figure 5.9 Temporal evolution of the median size d_{50} of the naproxen (NAP) particles milled with the use of 100 µm YSZ beads. Run 8 at the baseline conditions (u = 11.7 m/s, c = 0.4 and Q = 126 ml/min) and Run 9 at the intensified process conditions (u = 14.7 m/s, c = 0.543 and Q = 343 ml/min). At t = 0 min, the NAP particles have d_{50} = 16.60 ± 1.27 µm and d_{90} = 77.12 ± 2.10 µm.

Table 5.4 Power Applied per Unit Volume of Slurry (P_w), Measured Viscosity ($\mu_{L)}$ and Density (ρ_L) of the Milled Drug Suspensions, and the Calculated Microhydrodynamic Parameters (θ, u_b, ν, σ_b^{max}, a, and F) for Different Runs

Run No.	P_w (W/m^3)	μ_L (cP)	ρ_L (kg/m^3)	θ (m^2/s^2)	u_b (m/s)	ν (KHz)	σ_b^{max} (GPa)	a (mHz)	F (m$^{0.6}$/s$^{2.6}$)
1	3.13×10^{5}	5.97	1034	2.25×10^{-2}	2.40×10^{-1}	3.98	2.19	1.24×10^{-1}	5.26×10^{12}
2	2.92×10^{5}	5.73	1026	1.24×10^{-2}	1.78×10^{-1}	5.47	1.95	1.99×10^{-1}	2.87×10^{13}
3	2.71×10^{5}	5.51	1028	5.30×10^{-3}	1.16×10^{-1}	7.17	1.64	3.28×10^{-1}	1.53×10^{14}
4	2.29×10^{5}	5.63	1040	2.06×10^{-3}	7.24×10^{-2}	7.58	1.36	3.22×10^{-1}	3.70×10^{14}
5	6.88×10^{5}	5.04	1036	5.90×10^{-3}	1.22×10^{-1}	12.8	1.68	8.99×10^{-1}	1.46×10^{15}
6	1.25×10^{6}	4.83	1038	3.70×10^{-3}	9.76×10^{-2}	27.1	1.53	2.10	2.81×10^{15}
7	1.38×10^{6}	4.56	1037	4.20×10^{-3}	1.03×10^{-1}	28.7	1.57	2.45	3.31×10^{15}
8	2.08×10^{5}	4.93	1008	2.09×10^{-3}	7.29×10^{-2}	7.63	1.36	3.75×10^{-1}	3.77×10^{14}
9	1.38×10^{6}	4.78	1007	4.10×10^{-3}	1.02×10^{-1}	28.4	1.56	2.30	3.21×10^{15}

5.4 Summary and Conclusions

Wet stirred media milling is considered as the robust process for the production of poorly water-soluble drug nanoparticle suspensions. Besides its advantage in large scale production, the process is limited by long hour of operation, intense energy consumption and bead wear. In the present work, an intensification process methodology for WSSM has been developed with the objective of producing sub-100 nm particles at a reduced mill time, energy consumption, and bead wear. Two model poorly water- soluble drugs, Griseofulvin (GF) and Naproxen (NAP) were selected for this study, milled at a bench scale process having 200 ml batch volume with 10 wt% drug loading. The use of smallest beads (100 µm) in our base line process conditions enabled us to produce stable suspensions containing sub-100 nm (98 nm) GF particles after 6 h of milling with reduced energy consumption and reduced bead wear. Microhydrodynamic theory of beads clearly explains the following within the context of 100 µm beads (i) fastest particle breakage rate due to more number of stress events (ii) production of sub-100 nm particle due to high particle capture frequency (iii) reduced energy consumption due to low fluctuating motion of beads and (iv) reduced bead wear contamination due to low compressive stress between the beads. A milling intensity factor, which is proportional to the energy dissipation rate during deformation of the drug particles, explained the overall positive effects of the smaller beads. Further, an increased mill intensity factor was achieved by increasing the particle breakage rate via combined use of intense mill parameters such as rotor tip speed, bead load, and feed flow rate, which finally led to the production of 83 nm GF particles within 30 min of milling. Further reduction in both

particle size and milling time was not achieved due to the practical limitation of our mill such as maximum stirrer speed and difficulty to use/separate less than 100 µm beads.

A comparative analysis between the baseline and intensified process conditions to produce GF particle size of 100 nm showed a 13.6 times reduction in cycle time with energy savings up to 43% with use of intensified process conditions. Bead wear contamination levels of zirconium and yttrium in the milled drug particles was found to be proportional to the milling time, and 86.5% less bead wear (zirconium) contamination was observed with the reduced milling time. Similarly, milling of NAP with intensified process conditions also led to the faster preparation of sub-100 nm particles with reduced specific energy consumption and bead wear. Thus, the intensified process methodology developed in this Chapter presents an opportunity for formulators/engineers to design an intensified wet-milling process for faster production of sub-100 nm drug particles with energy savings and reduced bead wear contamination of final drug product.

CHAPTER 6

CONTINUOUS PRODUCTION OF DRUG NANOPARTICLE SUSPENSIONS VIA WET STIRRED MEDIA MILLING: A FRESH LOOK AT THE REHBINDER EFFECT

6.1 Introduction

Fast and efficient development of pharmaceutical formulations containing poorly water-soluble drug particles is of great interest to the pharmaceutical industry (Date and Patravale, 2004). By some estimates, 60% of drug candidates currently under investigation can be classified as Biopharmaceutical Classification System (BCS) Class II, for which the bioavailability is limited by solubility rate. Recent advances in combinatorial chemistry aided the discovery of new drug molecules with such low solubility characteristics (Muller and Peters, 1998; Niwa et al., 2011). Production of nanoparticles and microparticles of poorly water-soluble drugs can enhance the dissolution rate through the significant increase of the surface area (see e.g. the Noyes–Whitney equation (Noyes and Whitney, 1897)). Such small particles can be produced either by the so-called top-down approach, which includes jet milling (Chan et al., 2002), high pressure homogenization (Kamiya et al., 2009), and stirred media milling (Bilgili et al., 2004, 2006); or by the bottom-up approach (Anais et al., 2009; Chiou et al., 2008; Date and Patravale, 2004) which involves building up particles by precipitation of dissolved molecules. Both approaches have been widely used to produce microsuspensions (suspensions with particles having a mean or median size in the range 1–10 μm) and nanosuspensions (suspensions with particles having a mean or median size less than 1 μm) (Ain-Ai et al., 2008; Basa et al., 2008; Hu et al., 2004; Kesisoglou et al., 2007; Liversidge et al., 1995; Park et al., 2009; Tanaka et al., 2009).

A thorough search of pharmaceutical literature for the wet media milling of BCS Class II drugs shows that a great majority of the experimental data was obtained with the batch/recirculation operation mode. In batch operations, the mill is operated either vertically or horizontally, where agitation of the milling media (beads) is performed by a main rotating shaft, with the possibility of sub-shafts branching off. Batch mills are not widely used in large scale production due to scale-up issues; however, nanomilling of pharmaceuticals in small-scale batch operations has been documented (Bhakay et al., 2011; Lee et al., 2008; Sepassi et al., 2007). Recirculation mode uses a small milling chamber, recirculation pump, holding tank, and milling media containment screen to facilitate particle breakage. Similar to standard batch milling, particle breakage originates from the intense agitation of the beads and product suspension. A pump is employed to circulate the suspension from the holding tank, through the mill, and back into the holding tank (see Figure 6.1a). Elan's Nanocrystal Technology™ makes use of recirculation media milling to produce drug nanosuspensions in marketed products like: Rapamune (Wyeth), Emend (Merck), Tricor (Abbott), and Megace (Par Pharmaceutical) (Bruno et al., 1996), with a couple of review papers (Merisko-Liversidge et al., 2002; Merisko-Liversidge and Liversidge 2011) thoroughly discussing the recirculation milling process. Several research groups (Cerdeira et al., 2011; Ghosh et al., 2011; Singh et al., 2011) have recently used the recirculation milling mode to produce drug nanosuspensions in small batch sizes; however, a comparison to other milling modes was not performed. A comparison study of standard batch mode and recirculation mode of milling of drug nanosuspensions was performed using a planetary mill (Juhnke et al., 2010); however, no comparison or discussion of multi-pass (or cascade continuous mode) was presented.

Some researchers (Adjei et al., 1995; Annapragada et al., 1996; Verhoff et al., 2003; Czekai and Seaman, 1996, 1998) refer to the recirculation operation mode as a continuous milling process. Although the milling is performed 'continuously' in a milling chamber, no product is withdrawn continuously from the mill as 100% of mill output is circulated back to a holding tank, which allows the production of a *fixed batch size* as determined by the capacity of the holding tank (Figure 6.1a). The milling dynamics is partly coupled to the mixing dynamics in the holding tank that is usually assumed well-mixed. Figure 6.1b depicts a multi-pass continuous milling process: unmilled suspension is loaded into the holding tank, pumped to pass through the mill, and collected into the receiving tank. Using this milling mode, multiple passes can be performed by repeating the said procedure. It is possible to automate the multi-pass mode using two separate holding tanks with interconnected valves and pumps by which the suspension can be processed from one tank to the other in a swing or pendulum motion. Figure 6.1c depicts a true (cascade) continuous milling process where unmilled suspension is loaded into the holding tank and allowed to pass through n number of mills in series before being collected in the receiving tank. The multi-pass mode (Figure 6.1b) is intended to simulate the operation of true (cascade) continuous milling (Figure 6.1c). Since it is expensive to acquire n (usually 6–12) number of mills for research/development purposes at the lab-scale, the investigation of continuous milling was carried out using the multi-pass mode in this chapter.

In all major chemical industries, continuous processing is widely used for large-scale production. There is a growing interest in moving all pharmaceutical unit operations in drug product manufacture from batch processes to continuous processes. Recent

publications on continuous mixing have made the case for the feasibility of continuous drug product manufacture (see e.g. Berthiaux et al., 2008; Vanarase et al., 2010a, 2010b). This manufacturing strategy could bring the pharmaceutical industry advantages such as consistent and improved product quality, reduced waste, lower inventory and equipment costs, easy scale-up, flexibility, and short cycle times. Pharmaceutical unit operations such as tabletting, roller compaction, and capsule filling are already performed semi-continuously; whereas mixing, wet milling, most granulations, drying, and tablet coating are usually performed in the batch/recirculation mode. Although ample experimental studies of batch and recirculation mode of wet media milling exist in literature, little effort has been devoted to the cascade or multi-pass continuous modes. In the area of continuous wet stirred media milling of drugs, there are only a couple of patents available (Holland et al., 2006; Verhoff et al., 2003). Initial discussion on the feasibility of nanomilling Fenofibrate using a wet stirred media mill operating in single-pass mode was presented (Holland et al., 2006); however, the figures and examples provided only described recirculation milling. Another patent (Holland et al., 2006) presents what is believed to be the first documentation of cascade continuous mode of wet media milling of drugs, where Nabumetone nanoparticles were produced using five media mills in series. In both cases, only the final median particle size was provided; procedural details were missing, and the breakage dynamics was not studied.

Wet stirred media milling of poorly water-soluble drugs has been commonly performed in recirculation/batch mode (see preceding chapters) to understand the impact of formulation and processing parameters, and scant information is available on the continuous mode of operation.

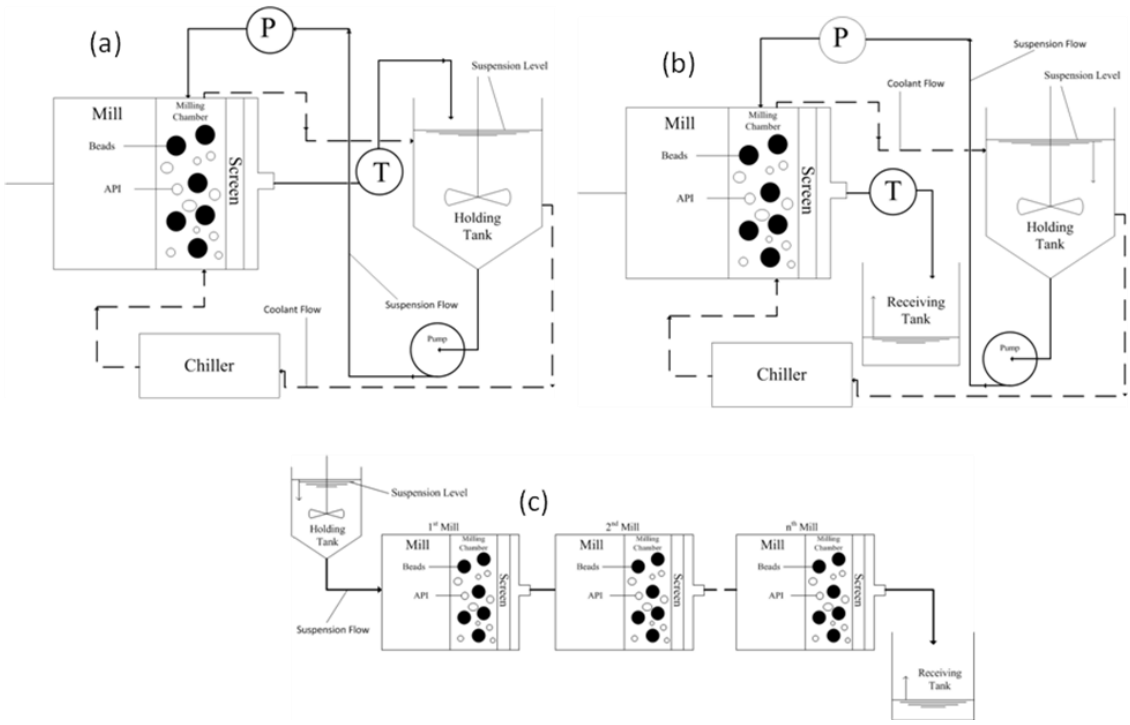

Figure 6.1 Schematic of recirculation, multi-pass continuous, and cascade continuous modes of wet media milling. 'P' represents pressure gauge and 'T' represents thermometer. (a) Recirculation – Suspension recirculates through the mill. (b) Multi-Pass Continuous – Suspension flows from holding tank, through mill, and into receiving tank. (c) Cascade Continuous - Suspension flows from holding tank, through mills in series, and into receiving tank (coolant flow for cascade continuous mode is not shown for clarity).Figures are not drawn to scale.

An objective of the current chapter is the *continuous production* of nanosuspensions of two BCS Class II drugs, i.e. Griseofulvin (GF) and Naproxen (NAP), using a single wet stirred media mill (Netzsch Microcer) in the multi-pass mode. Evolution of the particle size distribution (PSD) during recirculation and multi-pass continuous modes of operation was studied to describe the breakage dynamics along with the effects of a reduced suspension flow rate. Another objective of the present chapter is the *elucidation of the so-called Rehbinder effect* on fine milling. The Rehbinder effect is described as the facilitation of crystal cleavage and decrease in hardness of crystals caused by surface-

active agents. Adsorption of the surface-active agents can weaken the bonds in the crystal surface layer and lower the specific surface free energy (Butyagin, 1999; Rehbinder, 1958; Rehbinder and Shchukin, 1972; Shchukin, 2006). When GF particles were milled in the presence of hydroxypropyl methyl cellulose (HPMC) as the only stabilizer in a *Micros batch mill*, limited analysis (Bhakay et al., 2011) did not reveal a significant Rehbinder effect. Here, GF and NAP particles were milled in the presence/absence of a stabilizer combination, i.e., a polymer (hydroxypropyl cellulose, HPC) and an anionic surfactant (sodium lauryl sulfate, SLS), toward elucidating the Rehbinder effect. Laser diffraction, BET nitrogen adsorption, SEM imaging, and a microhydrodynamic analysis were used as tools to investigate the roles of the stabilizers. Milling the drugs in the absence of stabilizers produced primary nanoparticles and their aggregates, while milling in the presence of stabilizers produced smaller primary nanoparticles with minimal aggregation. This is the first study in pharmaceuticals literature that provides sufficient evidence for the existence of the Rehbinder effect. Not only do the stabilizers allow proper stabilization/dispersion of the milled suspensions, but they also do facilitate the breakage of the drug particles.

6.2 Experimental

6.2.1 Materials

GF (BP/EP micronized grade) and NAP (USP grade), were used for all wet media milling as reported in Chapter 5. SEM images of as-received drug particles are shown in Figure 6.2. An anionic surfactant, sodium lauryl sulfate (SLS), and a neutral polymer, hydroxypropyl cellulose (HPC, SL grade), were used as stabilizers.

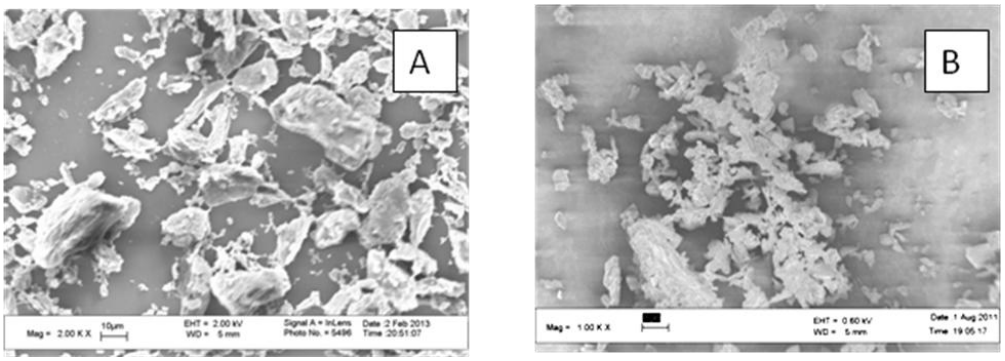

Figure 6.2 SEM images of BCS Class II drugs as received from the manufacturer: (a) Griseofulvin (GF) at 2 kX, (b) Naproxen (NAP) at 1 kX.

6.2.2 Methods

6.2.2.1 Preparation of Feed Suspensions. Feed drug suspensions were prepared by first weighing de-ionized water (Di-H_2O) inside a clean beaker. SLS was weighed and added to the water gradually for 15 min while mixing. HPC was then weighed and added gradually for 30 min while mixing. The HPC/SLS solution was then mixed for an additional 15 min to ensure that the HPC and SLS particles were properly dissolved. SLS and/or HPC addition steps were skipped for runs that do not use the stabilizer(s) (see Table 6.1). The drug particles were then weighed and added gradually for 40 min while mixing. Two samples (1 mL) were taken after 40 min of mixing for PSD analysis, corresponding to the 0^{th} turnover or pass sample in the dynamic study (see below). All mixing was performed using the low shear laboratory stirrer. To defoam and pre-cool the suspension, feed suspensions were kept in a refrigerator at about 8 ^{o}C for 1 h prior to milling.

Table 6.1 shows the formulations used for the wet media milling experiments. The drug loading was 10% for all runs performed. Unless otherwise specified, all weight percentages are with respect to water.

Table 6.1 Operating Conditions and Formulations of the Wet Media Milling Experiments

Run No.	Drug	Flow Rate (mL/min)	Milling Mode	Di-H_2O (mL)	Drug Loading (% w/w)[a]	HPC Concentration (% w/w)[a]	SLS Concentration (% w/w)[a]
1	GF	110	Recirculation	400	10	2.5	0.5
2	GF	110	Multi-Pass	445	10	2.5	0.5
3	GF	55	Recirculation	400	10	2.5	0.5
4	GF	55	Multi-Pass	445	10	2.5	0.5
5	GF	110	Multi-Pass	457	10	—	—
6	NAP	110	Recirculation	400	10	2.5	0.5
7	NAP	110	Multi-Pass	445	10	2.5	0.5
8	NAP	55	Recirculation	400	10	2.5	0.5
9	NAP	55	Multi-Pass	445	10	2.5	0.5
10	NAP	110	Multi-Pass	454.5	10	—	0.0825

[a]% w/w with respect to Di-H_2O (de-ionized water).

A suspension of 440 mL was used when operating in the recirculation mode. About 50 mL residual suspension must be retained within the milling chamber during each pass of the multi-pass mode of operation because running the mill empty could cause serious damage. Therefore, the suspension volume was increased to 490 mL when milling in multi-pass continuous mode to account for the 50 mL residual suspension. In the first part of this Chapter (Runs 1–4 and 6–9), HPC and SLS loading were 2.5% and 0.5%, respectively. Experiments were performed with both 110 and 55 mL/min flow rate. After milling, samples from Runs 1, 2, 6, and 7 were refrigerated at about 8 ^{o}C for 7 days. The refrigerated samples were analyzed using laser diffraction to assess the short-term physical stability of the suspensions. Stability studies were not performed for the other runs with identical formulations despite the difference in the suspension flow rate.

In the second part of this chapter, Runs 5 and 10 were designed to elucidate the effect of stabilizers on particle breakage by milling the drugs in the absence of stabilizers. No processing issue was encountered during GF milling and subsequent characterization. On the other hand, a thick foam was formed while attempting to prepare the NAP suspension without HPC/SLS (Run 10). Since the foam could not be milled as prepared, small batch size experiments were performed to determine the minimum amount of SLS required to properly wet the particles and to facilitate milling. It was determined that at 0.0825% SLS, the foam was reduced to such a level and consistency that milling could be performed. Such a small addition of SLS was not expected to significantly affect the analysis since the amount of SLS added was substantially less than the critical micelle concentration (CMC) of SLS (2.36 g/L CMC vs. 0.825 g/L SLS added). However, a

confounding effect cannot be completely ruled out due to this small SLS amount in NAP milling.

6.2.2.2 Milling Procedure. The mill was set up to operate either in recirculation mode (Figure 6.1a) or in multi-pass continuous mode (Figure 6.1b) by choice. In recirculation milling, the unmilled feed suspension was loaded into the 500 mL holding tank. The suspension then circulates continuously from the holding tank, through the mill, and back into the holding tank by a peristaltic pump. A complete passage of the bulk volume from the holding tank, through the mill, and back into the holding tank is referred to as a 'turnover'. The amount of time required to perform a single turnover was calculated by dividing the batch volume in the holding tank by the suspension flow rate. The number of turnovers performed during a milling experiment is given by the ratio of the total milling time to the turnover time. A total milling time of 64 min was used for all milling experiments performed in this study.

In multi-pass continuous milling, the unmilled suspension was loaded into the holding tank and pumped through the mill by the peristaltic pump and collected in the receiving tank; with each trip referred to as a 'pass'. When the MicroCer mill was operated in the multi-pass continuous mode, additional mixing and recirculation time had to be introduced to deal with the 50 mL residual suspension that must remain inside the milling chamber in between passes. The procedure was as follows: After the first pass of milling, the receiving tank suspension was poured back into the holding tank and mixed for 3 min with the paddle mixer set at 1000 rpm. A 1 mL sample was taken after 3 min.

The suspension was then circulated for 8 min with the mill rotor off while the paddle in the holding tank was rotated at 1000 rpm. This was performed to allow the

milled suspension and 50 mL unmilled residual suspension to mix completely. After 8 min, the well-mixed suspension was ready to pass through the mill and to be collected in the receiving tank once again (the second pass). The procedure mentioned above was repeated for all the remaining passes.

In both modes of milling, the mill rotor was rotated at 3600 rpm (tip speed of 13.2 m/s), with the suspension in the holding tank mixed at 400 rpm during milling. For runs operating with a flow rate of 110 mL/min, 1 mL samples were taken after the 1^{st}, 2^{nd}, 3^{rd}, 4^{th}, 7^{th}, 8^{th}, 12^{th}, and 16^{th} turnover or pass (64 min total, 4 min per turnover or pass). When switching to runs operating at a flow rate of 55 mL/min, samples were taken after the 1^{st}, 2^{nd}, 3^{rd}, 4^{th}, 5^{th}, 6^{th}, 7^{th}, and 8^{th} turnover or pass (64 min total, 8 min per turnover or pass). Multi-pass mode with a flow rate of 55 mL/min required 16 min of additional mixing/recirculating of the 50 mL residual suspensions with the produced suspension in-between the passes. Particle size analysis was performed on all samples (see *Particle Size Analysis* below).

Establishment of a steady-state operation in terms of particle size is important in continuous milling. The rotor reaches the set speed usually within few seconds, the peristaltic pump recirculates the suspension at a constant flow rate with small variability, and the intensive cooling of the milling chamber allows maintenance of low temperature in the suspension during milling. Therefore, in multi-pass continuous milling, it is theoretically expected that the process will reach a steady-state in each pass within a short period of time, as compared with the duration of the whole pass. Each pass (1^{st}, 2^{nd}, and so on) corresponds to a *different steady-state condition*, which will emulate responses from different mills in series in a large-scale cascade operation. To prove that the steady-

state was achieved relatively fast, samples were taken at the outlet of the mill at 15, 30, 60, 120, and 240 s *during* the 2nd pass of a GF suspension (110 mL/min flow rate), as opposed to the usual sampling done on the whole milled suspension obtained from the 2nd pass. The median particle sizes of the samples were measured by laser diffraction (see below) to be 684, 494, 498, 497, and 472 nm, respectively, with an average value of 529 nm (490 ± 13 nm excluding the 15 s sample). The 2nd pass sample collected *cumulatively* in the beaker (usual sampling) had a median size of 525 nm. These findings suggest that a steady-state was established within 15–30 s during the 2nd pass of the GF suspension. Considering the fact that the total duration of the 2nd pass was 4 min, the steady-state was indeed established fast. In addition, there was no need to discard the milled product obtained during the early 0–30 s period because the amount of suspension produced was small compared with the whole milled product during the 2nd pass. This approach was justified by the similarity between the averaged median size of the multiple time samples (490 nm, excluding the 15 s sample) and that from the whole sample accumulated in the beaker during the 2nd pass (525 nm). Of course, process engineers will opt to divert the product stream until a steady-state is established during cascade-continuous operation in manufacturing. Formulation and processing parameters may affect the attainment of steady-state and steady-state particle size, which is of practical importance; however, this aspect will not be treated here extensively.

6.2.2.3 Particle Size Analysis and SEM. Particle size analysis of the milled suspensions was performed by laser diffraction using a Coulter Beckmann LS 13-320 (Brea, CA, USA) as reported in previous chapters. Samples were taken during milling after the various turnovers or passes mentioned above and were diluted with 10 mL of the

relevant solution: HPC/SLS solution (Runs 1–4 and 6–9), de-ionized water (Run 5), and SLS solution (Run 10) prior to particle size measurements. To measure the particle size of the refrigerated samples after 7 days of storage, content of the sample vials was gently mixed by a stir bar to redisperse and homogenize the samples. All given sizes are volume-weighted values. Besides the usual 50% and 90% passing sizes (d_{50} and d_{90}), a Sauter-Mean Diameter (SMD) was also calculated from the size distribution, which was compared with the SMD calculated from the BET analysis. SEM imaging was performed as reported in Chapter 3 and Chapter 4.

6.2.2.4 Differential Scanning Calorimetry (DSC). A Mettler-Toledo Polymer Analyzer DSC (Model: PolyDSC) (Columbus, OH, USA) was used to obtain the onset melting temperature, peak melting temperature, and heat of melting of GF and NAP as received and after milling (Runs 5 and 10) as reported in Chapter 3.

6.2.2.5 Raman Spectroscopy and X-ray Powder Diffraction (PXRD). In order to verify the findings from the DSC analysis and elucidate any changes to the GF crystallinity upon milling, as-received and milled/dried GF samples were subjected to Raman Spectroscopy and X-ray Powder Diffraction (PXRD). Raman spectra were collected using a Mesophotonics SE 1000 Raman spectrometer (Chilworth Science Park, Southampton Hampshire, UK), which was calibrated to 2 cm^{-1} with a 250 mW near-infrared laser operating at 785 nm with a 130 µm diameter spot size. Data acquired with the Raman spectrometer represent an average of five scans, for a total of 50 seconds. All Raman data were as-recorded by the instrument. During the spectra acquisition, powder samples were placed on glass substrates. In PXRD, as-received and milled/dried GF particles were analyzed using a wide-angle Philips X'pert MRD Diffractometer (7609

RG, Almelo, Netherlands) with Cu K_α radiation (λ =1.5406Å). The tube voltage and amperage were set to 45 kV and 40 mA, respectively. The samples were scanned for 2θ ranging from 5^o to 40^o at a speed of ~0.01 2θ/s. Data were collected using Philips X'Pert DataCollector and analyzed using X'Pert Data Viewer.

6.2.2.6 BET Nitrogen Adsorption. Powder samples for the BET experiments were obtained from the suspension samples following the same drying procedure as that used for the preparation of the DSC samples. The dried samples were then degassed under vacuum at 80 ^{o}C for 24 h to remove atmospheric moisture bound to the particle surface prior to nitrogen adsorption. The powder specific surface area (SSA) of Runs 5 and 10 samples were determined from an 11-point nitrogen adsorption isotherm using a Nova 3200 BET analyzer (Quantachrome Instruments, Boynton Beach, Florida, USA). Assuming spherical primary particles, the Sauter-Mean Diameter (SMD) was calculated using SMD = 6/(ρ×SSA), where ρ is the true density of the drug (1.4 g/cm^3 for GF and 1.2 g/cm^3 for NAP).

6.2.2.7 Viscosity and Density of the Milled GF Suspensions. To be able to perform a microhydrodynamic analysis, the apparent shear viscosity of some of the milled GF suspensions (Runs 2 and 5) was determined using an R/S plus Rheometer (Brookfield Engineering, Middleboro, MA, USA) as reported in Chapter 3 and Chapter 4. Measurements were performed in duplicate to check for reproducibility. Density of the above suspensions (ρ_L) was determined as reported in Chapter 3 and chaprter 4. Measurements were performed in triplicate to check for reproducibility and the average was calculated.

6.3 Results and Discussion

6.3.1 Recirculation vs. Multi-Pass Continuous Operation

6.3.1.1 Characteristics of the Final GF and NAP Suspensions. GF and NAP particles were separately milled in the recirculation mode for 16 turnovers (Runs 1 and 6). They were also milled in the multi-pass continuous mode for 16 passes (Runs 2 and 7), while keeping formulation and process conditions the same (Table 6.1). For all these different runs, the total milling time was 64 min and the suspension flow rate was 110 mL/min. Irrespective of the milling mode, nanoparticles were obtained, and the final median particle size after 16 turnovers or passes were similar for these runs (Table 6.2). The flow rate was then reduced by half to 55 mL/min while leaving total milling time unchanged, i.e., 64 min (Runs 3, 4, 8, and 9). GF and NAP were milled in recirculation mode (Runs 3 and 8), with the turnover time increased from 4 to 8 min to account for the decreased flow rate. They were also milled in multi-pass continuous mode (Runs 4 and 9) while keeping formulation and process conditions the same. Table 6.2 shows that even after reducing the flow rate by half, nanoparticles with similar median sizes were obtained using both modes of milling after the completion of 8 turnovers or passes.

Overall, these results suggest that given sufficient total milling time (64 min), both the recirculation and multi-pass continuous modes led to similar particle sizes, irrespective of the suspension flow rate used. To gauge the reproducibility of the wet media milling process, GF runs (Runs 1 and 2) were repeated. It was observed that a repeat of Run 1 produced a final median particle size of 0.157 μm, yielding a 1.3 % difference when compared to the data shown in Table 6.2. Similarly, a repeat of Run 2 produced a final median particle size of 0.159 μm (a 0.6 % difference).

Table 6.2 Particle Size Statistics of the Suspensions Before and After Milling As Well As After 7-Day Storage

Run No.	Before Milling d_{50} (μm), d_{90} (μm)	After Milling d_{50} (μm), d_{90} (μm)	After 7-Day Storage d_{50} (μm), d_{90} (μm)
1	18.8, 54.8	0.159, 0.223	0.157, 0.224
2	16.3, 46.0	0.160, 0.229	0.157, 0.233
3	18.3, 53.3	0.157, 0.228	—
4	13.9, 34.9	0.154, 0.238	—
5	15.4, 31.4	6.04, 8.76	5.33, 8.80
6	12.9, 34.2	0.143, 0.238	0.137, 0.269
7	10.4, 29.0	0.147, 0.253	0.145, 0.286
8	15.7, 51.0	0.138, 0.229	—
9	14.6, 33.8	0.146, 0.327	—
10	17.8, 39.0	5.78, 15.3	14.5, 29.6

Note: 7 day stability testing was not performed on Runs 3, 4, 8, and 9.

Good reproducibility of the particle size of final drug suspensions has also been established in earlier work (Bhakay et al., 2013; Bilgili and Afolabi, 2012; Sievens-Figueroa et al. 2012), regardless of the variability in the initial as-received drug particle size provided that the suspensions had a wetting agent (e.g. SLS) and some stabilizers (e.g. HPC and SLS). A short-term physical stability study of several suspensions (Runs 1, 2, 5, 6, 7, and 10) was performed by analyzing particle size after seven days of storage (Table 6.2). Results indicate the amount of polymer and surfactant used was sufficient to stabilize the suspensions against both aggregation and ripening, as deduced from a comparison of the d_{50} and d_{90} values after milling and 7-day storage (similar particle sizes).

To develop a more fundamental understanding of the HPC–SLS synergy and the interactions with the specific drugs considered here, HPC–SLS adsorption on the respective drug surfaces must be studied (see Chapter 3). In the absence of stabilizers

(Run 5) or with minimal amount of surfactant (Run 10), aggregates of smaller particles formed during milling, rendering the suspensions unstable. A stability study was not performed on runs operating at the reduced flow rate as the formulation remained unchanged. In addition, a long-term stability was not performed as the suspensions were intended to be dried shortly after media milling in various drying applications (as in Bhakay et al., 2013; Sievens-Figueroa et al., 2012). Readers are referred to Bhakay et al., (2013) and Sievens-Figueroa et al., (2012) for the effects of drying of the drug nanosuspensions on the reconstitution of the nanoparticles. In aqueous dispersion of the dried products (coated microparticles and films), the formulations used in this study led to stable, well-dispersed suspensions with effective recovery of the drug nanoparticles.

A DSC study was performed on various samples to investigate the effect of milling on the drug crystallinity. DSC thermograms (Figure 6.3) exhibited sharp endothermic peaks associated with the melting of the crystalline drugs; no other thermal event was encountered. It should be noted that milling, especially dry milling and cryomilling, can induce defects in crystals as well as amorphous regions, which can lead to appearance of exothermic response like recrystallization and glass transition (see e.g. Feng et al., 2008; Sharma et al., 2009; Zarow et al., 2011). If crystal defects accumulate to a significant extent and/or amorphous content becomes appreciable, the melting temperature and the heat of melting can be reduced significantly (Feng et al., 2008). Polymorphic changes can also lead to such changes.

As presented in Table 6.3 for GF and NAP, both the onset and peak melting temperatures of the as-received samples remained the same after milling of GF (Run 5) and NAP (Run 10). No broadening of the melting point range was observed. Only a slight

decrease (5.4%) in the heat of melting (fusion) was observed for GF, whereas a 5.1% increase was observed for NAP.

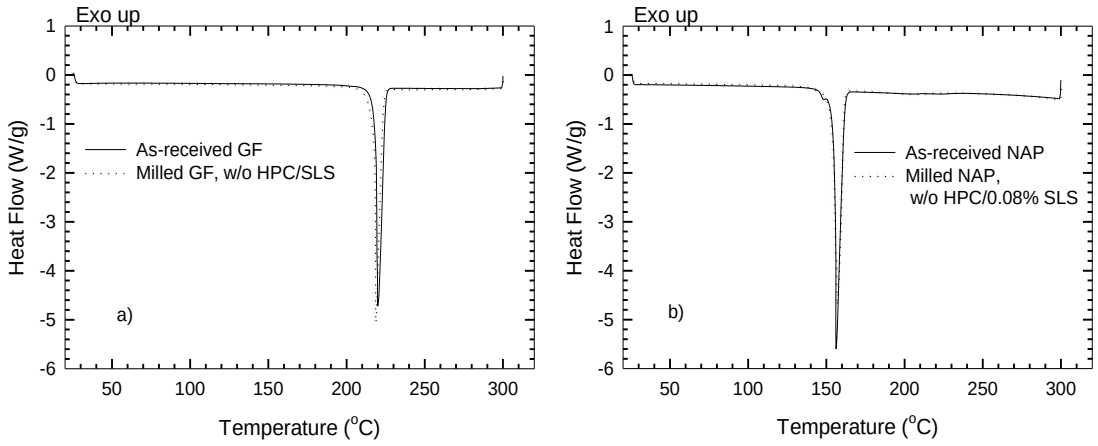

Figure 6.3 DSC thermograms of (a) as-received GF and milled/dried GF w/o stabilizers (Run 5), (b) as-received NAP and milled/dried NAP w/o HPC/0.08% SLS (Run 10).

Table 6.3 Melting Points and Heat of Melting of As-Received and Milled GF and NAP

Sample	Onset Melting Point (°C)	Peak Melting Point (°C)	ΔH_m (J/g)
As-received GF	218.0	220.1	111.1
Milled GF, w/o HPC/SLS[a]	217.3	219.2	105.1
As-received NAP	155.0	158.6	136.0
Milled NAP, w/o HPC/0.08% SLS[b]	153.9	157.9	142.9

[a]Run 5
[b]Run 10

These small deviations in the heat of melting could be attributed to experimental errors (sample weight, bulk density, and particle size differences in the samples as well as presence of SLS in NAP sample, etc.). Overall, the DSC results suggest that the crystalline nature of GF and NAP was largely preserved after milling and no polymorphic form change has occurred during milling; a cautionary note that small amount of amorphous content may not be accurately determined using the DSC.

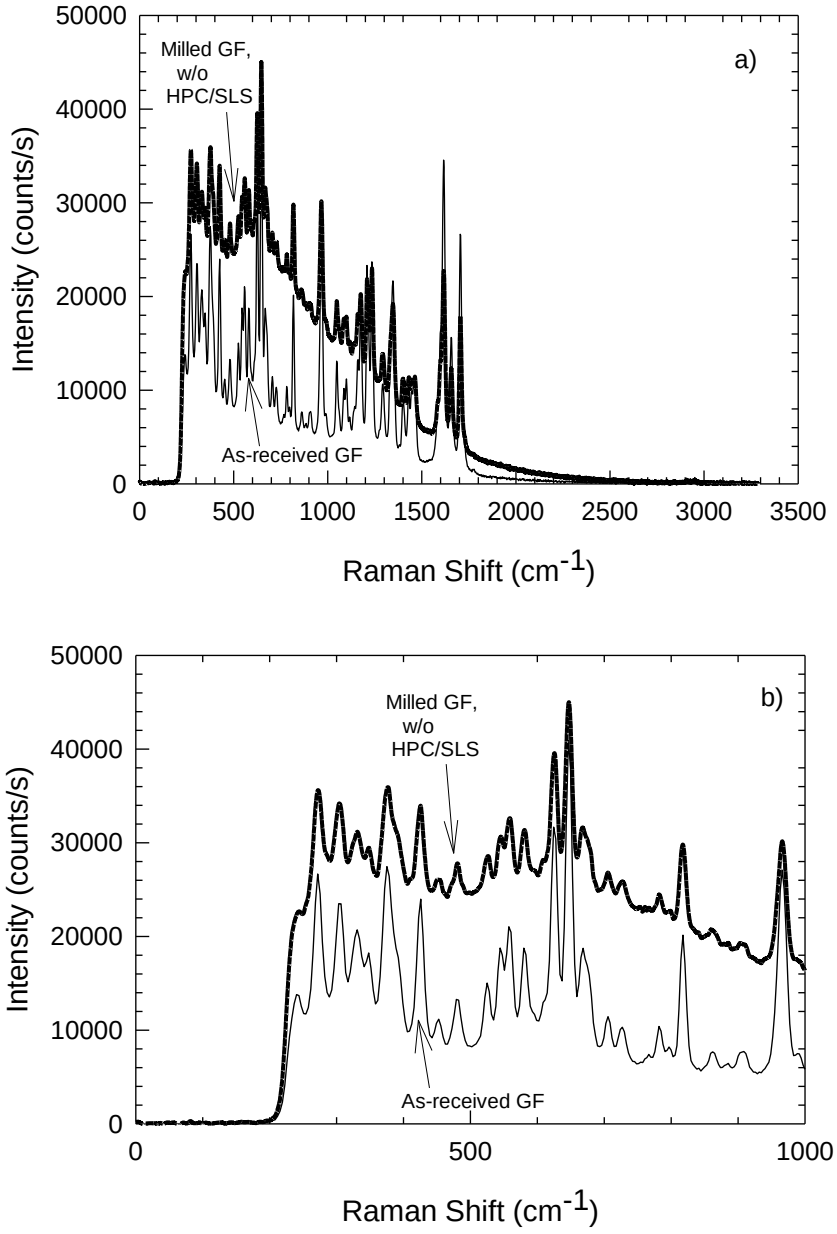

Figure 6.4 Raman spectra of as-received and milled/dried GF w/o HPC/SLS (Run 5): (a) the 0 to 3500 cm^{-1} region, (b) expanded view of the 0 to 1000 cm^{-1} region.

In order to support the findings from the DSC analysis, an extensive characterization was performed on as-received and milled/dried GF samples using Raman spectroscopy and PXRD. The Raman spectra of the as-received and milled/dried samples of GF were very similar, with characteristic peaks occurring at similar frequencies

(Figure 6.4). The occurrence of a doublet peak in the ~640 cm^{-1} region is attributed to the C–Cl stretching mode in the GF molecule (Feng et al., 2008; Zarow et al., 2011). Only a single peak would appear at this frequency if the samples were amorphous. More importantly, the ~820 cm^{-1} line, attributed to the cyclohexanone ring stretching vibration, is well-known to disappear upon a decrease in GF crystallinity (Zarow et al., 2011), while a sharp peak is still visible after milling in the milled sample.

The PXRD pattern of the milled/dried sample was similar to that of the as-received GF sample (Figure 6.5), with some reduction in peak heights. The peak positions were very similar to the published experimental and computed PXRD patterns of pure, crystalline GF in the literature (Feng et al., 2008; Zarow et al., 2011). Therefore, Raman spectra and PXRD patterns appear to support the findings from the DSC analysis in that wet media milling did not significantly change the crystalline nature of GF within the detection limits of the respective equipment. The reduction in PXRD peak heights could be attributed to small amount of defects formed at the particle surfaces and nanocrystalline nature of the particles produced by the wet media milling (Feng et al., 2008; Zarow et al., 2011). In the absence of water, cryomilling of GF and indomethacin led to significant reduction in crystallinity: transformation to amorphous form and crystal defects (Feng et al., 2008; Sharma et al., 2009; Zarow et al., 2011). Interestingly, in the presence of *water*, cryogrinding did not produce amorphous phase for indomethacin (Sharma et al., 2009). Plasticizing action of water on the newly formed amorphous content and ensuing rapid recrystallization could be one mechanism (Sharma et al., 2009). In wet media milling, besides having a plasticizing effect, water allows fast and

effective cooling during particle breakage, which can minimize formation of local hot spots on particle surfaces and thus reduce the extent of surface amorphization.

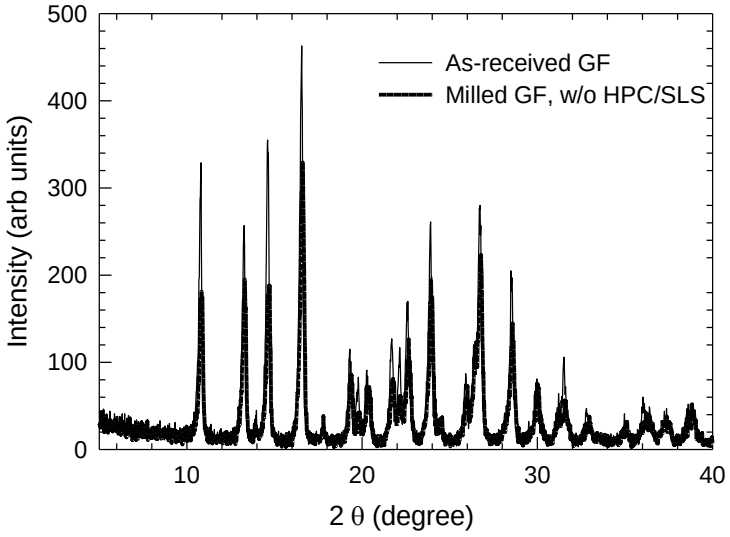

Figure 6.5 PXRD patterns of the as-received GF and milled/dried GF w/o HPC/SLS (Run 5).

6.3.1.2 Evolution of Particle Size during Milling: Effects of Operation Mode.

Samples were periodically taken from the holding tank at various turnovers or passes corresponding to different processing times. Note that the processing time is typically much larger than the total mean residence time, which is equal to the mean residence time during a single pass multiplied by the number of passes in the multi-pass mode (excluding the remixing time associated with the 50 mL residual suspension). The samples were analyzed using laser diffraction to study the evolution of the PSD. Since the analysis and discussion of the wet stirred media milling dynamics of drugs is scarce (see Bhakay et al., 2011), a thorough analysis will be given here. Figure 6.6 presents the d_{50} and d_{90} evolution during recirculation and multi-pass continuous milling of GF (Runs 1 and 2) and NAP (Runs 6 and 7) at a flow rate of 110 mL/min. For both GF and NAP

cases with either operation mode, upon an increase in processing time, the particle size was reduced almost monotonically and no apparent size increase was observed while an equilibrium (plateau or limiting) particle size was approached or attained after a high number of turnovers or passes (about 8 for GF and 12 for NAP). A size increase may occur in poorly stabilized suspensions during milling if the aggregation rate of produced fine particles exceeds the rate at which large particles and aggregates break (Bhakay et al., 2011). In view of this, the results suggest that particle breakage was the dominant mechanism and aggregation of the particles occurred at a smaller rate than the breakage in the presence of stabilizers during most of the milling process. Of course, as milling progressed long enough, aggregation rate increased upon production of finer (colloidal) drug particles, which could be a reason for the equilibrium (plateau) approached at the high number of turnovers/passes (Knieke et al., 2008, 2009). As the drug particle size decreases, number concentration in the suspension increases and the interparticle distance decreases, leading to more frequent collisions and potentially higher aggregation rate (Bhakay et al., 2011; Sommer et al., 2006). On the other hand, the drastic decrease in breakage rate and observed approach to a plateau size in Figure 6.6 can be partly explained by another factor: as milling progressed, finer particles were produced, which have a much lower specific breakage rate (breakage probability) than the coarser particles and thus are harder to break (Bilgili et al., 2004, 2006, 2008). Population balance models without any aggregation terms (Bilgili, 2007; Bilgili and Capece, 2011) were able to capture the sharp decrease in breakage rate even during the breakage of large microparticles. Considering that nanoparticles are even less likely to break than microparticles (Bilgili et al., 2004, 2006), it can be argued that the approach to or

attainment of a plateau size observed in Figure 6.6 is not solely explained by the aggregation of fine particles (especially nanoparticles), but also by the extremely low breakage probability of such particles.

Recirculation and multi-pass operation modes of GF milling seem to result in a similar evolution of the particle size at 110 mL/min (Figure 6.6). In the case of NAP, the recirculation mode had a slightly faster breakage rate than the multi-pass continuous mode after the first few turnovers/passes. Initially, larger particle size observed in the recirculation mode prior to milling (due to as-received PSD variability) caused a larger particle size in this mode as compared with the multi-pass mode during the first turnovers or passes. In general, at this high flow rate, the evolution of the PSD and final particle size after 16 turnovers or passes were very similar. Figure 6.7 illustrates the particle size evolution during GF (Runs 3 and 4) and NAP (Runs 8 and 9) milling at a reduced flow rate of 55 mL/min. Again, after the first or second turnover/pass, recirculation mode had a greater breakage rate than the multi-pass mode. The impact of the initial size difference seems to disappear after the second turnover/pass.

A cursory look at Figures 6.6 and 6.7 suggests that a larger disparity between the milling modes occurred when milling was performed at a reduced flow rate. This could be partly explained by the presence of 50 mL residual (unmilled) suspension (about 10% of the total suspension) that had to be left unprocessed in the milling chamber and tubing during each pass of the multi-pass mode. This residual suspension was mixed later on with the milled suspension in the receiving tank (see Figure 6.1b), and the mixed suspension was then used as the feed to the subsequent pass.

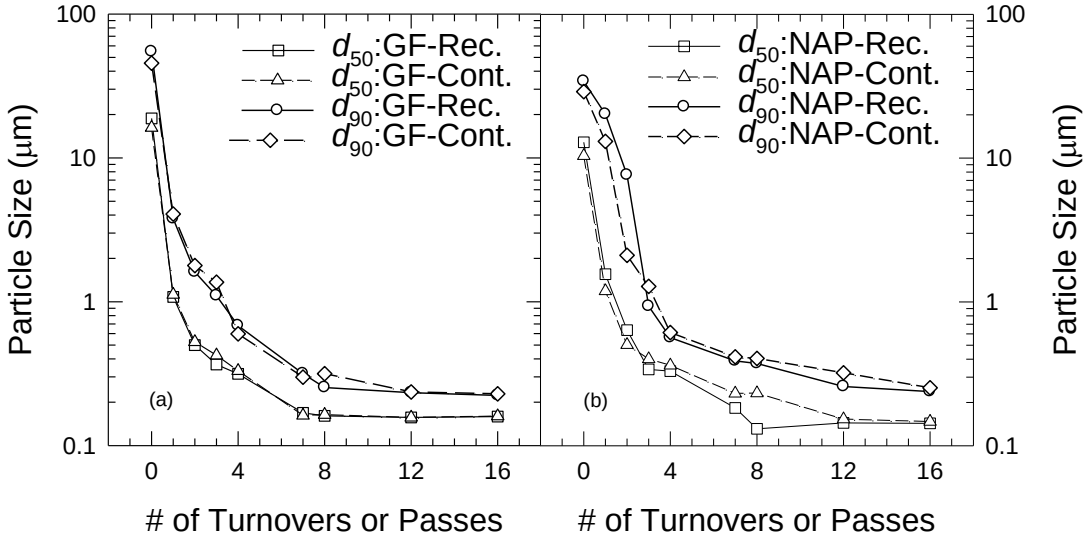

Figure 6.6 Evolution of d_{50} and d_{90} during recirculation and multi-pass continuous modes of wet media milling with 110 mL/min suspension flow rate: (a) Griseofulvin (GF) (Runs 1 and 2), (b) Naproxen (NAP) (Runs 6 and 7).

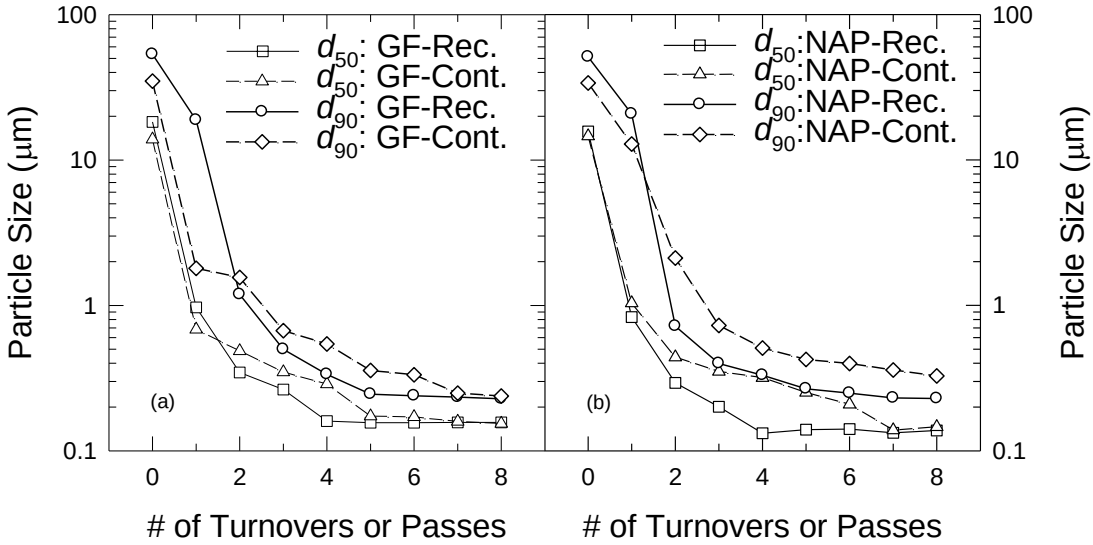

Figure 6.7 Evolution of d_{50} and d_{90} during recirculation and multi-pass continuous modes of wet media milling with 55 mL/min suspension flow rate: (a) Griseofulvin (GF) (Runs 3 and 4), (b) Naproxen (NAP) (Runs 8 and 9).

Hence, some 10% of the particles were subjected to no milling action in a given pass during the multi-pass mode, which may have contributed to the observed smaller breakage rate for both GF and NAP. This may also explain the larger d_{90} for NAP even after 8 turnovers in the multi-pass mode as compared with that in the recirculation mode (see Runs 8 and 9 in Table 6.2). This effect of the residual suspension is expected to disappear as the number of passes increases because further mixing of the residual suspension and the milled suspension takes place. There were 8 passes associated with 55 mL/min flow rate as opposed to 16 passes at 110 mL/min, leading to a reduction of the number of times the residual suspension in the milling chamber was mixed with the milled product in the holding tank and subsequently milled for the former case. It should be noted that the effect of the residual suspension will completely disappear as the ratio of residual suspension to total suspension volume decreases (larger scales and/or larger product volumes).

6.3.1.3 Effects of the Suspension Flow Rate. To analyze the milling dynamics more quantitatively, the median particle size (d_{50}) data presented in Figures 6.6 and 6.7 were fitted by the following two-parameter empirical model shown in Eq. (2.7) (See Chapter 2.3).Table 6.4 presents the values of the parameters d_{lim} and τ_{p} as well as some fitting statistics. The coefficient of determination (R^2) and the sum of squared-residuals (SSR) gauge the accuracy with which the model explains the deviations from the experimental data. An R^2 value approaching 1 and small SSR values reflect good accuracy. Table 6.4 shows an acceptable fit of the data (R^2 values greater than or equal to 0.92). COV% is defined as the ratio of the standard deviation to the mean of the estimated parameter, where a lower value makes the parameter more precise and more

certainly non-zero. In addition, p-values less than 0.05 indicate that the parameters are non-zero and statistically significant. All p-values (not shown in table) for the parameters shown in Table 6.4 were found to be less than 0.006, signifying the statistical significance of the model parameters.

The estimated d_{lim} values (Table 6.4) are almost identical to the experimental median particle sizes obtained after total milling time of 64 min (Table 6.2), except for Runs 4 and 8, thus giving some credence to the purely empirical model (Eq. (2.7)). Even for Runs 4 and 8, the experimental median size was within two standard deviation of the estimated d_{lim}.

Table 6.4 Parameter Estimates from the Empirical Model Fit (Eq. (2.7)) to the Milling Data with Statistical Analysis

Run No.[a]	d_{lim}, COV% (μm), (–)	τ_p, COV% (min), (–)	R^2 (–)	*SSR* (–)
1	0.159 (5.98)	5.59 (8.93)	0.980	1.32×10^{-2}
2	0.156 (6.37)	6.06 (8.93)	0.980	1.39×10^{-2}
3	0.155 (4.75)	6.45 (9.25)	0.983	9.76×10^{-3}
4	0.128 (12.8)	16.3 (12.1)	0.978	9.66×10^{-3}
6	0.148 (8.84)	4.67 (10.8)	0.969	3.16×10^{-2}
7	0.179 (12.0)	5.88 (17.8)	0.920	5.09×10^{-2}
8	0.136 (3.40)	5.78 (7.29)	0.990	5.50×10^{-3}
9	0.145 (18.5)	12.5 (17.7)	0.925	4.20×10^{-2}

[a]Note: Data for Runs 5 and 10 were not fitted as the suspensions were not physically stable.

The main interest lies in the time constant (τ_p). Comparing τ_p values of different milling modes at a flow rate of 110 mL/min (Runs 1 vs. 2 for GF and Runs 6 vs. 7 for NAP), analysis from the model fit illustrate that the breakage in the recirculation mode of milling was slightly faster than the breakage in the multi-pass continuous mode. Comparing the same processes at a reduced flow rate (Runs 3 vs. 4 and Runs 8 vs. 9) led to confirm this finding. Moreover, an additional evidence for the increased disparity between the recirculation and multi-pass continuous modes of milling at the lower

suspension flow rate (55 mL/min) can be observed. This was partly ascribed to the 50 mL residual suspension in the multi-pass mode, but it could also be related to the degree of back-mixing taking place in the milling chamber (see below).

A comparison of the empirical model fit parameters from Runs 1 vs. 3, Runs 2 vs. 4, Runs 6 vs. 8, and Runs 7 vs. 9 in Table 6.4 shows that the runs with a suspension flow rate of 55 mL/min had a larger characteristic time constant than the runs with a suspension flow rate of 110 mL/min. This suggests a slower overall breakage rate at the lower suspension flow rate. Comparing Figures 6.6 and 6.7 suggests a wider PSD at the reduced flow rate. Since a study of the residence time distribution (RTD) of particles in the mill is beyond the scope of this chapter, few limited studies will be mentioned from the literature to discuss the effects of the suspension flow rate from the RTD perspective. During wet media (bead) milling of various materials, an increase in the suspension flow rate caused a tightening of the RTD (Deutsche Keramische Gesellschaft, 2009; Kula and Schütte, 1987; Stehr, 1982) (less back-mixing) or that a decrease led to widening of the RTD (Stehr and Schwedes, 1983). Within the context of the convection–dispersion model (Schwedes and Bunge, 1993; Stehr, 1984), the RTD in a wet stirred media mill may be described by a single dimensionless number called Péclet (Pe) number: $Pe = VL/D$. Here, V is the average axial velocity of the suspension, L is the length of the horizontal mill chamber, and D is the axial dispersion coefficient. A Pe value of 0 describes an ideal, perfectly well-mixed vessel (perfect back-mixing), whereas a Pe value of ∞ describes ideal, plug-flow vessel (no back-mixing). Obviously, real systems operate somewhere in between these two extreme, idealized back-mixing scenarios: Pe for stirred bead mills usually varies from 0.6 to 5 depending on the operational conditions (Schwedes and

Bunge, 1993). This suggests that the mixing condition in stirred media mills is closer to that of a perfectly well-mixed vessel (Folger, 1999). From the definition of Péclet (Pe) number, one can see that an increase in the suspension flow rate leads to a larger Pe (tighter RTD) through a proportional increase in *V* (with negligibly small increase in *D*), which in turn leads to a tighter and usually finer PSD during milling (Deutsche Keramische Gesellschaft, 2009; Schwedes and Bunge, 1993; Stehr, 1982, 1984; Stehr and Schwedes, 1983). Population balance modeling of continuous mills demonstrated that the PSD is tighter and finer for a mill with no back-mixing (plug-flow) than that with perfect mixing (Bilgili and Scarlett, 2005), thus suggesting a higher overall breakage rate for the plug-flow case. In summary, the wider PSD and reduced overall breakage rate associated with the decrease in the suspension flow rate could be explained by a decrease in the Péclet (Pe) number (widening of the RTD).

6.3.2 Role of Stabilizers in Wet Media Milling

During wet media milling of materials, stabilizers such as polymers and surfactants, also known as grinding aids, can affect or play a major role in three phenomena: stabilization of the suspension and proper dispersion of the product particles, microhydrodynamics during media milling as affected by suspension rheology, and particle strength (El-Shall and Somasundaran, 1984; Klimpel, 1999). In a suspension, electrically neutral polymers like HPC stabilize particles by steric forces that are created by protruding large chains after polymer adsorption onto the particle surfaces (steric mechanism); whereas anionic surfactants like SLS can render the particles negatively charged after adsorption, which increases the electrostatic repulsion among adjacent particles and thereby preventing particle aggregation (electrostatic mechanisms) (El-Shall and Somasundaran, 1984;

Klimpel, 1999). Combination of polymers (like HPC) and surfactants (like SLS) is known to have synergistic stabilizing effects (Basa et al., 2008; Ryde and Ruddy, 2002). It is interesting to note that most pharmaceuticals literature on wet media milling focused on the first phenomena, i.e., stabilization and proper dispersion of the particles (e.g. Bruno et al., 1996; Ghosh et al., 2011; Lee et al., 2008; Singh et.al., 2011), thus largely neglecting the impact of the stabilizers on the microhydrodynamics and the particle strength (associated with the Rehbinder effect). The so-called Rehbinder effect (Rehbinder, 1958) is defined as the reduction in surface energy and surface structure change upon adsorption of surface-active agents, which leads to an increase in ductility, reduced hardness, and enhanced crack propagation in various materials (Butyagin, 1999; Karpenko, 1974; Rehbinder and Shchukin, 1972; Shchukin, 2006), thus potentially enhancing the breakage of particles during wet milling operations (Butyagin, 1999; Rehbinder, 1958; El-Shall and Somasundaran, 1984). Unfortunately, up to now, sufficient experimental data are not available to prove or disprove the Rehbinder effect during milling processes (Kissa, 1999; Tadros, 1994) perhaps due to the aforementioned confounding effects of the stabilizers.

6.3.2.1 Stabilization and Rehbinder Effect. Milling experiments were carried out under identical conditions (same set points for the process variables) in the presence and absence of stabilizers (HPC/SLS) toward elucidating the roles of stabilizers. To this end, particle sizing via laser diffraction (LD), SEM imaging, and BET nitrogen adsorption were used. The Sauter-Mean Diameter (SMD) was calculated separately from the LD particle size distribution data on milled suspension samples and the specific surface area (SSA) (BET adsorption on dried suspension samples). No BET adsorption was performed

on samples with the stabilizers as the particle surfaces were covered by excessive amounts of the stabilizers, which could prevent accurate measurement of the SSA without yielding a good estimate of the primary particle size. Table 6.5 summarizes the calculated SMD values. A suspension of GF without the stabilizers (HPC/SLS) was prepared and milled in the multi-pass continuous mode (Run 5). The PSD was obtained and compared to that of the milled GF in the presence of the stabilizers (Run 2).

Table 6.5 Sauter-Mean Diameter (SMD) of the Milled GF and NAP

Run No.	Drug	Stabilizers Added Before Milling	Stabilizers Added After Milling	Measurement Method[a]	SMD (μm)
2	GF	2.5% HPC/0.5% SLS	—	LD	0.153
5	GF	—	—	LD	1.48
5	GF	—	—	BET	0.522
5	GF	—	2.5% HPC/0.5% SLS	LD	0.479
7	NAP	2.5% HPC/0.5% SLS	—	LD	0.130
10	NAP	0% HPC/0.08% SLS	—	LD	0.563
10	NAP	0% HPC/0.08% SLS	—	BET	1.12

[a]LD (laser diffraction) was performed on wet suspension samples, whereas BET nitrogen adsorption was performed on oven-dried suspensions after degassing.

Figure 6.8 illustrates that in the absence of the stabilizers, GF suspension exhibits a bimodal PSD, possibly indicating the presence of primary nanoparticles and their aggregates of various sizes (to be confirmed with SEM imaging and BET adsorption analysis). On the other hand, the PSD of GF suspension milled with the stabilizers shows a tight, unimodal distribution of particle sizes in the range of about 100–200 nm. Figure 6.9 presents the SEM images of the dried samples from Runs 2 and 5. Figure 6.9a shows GF milled in the absence of the stabilizers (Run 5) at low magnification, with mostly aggregated particles sized between 1 and 20 μm in size. Further magnification of these

particles (Figure 6.9b) shows the existence of primary nanoparticles with a size range of 150–600 nm. To compare these results, SEM images of the GF milled in the presence of the stabilizers in both recirculation and multi-pass continuous modes (Runs 1 and 2) (Figure 6.9c and 6.9d) are shown, where primary particles sized between 100–200 nm can be observed.

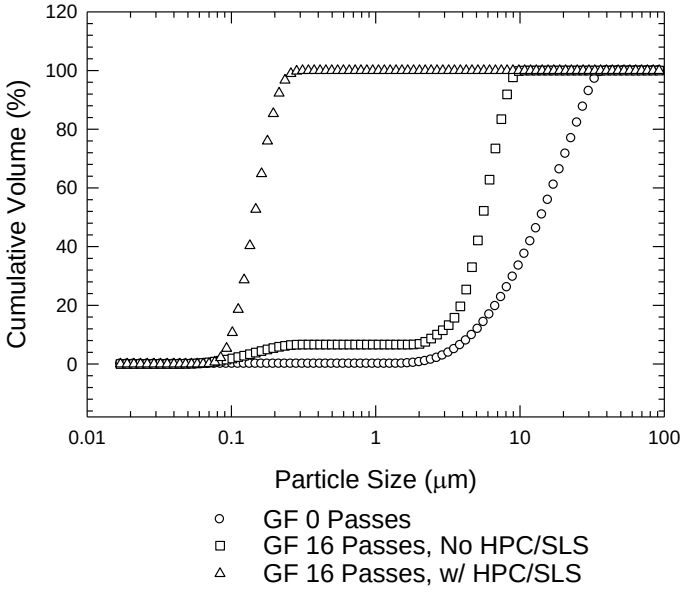

Figure 6.8. Effect of polymer/surfactant (HPC/SLS) on the particle size distribution of milled GF (Runs 2 and 5).

The SEM imaging appears to corroborate the laser diffraction results: Run 5 suspension, being unstable in the absence of the stabilizers, consists of some nanoparticles and their aggregates (primary particle sizes in the size range of 150–600 nm), whereas Run 2 suspension, being stable in the presence of the stabilizers, consists of primary nanoparticles in the size range of 100–200 nm (see both Figure 6.9d and Figure 6.8) with minimal amount of aggregates. This suspension was also physically stable over 7-day storage (see Table 6.2).

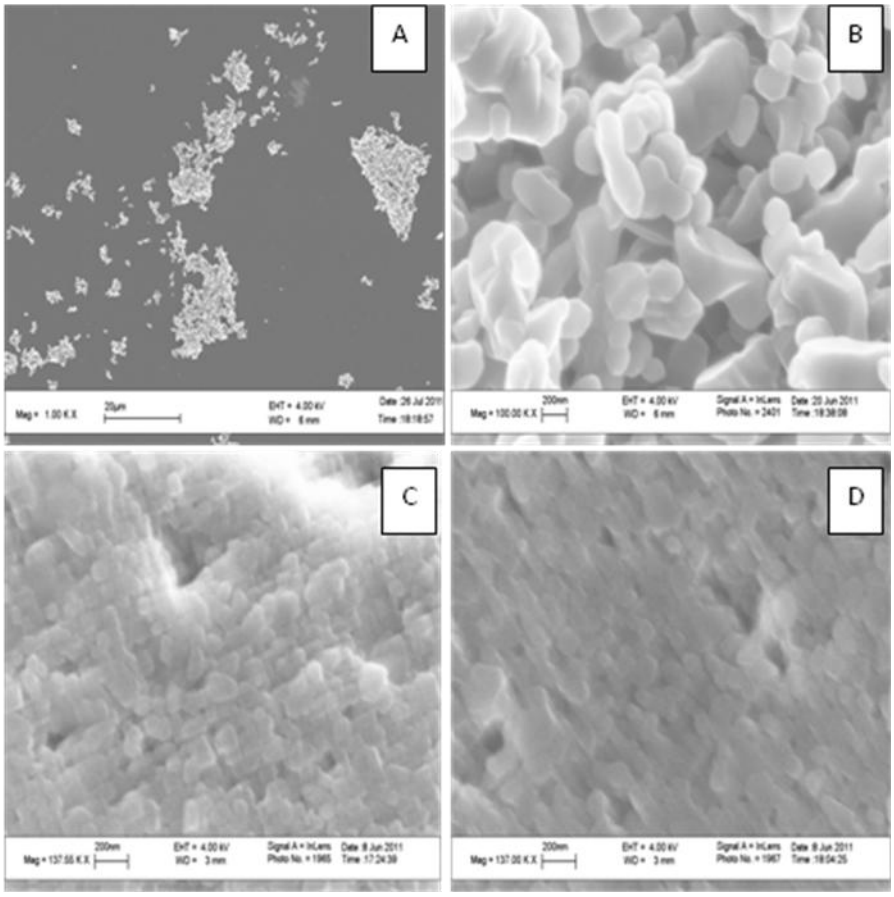

Figure 6.9 SEM images of milled Griseofulvin (GF): (a) milled in multi-pass continuous mode for 16 passes w/o HPC/SLS at 1.5 kX (Run 5), (b) milled in multi-pass continuous mode for 16 passes w/o HPC/SLS at 100 kX (Run 5), (c) milled in recirculation mode for 16 turnovers w/ HPC/SLS at 137 kX (Run 1), (d) milled in multi-pass continuous mode for 16 passes w/ HPC/SLS at 137 kX (Run 2).

In the absence of the stabilizers (HPC/SLS), the nanoparticles formed by the breakage of GF particles in Run 5 aggregated extensively in the suspension due to their large surface area, high number concentration, and strong attractive interparticle forces (van der Waals and hydrophobic interactions (El-Shall and Somasundaran, 1984; Kissa, 1999). On the other hand, due to the synergistic stabilizing action of adsorbed HPC/SLS (Basa et al., 2008; Ryde and Ruddy, 2002), the nanoparticles were protected against aggregation during the milling and storage, and thus a stable suspension formed in Run 2.

Besides its interaction with HPC, SLS helps wetting the particles and aggregates that may have formed instantaneously during the milling. SLS also helps fluid penetration into aggregate pores, which may in turn facilitate the deaggregation of these aggregates into primary particles during the milling (Kissa, 1999).

All of these aspects that relate to the stabilization/dispersion phenomena are widely recognized within the pharmaceuticals field. Polymers and surfactants have a major role in wet media milling: they stabilize particles against aggregation and ensure the production of a stable, properly dispersed suspension. On the other hand, a more important conclusion can be drawn from the aforementioned SEM images: the primary GF nanoparticles formed in the presence of the stabilizers (Run 2, 100–200 nm) appear to be smaller than those formed in the absence of the stabilizers (Run 5, 150–600 nm). In other words, the stabilizers facilitated the particle breakage and caused the formation of smaller primary particles during the milling. This is the first piece of evidence for the Rehbinder effect of HPC/SLS during the wet milling of GF particles. To gather additional evidence, Sauter-Mean Diameter (SMD) values calculated from LD and BET analysis were compared (see Table 6.5). The SMD values obtained from the LD data were 1.48 µm for Run 5 sample (no stabilizers) and 0.153 µm for Run 2 sample (with the stabilizers). From the BET analysis, SSA and SMD values were 8.21 m^2/g and 0.522 µm for Run 5 sample. The SMD calculated from SSA (BET nitrogen adsorption) is a good measure of the true primary particle size in a powder with aggregates (Vital et al., 2008). For Run 5 (without stabilizers), the SMD value of 0.522 µm (BET) vs. 1.48 µm (LD) confirms that Run 5 particles in the suspension consist of nanoparticles and their aggregates. More importantly, while noting the difference in the respective measurement

techniques, with the SMD value of 0.522 µm (BET) and the observed primary particle size range of 150–600 nm (SEM), it can be confirmed that Run 5 (no stabilizers) primary particles are indeed larger than those of Run 2 (with stabilizers), thus giving credence to the existence of the Rehbinder effect.

It is argued that stabilizers can be added to a milled drug suspension (without stabilizers) at the end of the milling process, which may result in a similar PSD to that obtained with initial addition of the stabilizers (standard procedure). If this were the case, the Rehbinder effect could be refuted because the stabilizers would not appear to facilitate the particle breakage (Bhakay et al., 2011). Toward testing this hypothesis, HPC/SLS was dissolved in 50 mL Run 5 sample by mixing for 15 min (GF suspension obtained from the 16 passes of the multi-pass continuous milling in the absence of the stabilizers) to prepare a suspension with 2.5% HPC and 0.5% SLS while keeping GF loading at 10%. This sample was then sonicated for 35 min to facilitate the efficient deaggregation of the aggregates in Run 5 based on the learning from a comprehensive redispersion study on drug nanoparticle deaggregation (Bhakay et al., 2013). PSD data obtained from laser diffraction of Run 5 sample after HPC/SLS addition shows an SMD of 0.479 µm (Table 6.5), which was much larger than the SMD value for the Run 2 sample (0.153 µm) with the stabilizers added at the beginning of the milling. Similar information can be gained from a comparison of the SEM images in Figure 6.9d (Run 2) and 10 (Run 5, after HPC/SLS addition): the primary particles appear to be smaller when the stabilizers were added at the beginning of the milling (Figure 6.9d) as opposed to the case where the stabilizers were added at the end of milling (Figure 6.10). Hence, the Rehbinder effect cannot be refuted.

Similar to the analysis performed on GF, the PSD of NAP milled with no HPC/0.08% SLS (Run 10) was obtained and is shown in Figure 6.11, along with NAP milled in the presence of HPC/SLS (Run 7). Figure 6.11 suggests that NAP milled with no HPC/0.08% SLS produced a bimodal distribution, which indicates the presence of primary nanoparticles and their aggregates (see also Figure 6.12), while the PSD of NAP milled with stabilizers shows a tight, unimodal distribution with particle sizes in the range of 50–250 nm. The LD analysis yielded SMD values of 0.130 µm and 0.563 µm for Runs 7 and 10 respectively (Table 6.5). BET adsorption analysis yielded an SMD value of 1.12 µm (SSA = 4.45 m^2/g). SEM image of Run 10 viewed under low magnification is provided in Figure 6.12a: aggregated particles can be seen. Further magnification of these aggregated particles (Figure 6.12b) shows evidence of primary particles with a size range of about 200–1000 nm. Figures 6.12c and 6.12d (Runs 6 and 7) show primary nanoparticles sized mostly between 100–200 nm when HPC/SLS combination was used during the milling. The above results from SMD data and SEM imaging confirms the presence of larger primary particles in the case of no HPC/0.08% SLS than in the case of 2.5% HPC/0.5% SLS, and that the suspension was not properly stabilized in the former case. These findings provide evidence for the Rehbinder effect in NAP milling; however, a cautionary note that the presence 0.08% SLS (albeit much smaller than the CMC of SLS) may confound some of the above findings in NAP case. However, it was not feasible to process NAP particles consistently and reproducibly due to poor wetting of NAP in the absence of the surfactant.

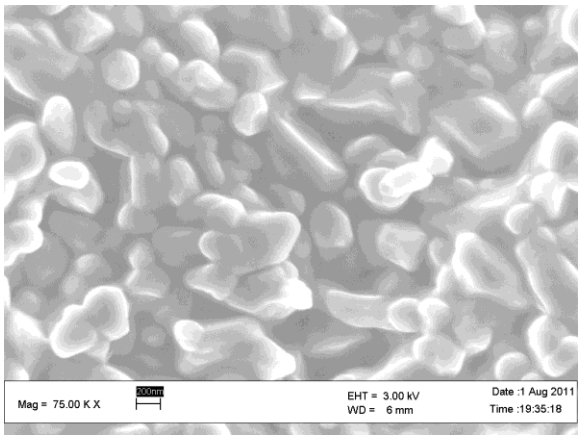

Figure 6.10 SEM image (magnification at 75 kX) of Griseofulvin (GF) particles after milling in multi-pass continuous mode for 16 passes in the absence of HPC/SLS (Run 5) followed by addition of 2.5% HPC and 0.5% SLS with sonication for 35 min.

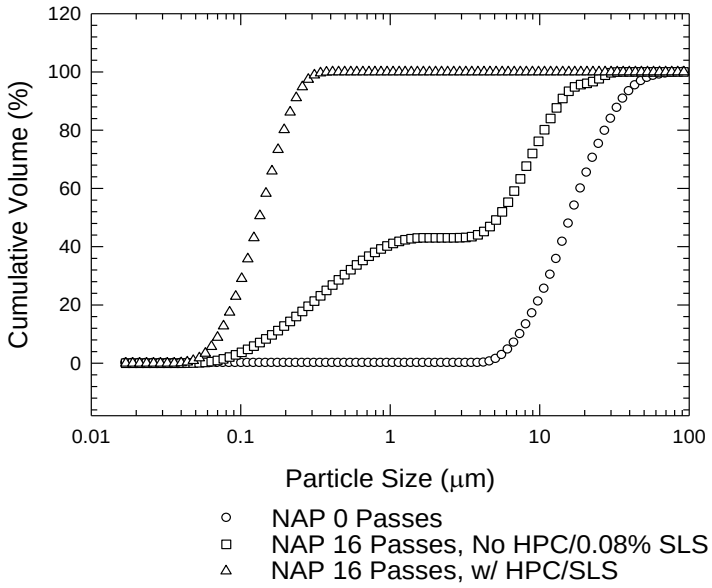

Figure 6.11 Effect of polymer/surfactant (HPC/SLS) on the particle size distribution of milled Naproxen (NAP) (Runs 7 and 10).

6.3.2.2 Suspension Rheology and Microhydrodynamics. One may argue that the aforementioned positive effects of the presence of stabilizers in the production of finer primary drug particles and stable nanosuspensions could have resulted from the

stabilizers' impact on the suspension rheology and microhydrodynamics in the mill. Toward testing this hypothesis, the apparent shear viscosity of the milled GF suspensions (Runs 2 and 5) as a function of shear rate was measured (see Figure 6.13).

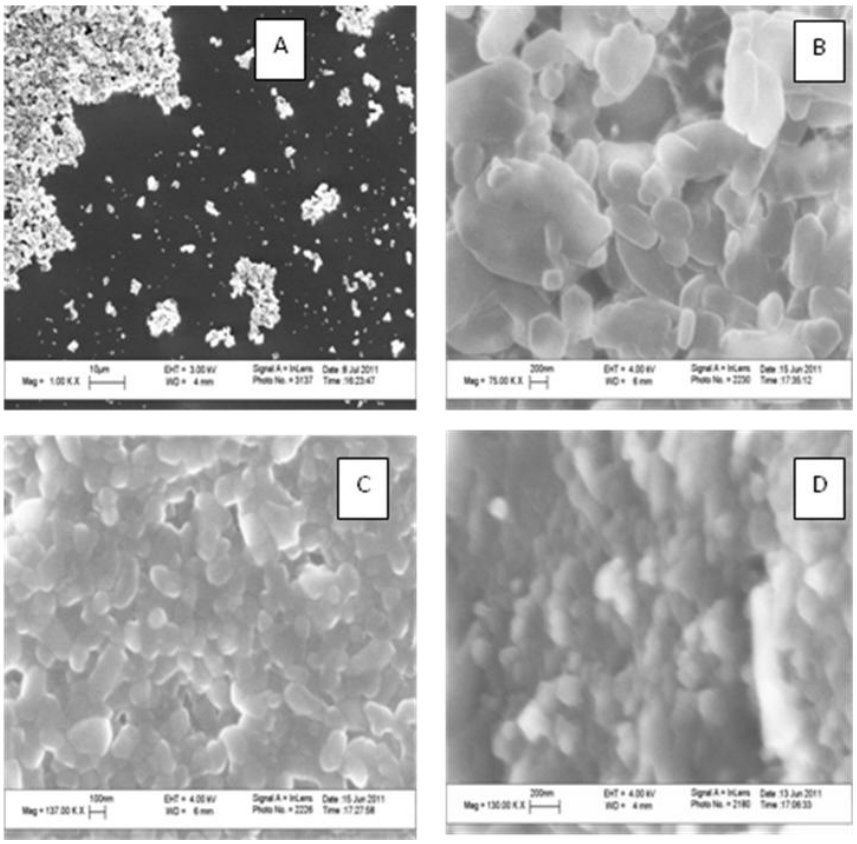

Figure 6.12 SEM images of milled Naproxen (NAP): (a) milled in multi-pass continuous mode for 16 passes w/o HPC and with 0.08% SLS at 1.0 kX (Run 10), (b) milled in multi-pass continuous mode for 16 passes w/o HPC and with 0.08% SLS at 75 kX (Run 10), (c) milled in recirculation mode for 16 turnovers w/ HPC/SLS at 137 kX (Run 6), (d) milled in multi-pass continuous mode for 16 passes w/ HPC/SLS at 130 kX (Run 7).

The stabilized GF suspension with minimal aggregation (Run 2, with HPC/SLS) exhibits a Newtonian fluid behavior above a shear rate of 150 1/s, whereas the unstable GF suspension with aggregates (Run 5, without HPC/SLS) exhibits a strong shear-thinning behavior due to extensive deaggregation of the aggregates with increasing shear rate. The apparent viscosity of Run 5 suspension tends to plateau as the shear rate approaches 1000

1/s. These observations are in line with other suspension rheology studies (Barthelmes et al., 2010; Bernhardt et al., 2010; Vital et al., 2008). Although the shear rate in media mills usually exceeds 1000 1/s, most earlier work considered 1000 1/s as a representative value for the high shear rate in their analysis (Barthelmes et al., 2010; Bernhardt et al., 2010; Knieke et al., 2010; Vital et al., 2008). As can be seen from Figure 6.13, for both suspensions, the apparent shear viscosities approach a constant value near 1000 1/s; hence, taking the viscosity value at a shear rate of 1000 1/s does not cause a serious flaw within the context of the microhydrodynamic analysis presented below.

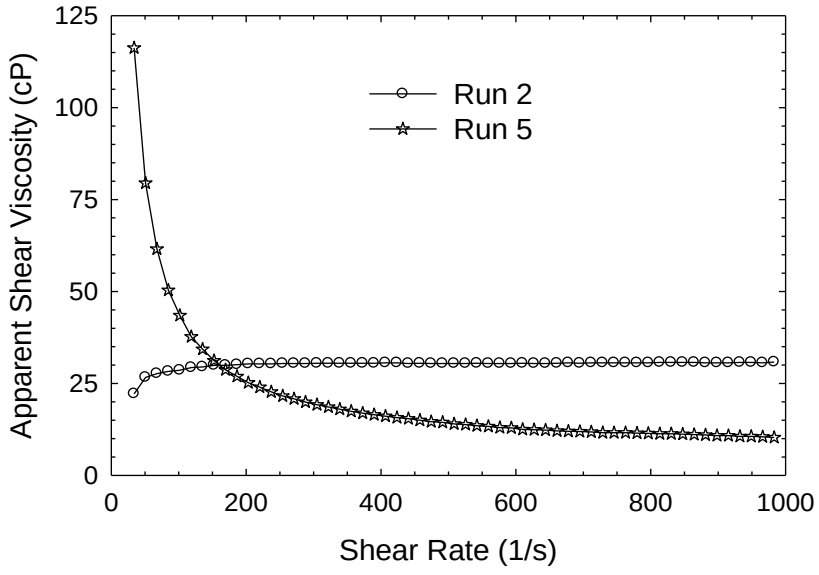

Figure 6.13 Variation of the apparent shear viscosity as a function of the shear rate at 25 ^{o}C for the milled Griseofulvin (GF) suspensions: with stabilizers (Run 2) and without stabilizers (Run5).

A microhydrodynamic analysis of wet stirred media mills has been recently developed to simulate the impact of mill rotor speed and bead type/size on the bead–bead collisions and to relate the responses from these simulations to some general observations from wet media milling experiments (Eskin et al., 2005a, 2005b). The

microhydrodynamic analysis have been used to explain the experimentally observed "viscous dampening" phenomenon (see Chapter 3) during the wet media milling of high drug–polymer loaded suspensions (Bilgili and Afolabi, 2012). According to this theoretical approach, the specific power applied to the mill rotor (P_w) dissipates through the fluctuating motions of the beads at the micro-scale, which is mathematically expressed in Chapter 2.4. Table 6.6 presents the measured parameters P_w, ρ_L, and μ_L and calculated values of θ, u_b, and ν. Milling in the absence of the stabilizers (Run 5) led to slightly higher θ, u_b, and ν values than milling in the presence of the stabilizers (Run 2).

Table 6.6 Measured Parameters (P_w, ρ_L, and μ_L) and Calculated Microhydrodynamic Parameters (θ, ν, and u_b) for Milling of GF

Run No.	P_w (W/m^3)	ρ_L (kg/m^3)	μ_L (cP)	θ (m^2/s^2)	ν (1/s)	u_b (m/s)
2	1.24×10^{6}	1037	31.0	2.28×10^{-2}	6.47×10^{3}	2.41×10^{-1}
5	7.89×10^{5}	1008	10.4	2.61×10^{-2}	6.92×10^{3}	2.58×10^{-1}

The microhydrodynamic analysis suggests that slightly faster particle breakage and finer primary particles should have been observed in the absence of the stabilizers because the higher values of θ, u_b, and ν mean more intense and frequent bead–particle collisions in the mill. However, the experimental findings presented earlier suggest otherwise. Therefore, the aforementioned positive effects associated with the use of the stabilizers (proper stabilization/dispersion and facilitation of the particle breakage or Rehbinder effect) did occur despite the less favorable microhydrodynamics in the mill.

6.4 Summary and Conclusions

Two poorly water-soluble drugs, Griseofulvin and Naproxen, were milled in a wet stirred media vessel using the recirculation mode and the multi-pass continuous mode at two different suspension flow rates. Breakage dynamics was assessed using an empirical model fit of the median particle size. The roles of stabilizers (HPC and SLS) have been elucidated by performing experiments in the presence/absence of stabilizers and characterizing the milled suspensions and dried suspensions via laser diffraction, BET nitrogen adsorption, and SEM imaging. Based on characterization with DSC (on both GF and NAP), PXRD (on GF), and Raman spectroscopy (on GF), the crystallinity of the drugs has been largely preserved after wet media milling. Continuous production of drug nanoparticles and stable nanosuspensions has been successfully demonstrated in the multi-pass continuous mode, which in general yielded similar PSDs to those obtained from the recirculation mode especially at the high flow rate. The deviations observed between the two operation modes is attributed to the 50 mL residual suspension in each pass during the multi-pass operation mode. The observed decrease in the breakage rate during the milling and approach to a plateau size upon prolonged milling were explained thoroughly in view of the lower specific breakage rate (breakage probability) of produced finer particles and the equilibrium between breakage and aggregation. When the flow rate was halved keeping the same total milling time (half number of passes), the overall breakage rate decreased and PSD widened because of a decrease in the Péclet number (widening of the residence time distribution). This also led to more disparity between the two modes of operation. The implications of the findings from a formulation/process development perspective are

a) Formulation development with nanosuspension formulations, even those intended for continuous manufacturing, can be performed in the batch or recirculation mode. The formulation, stabilization, and processing knowledge generated can be transferred to continuous operations without major difficulty.

b) Multi-pass mode can be automated to allow passes between two holding tanks in a swing/pendulum fashion, which will reduce development time significantly toward predicting the number of mills required for true (cascade) continuous milling operation.

c) In a true continuous milling process, a cascade of 6–12 media mills in series can lead to production of drug nanosuspensions. The exact number depends on the drug properties, formulation, and specific milling equipment as well as the desired/target drug particle size.

Through a comparative analysis of laser diffraction data, SEM images, and BET-based Sauter-Mean Diameter, this study has provided sufficient evidence for the existence of the Rehbinder effect during the milling of poorly water-soluble drugs. Not only do polymers/surfactants allow proper stabilization/dispersion of the nanoparticles in the suspensions (major effect), but they also facilitate drug particle breakage (minor–moderate effect). These positive effects of the stabilizers did occur despite the less favorable microhydrodynamics in the mill. In a future study, polymers and surfactants with a wide concentration range will be separately studied to elucidate their individual roles in the Rehbinder effect.

CHAPTER 7

OVERALL SUMMARY AND CONCLUSIONS

In the preceding chapters, a comprehensive investigation of the production of Griseofulvin nanosuspensions in a wet stirred media mill operating in both the recirculation and continuous modes has been carried out. From a process engineering perspective, many important conclusions can be drawn. The findings in the preceding chapters suggest that physically stable nanosuspensions of BCS Class II drugs can be produced via wet stirred media milling (WSMM) with a judicious and synergistic use of cellulosic polymers and surfactants. This solvent-free process appears to be robust, yielding reproducible suspensions with high drug loading and minimal media contamination. It can be carried out in batch, recirculation, and multi-pass continuous modes successfully. The as-received and milled particles of two BCS class II drugs namely Griseofulvin (GF) and Naproxen (NAP) were characterized to investigate the crystalline state of the particles. Characterization with DSC (on both GF and NAP), PXRD (on GF), and Raman spectroscopy (on GF), suggests that the crystallinity of the drugs has been largely preserved after wet media milling.

The dissertation work also contributed to the fundamental understanding of the preparation of stable drug nanoparticles suspensions; specifically it (1) indicated the need for a minimum polymeric stabilizer-to-drug ratio for proper stabilization of drug nanosuspensions as dictated by polymer adsorption and synergistic interactions between a polymeric stabilizer and a surfactant, (2) demonstrated the existence of an optimum polymer concentration from a breakage rate perspective in the presence of a surfactant,

which results from the competing effects of viscous dampening and enhanced steric stabilization at higher polymer concentration, (3) developed fundamental understanding of the breakage dynamics–processing–formulation relationships and rationalized preparation of a single highly drug-loaded batch (20% or higher) instead of multiple dilute batches, (4) developed an intensified process for faster preparation of sub-100 nm particles with reduced specific energy consumption and media wear (i.e. minimal drug contamination), and (5) provided evidence for the proof of the Rehbinder effect during the milling of drugs. Not only do the polymers and surfactants allow proper physical stabilization of the nanoparticles in the suspensions, but they also do facilitate drug particle breakage.

To understand the governing mechanism(s) during particle formation, a detailed the roles of stabilizers, i.e., cellulosic polymers and surfactants, were investigated in Chapter 3. Although polymers and surfactants are commonly used as stabilizers to impart physical stability to the suspensions produced by WSMM of poorly-water soluble drugs, scant information is available in pharmaceutical literature regarding their impact on the breakage kinetics. A combined microhydrodynamics–polymer adsorption analysis was implemented in Chapter 3 to elucidate the roles of stabilizers with a focus on the kinetics. Griseofulvin (GF) was milled at various concentrations of hydroxypropyl cellulose (HPC) in the presence–absence of sodium dodecyl sulfate (SDS). Particle sizing, scanning electron microscopy, thermal analysis, and rheometry were used to determine the breakage kinetics, adsorption isotherm, and apparent viscosity, which were then used to analyze the aggregation state of the milled suspensions and the microhydrodynamics. In the absence of SDS, an increase in HPC concentration slowed the particle aggregation

leading to faster apparent breakage. On the other hand, due to a synergistic stabilizing action of HPC with SDS, lower HPC concentration was needed to stabilize the suspensions, and an optimum HPC concentration for the fastest apparent breakage was identified. The microhydrodynamic analysis quantified, for the first time, the viscous dampening effect of polymers, while only the combined analysis could explain the observed optimum.

As the WSMM process is expensive and energy-intensive, it was important to study the breakage kinetics, which determines the cycle time and production rate for a desired fineness. To this end, the impact of stirrer speed, bead concentration, and drug loading on the breakage kinetics was explored via a microhydrodynamic model for the bead–bead collisions. Suspensions of GF were prepared in the presence of two stabilizers: HPC and SDS. Laser diffraction, scanning electron microscopy, and rheometry were used to characterize them. Various microhydrodynamic parameters including a newly defined milling intensity factor was calculated. An increase in either the stirrer speed or the bead concentration led to an increase in the specific energy and the milling intensity factor, consequently faster breakage. On the other hand, an increase in the drug loading led to a decrease in these parameters and consequently slower breakage. While all microhydrodynamic parameters provided significant physical insight, only the milling intensity factor was capable of explaining the influence of all parameters directly through its strong correlation with the process time constant. Besides guiding process optimization, the analysis rationalizes the preparation of a single highly drug-loaded batch (20% or higher) instead of multiple dilute batches.

Chapter 5 presents the design of an intensified WSMM process for the *production of truly nanosized drug particles (1-100 nm) with acceptable physical stability and minimal bead wear*. In pharmacutical literature, 100–300 nm particles were prepared by several hours to days of milling with relatively high energy consumption. A combined experimental and theoretical approach (microhydrodynamic model) was adopted with the ultimate objective of achieving faster production of sub-100 nm BCS class II drug particles with reduced energy consumption. The impact of media (bead) size on the energy consumption and breakage kinetics GF and naproxen (NAP) were elucidated. The baseline process with the optimal bead size was intensified by increasing the stirrer tip speed, bead loading, and suspension flow rate systematically, as guided by the microhydrodynamic model of the process. In all milling experiments, the suspensions were physically stabilized using a low molecular weight neutral polymer -hydroxypropyl methyl cellulose (HPMC-E3) and SDS. Static light scattering, dynamic light scattering, scanning electron microscopy, and powder X-ray diffraction were used to characterize the milled drug particles. Experimental and microhydrodynamic analysis of the milling beads showed that the smallest beads were effective in achieving sub-100 nm median size particles at the end of 6 h, with reduced specific energy consumption due to their relative high energy dissipation rate during the deformation of the particles (mill intensity factor). As guided by the microhydrodynamic model, the mill intensity factor was further increased by the combined use of intense mill parameters, which led to a GF particle size of 83 nm within 30 min of milling. Experimental investigation to produce GF particle size of 100 nm (ball-park size) with use of intensified process showed a 13.6 times reduction in cycle time compared to the baseline process with energy savings up to 43%.

This also led to 86.5% less bead wear (zirconium) contamination in the GF drug suspension as measured by inductive coupled plasma mass spectrometry analysis. Similarly, milling of NAP with intensified process conditions also led to the faster preparation of sub-100 nm particles with reduced specific energy consumption and bead wear. The use of small beads (100 μm) has enabled the intensification of the process, increase the breakage rate, and reduce the energy consumption without causing gross contamination of the drug product with worn-out beads. The intensified process methodology developed in Chapter 5 presents an opportunity for formulators/engineers to design an intensified wet-milling process for production of sub-100 nm drug particles with reduced cycle time and acceptable media contamination and/or to optimize existing wet-milling processes.

In Chapters 3–5, nanoparticles of BCS Class II drugs were produced during WSMM operating in recirculation mode. Scant information is available in the pharmaceutical literature regarding the continuous production of drug nanoparticles via wet media milling. GF and NAP were milled in both recirculation mode and multi-pass continuous mode to study the breakage dynamics and to determine the effects of suspension flow rate (Chapter 6). The evolution of the median particle size was measured and described by an empirical breakage model. The results in Chapter 6 indicate that the two operation modes could produce drug nanosuspensions with similar particle size distributions (PSDs). A reduced suspension flow rate slowed the breakage rate and led to a wider PSD and more differentiation between the two operation modes. The latter part of Chapter 6 focused on the roles of stabilizers (HPC and SDS) and elucidation of the so-called Rehbinder effect (reduction in particle strength due to adsorbed stabilizers such as

polymers and surfactants). Milling the drugs in the absence of the stabilizers produced primary nanoparticles and their aggregates, while milling with the stabilizers produced smaller primary nanoparticles with minimal aggregation. Using laser diffraction, BET nitrogen adsorption, SEM imaging, and a microhydrodynamic analysis of milling, this study, for the first time, provides sufficient evidence for the existence of the Rehbinder effect during the milling of drugs. Not only do the polymers and surfactants allow proper stabilization of the nanoparticles in the suspensions, but they also do facilitate drug particle breakage.

CHAPTER 8

FUTURE WORK

8.1 Develop a Multi-Scale Modeling Approach for WSMM

To gain a fundamental insight into the kinetics of particle breakage and aggregation as well as the stabilization behavior, a multi-scale modeling approach can be employed. In this approach, the combined use of the population balance model (PBM) (process or macro-scale) along with the microhydrodynamic model (micro-scale) will be investigated. The multi-scale modeling approach will be adopted for a recirculation mill so as to model the temporal evolution of the particle size distribution during milling. In Chapters 3 and 4, the impacts of processing/formulation parameters on the microhydrodynamics have been investigated. However, fitting and prediction of the particle size distribution at the macro-scale via the population balance model has not been investigated (see e.g. Bilgili and Scarlett 2005; Bilgili et al. 2006a, 2006b; Sommer et al. 2006 for population balance equation). Birth and death terms for particle aggregation will be introduced. As a major novelty, the specific breakage rate k will be correlated to granular temperature θ, thus enabling a first connection between the micro–macro scales. PBM should also be used to elucidate diferrent breakage and aggregation mechanism.

8.2 Process Intensification for Formation of Sub-100 Nm Particles with Multiple Drugs: Surfactant-Free Suspensions for Sterile Filtration (Along with Process Intensification)

In Chapter 5, an intensified wet media milling process for faster production of dense, stable drug suspensions with sub-100 nm particles was investigated. The synergistic combination of a polymer anda surfactant was employed, and small milling beads were

used along with intensified process conditions: a high flow rate, high mill tip speed, and a high bead concentration. The short-term physical stability of the drug suspensions was also investigated and the suspensions were stable. The use of surfactants have been identified to be the most effective class of dispersants improving the wettability and redispersibility as compared with soluble polymers and sugars (Bhakay et al., 2012). However, the use of surfactants can affect the long term stability of the suspension upon storage due to Ostwald ripening (Verma 2011; Ghosh, 2011). Other issues such as toxicity of the surfactants due to excess use are a concern in most formulations (Liversidge and Cundy 1995). For inhalation applications, the use of surfactant is either prohibited or utilized at extremely low concentrations due to the toxicity (Suzuki et al. 2000). Future work will focus on the use of multiple drugs along with acceptable polymers/surfactants. Future work should also explore the long term stability of such drug suspensions.

8.3 Formulation Doe for Multiple Drugs and Relate Milling Performance to Physicochemical, Mechanical, and Surface Properties of the Drugs

The task aims at producing stable nanosuspensions of five BCS Class II drugs namely griseofulvin, naproxen, fenofibrate, azodicarbonamide, and phenylbutazone using a combination of HPC and SDS and superdisintegrants. Impact of wet-milled superdisintegrants, as novel dispersants, on the physical stability of the drug suspensions will also be investigated. Few systematic studies related the milling performance to the physicochemical and surface properties of the drugs. Lee et al. (2005; 2008) studied the effect of hydrophobicity of copolymers; Choi et al. (2005) studied the surface energy of polymers on drug stabilization; Choi et al. (2008) and Sepassi et al. (2007) studied the

effect of polymer molecular weight; George and Ghosh (2013) investigated the material property variables (drug and stabilizer) that control the critical quality attributes (CQA) defining a nanosuspension formulation; Cerdeira et al. (2011) investigated the role of milling parameters and particle stabilization of drug materials with similar mechanical properties. The Young's modulus of the drug crystal was measured using in house software and the Hertzian calculation model. Their result suggests that similar mechanical properties of drugs exhibited similar milling behavior. Future work will investigate how milling performance of multiple drugs relate to their physicochemical, mechanical, and surface properties. The physical stability of the suspension should be assessed. Elucidate the structure and the state of the polymer (mono-layer vs. multi-layer coverage) on the surface of drug by experiments and models.

8.4 Is the Adsorbed Polymer or Surfactant Responsible for the Rehbinder Effect?

Chapter 6 sheds light on the role of the combination of polymer and surfactant on the particle strength (Rehbinder effect) and suggests that either stabilizer could have affected the strength of the drug particles. A systematic study with each type of stabilizer (i.e. polymer or surfactant) alone can elucidate whether the observed Rehbinder effect originated from either one of the stabilizers or both.

8.5 Effect of Temperature during WSMM

The effect of temperature during WSMM should be investigated along with different degrees of cooling should be considered.

8.6 Influence of Different Bead Materials along with Bead Mixtures of Various Sizes on the Millng Performance of Multiple Drugs

The task aims at investigating the influence of various bead materials (i.e. density of grinding beads) along with the mixtures of the beads for the milling of multiple drugs. Crosslinked polystyrene beads and yttrium stabilized zirconia bead is currently used for the production of nanosuspension in the literature. Scant information exists on the impact of bead mixtures on the milling performance of multiple drugs. Future work will involve a systematic design of experiment to investigate the impact of bead mixtures on the milling performance of multiple drugs. The impact of the ratio of drug particle size to the bead size should be further examined using the microhydrodynamic model.

APPENDIX A

SUPPLEMENTARY MATERIAL

Figures A.1 to A.6 shows supplementary material used in the text.

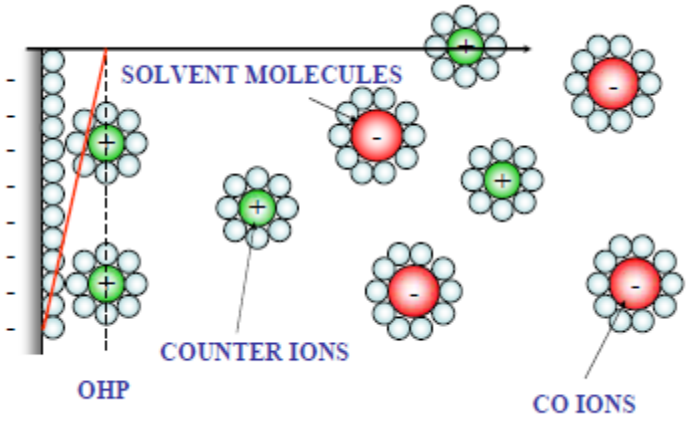

Figure A.1 Electrical double layer.

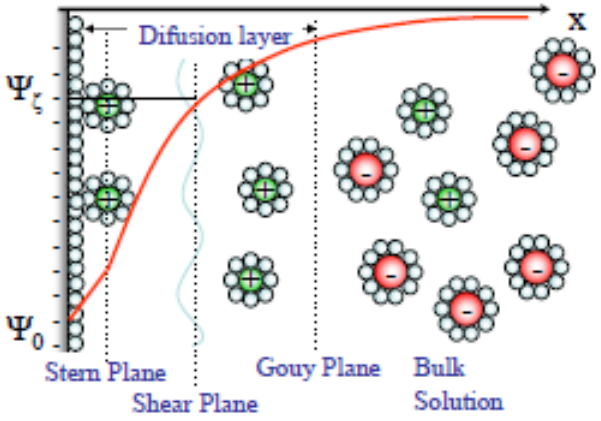

Figure A.2 Zeta potential.

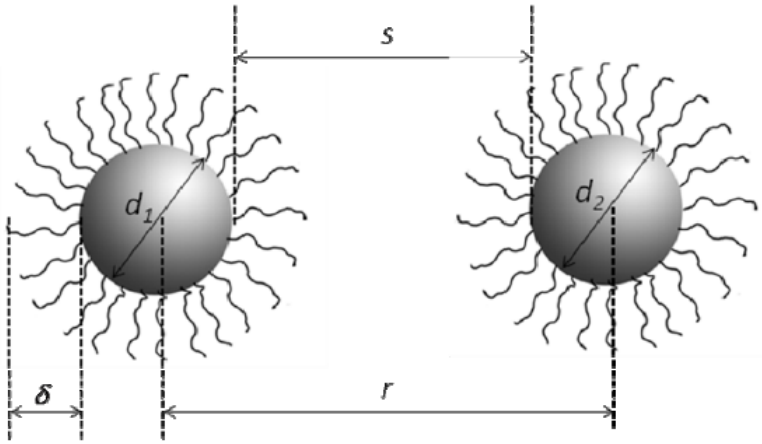

Figure A.3 Schematic representation of two coated nanoparticles of diameters d_1 and d_2 separated by surface to surface distance (s) and center to center distance (r).

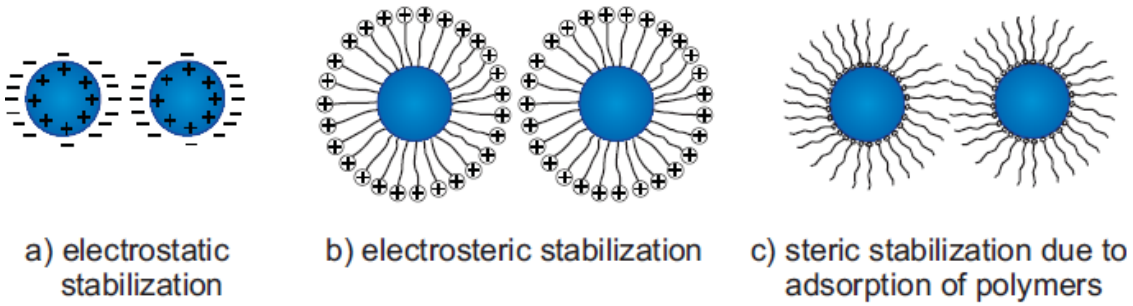

Figure A.4 Possibilities for stabilization.

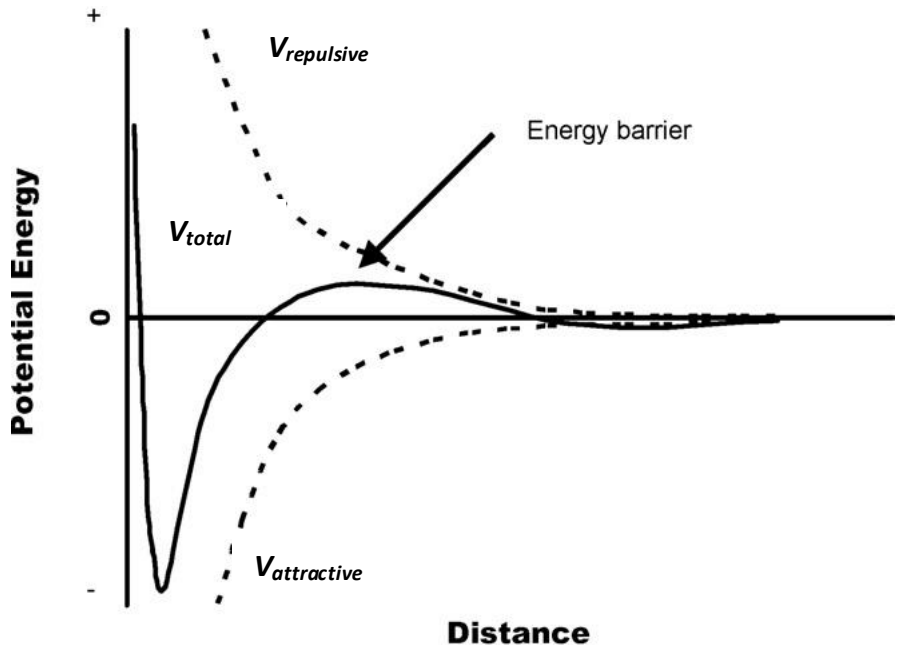

Figure A.5 Typical energy versus distance profiles of DLVO theory.

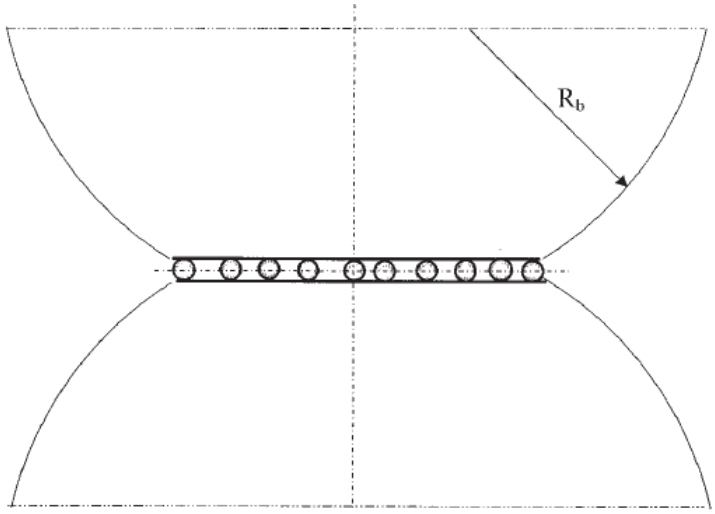

Figure A.6 Bead–bead interaction.

APPENDIX B

TYPICAL FLOW BEHAVIOR OF SUSPENSIONS

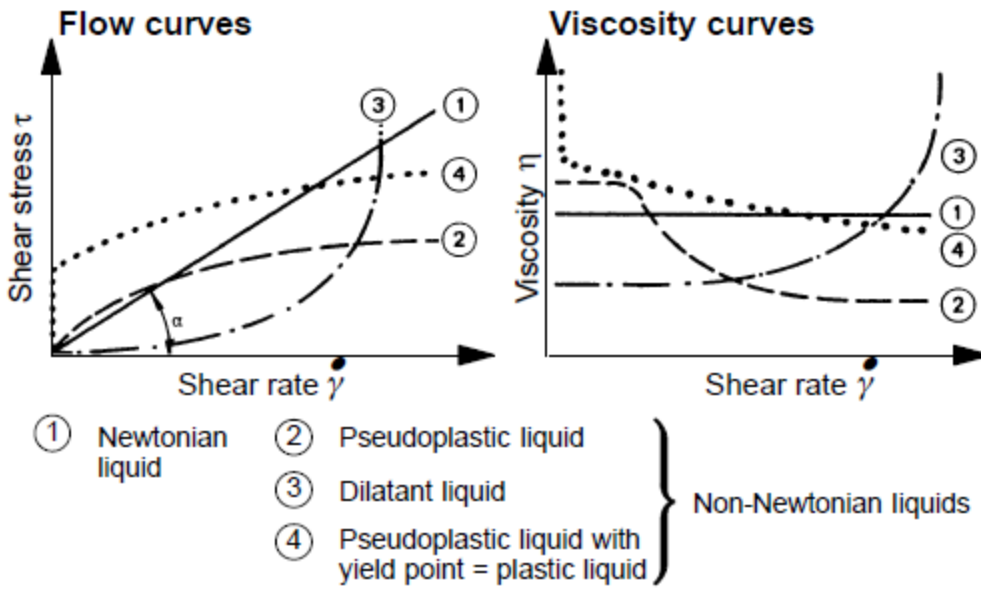

Figure B.1 Various types of common flow behavior (Edited from source: Schramm, G., 2000. "A practical approach to rheology and rheometry". Gebrueder HAAKE GmbH, Karlsruhe, Dieselstrasse, Germany, pp. 20–25)

Newtonian behavior (curve 1) is observed in dilute stable dispersion of spherical particles. For Newtonian fluids, the apparent viscosity stays relatively constant with shear rate. The flow curve (1) is known to be ideal. All other liquids not exhibiting this "ideal" flow behavior are called "Non-Newtonian liquids". Liquids which show pseudoplastic flow behavior under certain conditions of stress and shear rates – often just called "pseudoplastic liquids" or shear thinning liquids. The structures formed by the drug particles either due to aggregation are destroyed or deaggregated with increasing shear rates thereby leading to a lower viscosities. For most liquid materials the shear-thinning effect is reversible – often with some time lag – i.e. the liquids regain their original high

viscosity when the shearing is slowed down or is even terminated: the chain-type molecules return to their natural state of non-orientation, deformed droplets return to ball shape and the aggregates reform due to Brownian motion (Schramm, 2000). Dilatant liquid or shear thickening occurs when an increase in the shear rate increases the viscosity. Shear thickening mostly occurs at high solid loadings and high shear rates due to densely packed particles. Pseudoplastic liquids or shear thinning liquids with a yield point is known to exhibit plasticity (Schramm, 2000). Schramm (2000) describes the plastic fluid as dispersions which at rest can build up an intermolecular /interparticle network of binding forces (polar forces, van der Waals forces, etc.). These forces restrict positional change of volume elements and give the substance a solid character with an infinitely high viscosity. The shear thickening behavior and the plastic fluid behavior was not investigated in this work.

REFERENCES

Adam, J., Drumm, R., Klein, G., Veith, M., 2008. Milling of zirconia particles in a stirred media mill. J. Am. Ceram. Soc. 91, 2836–2843.

Adjel, A.L., Lee, D.Y., Hlinak, A.J., 1995. Apparatus for the continuous milling of aerosol pharmaceutical formulations in aerosol propellants. US Pat. 5687920.

Afolabi, A., Bilgili, E., 2011. Impact of processing and formulation parameters on drug nanoparticle suspensions produced via wet stirred media milling. Annu. Meet. AIChE, Paper No: 397b, Minneapolis, MN, Oct. 2011.

Afolabi, A., Akinlabi, O., Bilgili, E., 2013. Impact of process parameters on the breakage kinetics of poorly water-soluble drugs during wet stirred media milling: a microhydrodynamic view. Eur. J. Pharm. Sci. (under review).

Ain-Ai, A., Gupta, P.K., 2008. Effect of arginine hydrochloride and hydroxypropyl cellulose as stabilizers on the physical stability of high drug loading nanosuspensions of a poorly soluble compound. Int. J. Pharm. 351, 282–288.

Anais, J.P., Razzouq, N., Carvalho, M., Fernandez, C., Astier, A., Paul, M., Astier, A., Fessi, H., Lorino, A.M., 2009. Development of α-Tocopherol Acetate nanoparticles: influence of preparative processes. Drug Dev. Ind. Pharm. 35, 216–223.

Annapragada, A., Adjei, A., 1996. Numerical simulation of milling processes as an aid to process design. Int. J. Pharm. 136, 1–11.

Ashby, M.F., 1999. Material selection in mechanical design, Butterworth Heinemann, Burlington, MA.

Baert, L., Van't Klooster, G., Dries, W., François, M., Wouters, A., Basstanie, E., Iterbeke, K., Stappers, F., Stevens, P., Schueller, L., Van Remoortere, P., Kraus, G., Wigerinck, P., Rosier, J. 2009. Development of a long-acting injectable formulation with nanoparticles of rilpirivine (TMC278) for HIV treatment, Eur. J. Pharm. Biopharm. 72, 502–508.

Barthelmes, G., Pratsinis, S.E., Buggisch, H., 2003. Particle size distributions and viscosity of suspensions undergoing shear-induced coagulation and fragmentation. Chem. Eng. Sci. 58, 2893–2902.

Basa, S., Muniyappan, T., Karatgi, P., Prabhu, R., Pillai, R., 2008. Production and in vitro characterization of solid dosage form incorporating drug nanoparticles. Drug Dev. Ind. Pharm. 34, 1209–1218.

Berglund, K.D., Przybycien, T.M., Tilton, R.D., 2003a. Coadsorption of sodium dodecyl sulfate with hydrophobically modified nonionic cellulose polymers. 1. Role of polymer hydrophobic modification. Langmuir 19, 2705–2713.

Berglund, K.D., Przybycien, T.M., Tilton, R.D., 2003b. Coadsorption of sodium dodecyl sulfate with hydrophobically modified nonionic cellulose polymers. 2. Role of surface selectivity in adsorption hysteresis. Langmuir 19, 2714–2721.

Bernhardt, C., Reinsch, E., Husemann, K., 1999. The influence of suspension properties on ultra-fine grinding in stirred ball mills. Powder Technol. 105, 357–361.

Berthiaux, H., Marikh, K., Gatumel, C., 2008. Continuous mixing of powder mixtures with pharmaceutical process constraints. Chem. Eng. Process. 47, 2315–2322.

Bhakay, A., Merwade, M., Bilgili, E., Davé, R.N., 2011. Novel aspects of wet milling for the production of microsuspensions and nanosuspensions of poorly water soluble drugs. Drug Dev. Ind. Pharm. 37, 963–976.

Bhakay, A., Davé, R., Bilgili, E., 2013. Recovery of BCS Class II drugs during aqueous redispersion of core-shell type nanocomposite particles produced via fluidized bed coating. Powder Technol. 236, 221–234.

Bilgili, E., Hamey, R., Scarlett, B., 2004. Production of pigment nanoparticles using a wet stirred media mill with polymeric media. China Particuol. 2, 93–100.

Bilgili, E., Scarlett. B., 2005. Numerical simulation of open-circuit continuous mills using a non-linear population balance framework: incorporation of non-first-order effects. Chem. Eng. Technol. 28, 153–159.

Bilgili, E., Hamey, R., Scarlett. B., 2006. Nano-milling of pigment agglomerates using a wet stirred media mill: Elucidation of the kinetics and breakage mechanisms. Chem. Eng. Sci. 61, 149–157.

Bilgili, E., 2007. On the consequences of non-first-order breakage kinetics in comminution processes: absence of self-similar size spectra. Part. Part. Syst. Charact. 24, 12–17.

Bilgili, E., Bernstein, B., Hamey, R., Arastoopour, H., 2008. Some novel applications of grinding and milling technologies: Milling of soft materials and nanomilling. Fine Part. Technol. Charact. Research Signpost, Kerala, Ed.: Meftuni Yekeler, pp. 41–67.

Bilgili, E., Capece, M., 2011. Quantitative analysis of multi-particle interactions during particle breakage: a discrete non-linear population balance framework. Powder Technol. 213, 162–173.

Bilgili, E., Afolabi, A., 2012. A combined microhydrodynamics–polymer adsorption analysis for elucidation of the roles of stabilizers in wet stirred media milling. Int. J. Pharm. 439, 193–206.

Bisrat, M., Nystrom, C., 1988. Physicochemical aspects of drug release. VIII. The relation between particle size and surface specific dissolution rate in agitated suspensions. Int. J. Pharm. 47, 223–231.

Bose, S., Schenck, D., Ghosh, I., Hollywood, A., Maulit, E., Ruegger, C., 2012. Application of spray granulation for conversion of nanosuspensions in to dry powder form. Eur. J. Pharm. Sci. 47, 35-43.

Breitung-Faes, S., Kwade, A., 2008. Nano particle production in high-power density mills, Chem. Eng. Res. Des. 86, 390–394.

Bruno, J.A., Doty, B.D., Gustow, E., Illig, K.J., Rajagopalan, N., Sarpotdar, P., 1996. Method of grinding pharmaceutical substances. US Pat. 5518187.

Butyagin P., 1999. Rehbinder's predictions and advances in mechanochemistry. Colloids Surf. A. 160, 107–115.

Castro, L.L., Goncalves, G.R.R., Skeff Neto, K., Morais, P.C., 2008. Role of surfactant molecules in magnetic fluid: Comparison of Monte Carlo simulation and electron magnetic resonance. Phys. Rev. E. 78, 0615071 - 06150711.

Cerdeira, A.M., Mazzotti, M., Gander, B., 2010. Miconazole nanosuspensions: Influence of formulation variables on particle size reduction and physical stability. Int. J. Pharm. 396, 210–218.

Cerdeira, A.M., Mazzotti, M., Gander, B., 2011. Role of Milling Parameters and Particle Stabilization on Nanogrinding of Drug Substances of Similar Mechanical Properties. Chem. Eng. Technol. 34, 1427–1438.

Cerdeira, A.M., Mazzotti,M., Gander, B., 2013. Formulation and drying of miconazole and itraconazole nanosuspensions, Int. J. Pharm. 443, 209–220.

Chan, L.W., Lee, C.C., Heng, P.W.S., 2002. Ultrafine grinding using a fluidized bed opposed jet mill: effects of feed load and rotational speed of classifier wheel on particle shape. Drug. Dev. Ind. Pharm. 28, 939–947.

Chiou, H., Chan, H.K., Prud'homme, R.K., Raper, J.A., 2008. Evaluation on the use of confined liquid impinging jets for the synthesis of nanodrug particles. Drug Dev. Ind. Pharm. 34, 59–64.

Cho, H., Waters, M.A., Hogg, R., 1996. Investigation of the grind limit in stirred-media milling. Int. J. Miner. Process. 44–45, 607–615.

Choi, J.-Y., Park, C.H., Lee, J., 2008. Effect of polymer molecular weight on nanocomminution of poorly soluble drug. Drug Deliv. 15, 347–353.

Czekai, D.A., Seaman, L.P., 1996. Continuous media recirculation milling process. US Pat. 5513803.

Czekai, D.A., Seaman, L.P., 1998. Continuous method of grinding pharmaceutical substances. US Pat. 5718388.

Date, A.A., Patravale, V.B., 2004. Current strategies for engineering drug nanoparticles. Curr. Opin. Colloid. Interface. Sci. 9, 222–235.

Davies, J., Binner. J.G.P., 2000. Coagulation of electrosterically dispersed concentrated alumina suspensions for paste production. J. Eur. Ceram. Soc. 20, 1555–1567.

Deng, Z., Xu, S., Li, S., 2008. Understanding a relaxation behavior in a nanoparticle suspension for drug delivery applications. Int. J. Pharm. 351, 236–243.

Derjaguin, B., Landau, L., 1941. A theory of the stability of strongly charged lyophobic sols and the coalescence of strongly charged particles in electrolyte solution. Acta. Phys. Chim. USSR. 14, 633–658.

Deutsche Keramische Gesellschaft. 2009 Agitator bead mills for dispersing and comminution - Applications for ceramic processing. Ceram. Forum Int. 86, E23–E28.

El-Shall, H., Somasundaran, P., 1984. Physico-chemical aspects of grinding: a review of use of additives. Powder Technol. 38, 275–293.

Eskin, D., Zhupanska, O., Hamey, R., Moudgil, B., Scarlett, B., 2005a. Microhydrodynamics of stirred media milling. Powder Technol. 156, 95–102.

Eskin, D., Zhupanska, O., Hamey, R., Moudgil, B., Scarlett, B., 2005b. Microhydrodynamic analysis of nanogrinding in stirred media mills. AlChE J. 51, 1346–1358.

Eskin, D., Miller, M.J., 2008. A model of non-Newtonian slurry flow in a fracture. Powder Technol. 182, 313–322.

Evertsson, H., Nilsson, S., 1997. Microviscosity in clusters of ethyl hydroxyethyl cellulose and sodium dodecyl sulfate formed in dilute aqueous solutions as determined with fluorescence probe techniques. Macromolecules 30, 2377–2385.

Fadhel, H., Frances, C., 2001. Wet batch grinding of alumina in a stirred bead mill. Powder Technol. 119, 257–268.

Feng, T., Pinal, R., Carvajal, T., 2008. Process induced disorder in crystalline materials: differentiating defective crystals from the amorphous form of griseofulvin. J. Pharm. Sci., 97, 3207–3221.

Fleer, G.J., Lyklema, J., Parfitt, G.D., Rochester, C.H., 1938. In Adsorption from solution at the solid/liquid interface. Academic Press, London.

Florence, A.T., Attwood, D., 1981. Physicochemical Principles of Pharmacy. Chapman and Hall, London.

Fogler, H.S., 1999. Elements of Chemical Reaction Engineering. 3rd Ed. Prentice Hall, Upper Saddle River, NJ.

Ghosh, I., Bose, S., Vippagunta, R., Harmon, F., 2011. Nanosuspension for improving the bioavailability of a poorly soluble drug and screening of stabilizing agents to inhibit crystal growth. Int. J. Pharm. 409(1–2), 260–268.

Ghosh, I., Schenck, D., Bose, S., Liu, F., Motto, M, 2013. Identification of critical process parameters and its interplay with nanosuspension formulation prepared by top down media milling technology. Pharm. Dev. Tech. 18, 719-729.

Ghosh, I., Schenck, D., Bose, S., Ruegger, C., 2012. Optimization of formulation and process parameters for the production of nanosuspension by wet media milling technique: Effect of Vitamin E TPGS and nanocrystal particle size on oral absorption. Eur. J. Pharm. Sci. 47, 718–728.

Gidaspow, D., 1994. Multiphase Flow and Fluidization: Continuum and Kinetic Theory Descriptions. Academic Press, Boston, MA.

Hancock, B., Zografi, G., 1997. Characteristics and Significance of the Amorphous State in Pharmaceutical Systems. J. Pharm. Sci. 86, 1–12

Haskel, J.R., 2003. Laboratory scale milling process. Eur Pat. 1339390 A2

Hennart, S.L.A., Domingues, M.C., Wildeboer, W.J., van Hee, P., Meesters, G.M.H. 2010. Study of the process of stirred ball milling of poorly water soluble organic products using factorial design, Powder Technol. 198, 56–60.

Holland, S.J., Knight, W.A., Leonard, G.S., 2006. Wet Milling Process, US Pat. 2006/0214037.

Hu, J., Johnston, K.P., Williams, R.O., 2004. Nanoparticle engineering processes for enhancing the dissolution rates of poorly water soluble drugs. Drug Dev. Ind. Pharm., 30, 233–245.

Hunter. R.J., 1986. Foundations of colloid science. Vol 1. Oxford University Press, New York, NY.

Israelachvili, J., 1992. Intermolecular and Surface Forces. 2nd Ed. Academic Press, New York, NY.

Jankovic, A., 2003. Variables affecting the fine grinding of minerals using stirred mills. Minerals Engineer. 16, 337–345.

Juhnke, M., Berghausen, J., Timpe, C., 2010. Accelerated formulation development for nanomilled active pharmaceutical ingredients using a screening approach. Chem. Eng. Technol. 33, 1412–1418.

Juhnke, M., Märtin, D., John, E., 2012. Generation of wear during the production of drug nanosuspensions by wet media milling, Int. J. Pharm. 81, 214–222

Kamiya, S., Kurita, T., Miyagishima, A., Arakawa, M., 2009. Preparation of griseofulvin nanoparticle suspension by high pressure homogenization and preservation of the suspension with saccharides and sugar alcohols. Drug Dev. Ind. Pharm. 35, 1022–1028.

Karpenko, G.V., 1974. The 45th anniversary of the Rehbinder effect. Fiziko-Khimicheskaya Mekhanika Materialov, 10, 5–7.

Kawatra, S.K., 2006. Advances in Comminution. SME, Inc., Littleton, Colorado, pp. 99–114.

Kesisoglou, F., Panmai, S., Wu, Y., 2007. Nanosizing-Oral formulation development and biopharmaceutical evaluation. Adv. Drug Deliv. Rev. 59, 631–644.

Kim, C.-J., 2004. Surface Chemistry and Colloids, Advanced Pharmaceutics: Physicochemical Principles, CRC Press, pp. 193–256.

Kissa, E., 1999. Dispersions: Characterization, Testing, and Measurement. Marcel Dekker, New York, NY, pp. 240–241.

Klimpel, R.R., 1999. The selection of wet grinding chemical additives based on slurry rheology control. Powder Technol. 105, 430–435.

Knieke, C., Sommer, M., Peukert, W., 2009. Identifying the apparent and true grinding limit. Powder Technol. 195, 25–30.

Knieke, C., Steinborn, C., Romeis, S., Peukert, W., Breitung-Faes, S., Kwade, A., 2010. Nanoparticle production with stirred-media mills: opportunities and limits. Chem. Eng. Technol. 33, 1401–1411.

Knieke, C., Azad, M.A., Davé, R.N., Bilgili, E., 2013. A study of the physical stability of wet media-milled fenofibrate suspensions using dynamic equilibrium curves. Chem. Eng. Res. Des., doi: 10.1016/j.cherd.2013.02.008, in press.

Kula, M.R., Schütte, H., 1987. Purification of proteins and the disruption of microbial cells. Biotechnol. Progr. 3, 31–42

Law, S.L., Kayes, J.B., 1983. Adsorption of non-ionic water-soluble cellulose polymers at the solid-water interface and their effect on suspension stability. Int. J. Pharm. 15, 251–260.

Lee, J., 2003. Drug nano- and microparticles processes into solid dosage forms: Physical properties. J. Pharm. Sci. 92, 2057–2068.

Lee, J., Cheng, Y., 2006. Critical freezing rate in freeze drying nanocrystal dispersions. J. Control. Release 111, 185–192.

Lee, J., Choi, J.Y., Park, C.H., 2008. Characteristics of polymers enabling nano-comminution of water-insoluble drugs. Int. J. Pharm. 355, 328–336.

Lee, K., Sathyagal, A., N., McCormick, A., V., 1998. A closer look at an aggregation model of the Stöber process. J. Colloids Surf. A., *144*, 115-125.

Leuner, C., Dressman, J., 2000. Improving drug solubility for oral delivery using solid dispersions. Eur. J. Pharm. Biopharm. 50, 47–60.

Lian, J., Garay, J.E., Wang, J., 2007. Grain size and grain boundary effects on the mechanical behavior of fully stabilized zirconia investigated by nanoindentation, Scr. Mater. 56, 1095–1098.

Lipinski, C.A., 2002. Poor aqueous solubility: an industry wide problem in drug discovery. American Pharm. Rev. 5, 82–85.

Liversidge, G., Cundy, K., Bishop, J., Czekai, D., 1992. Surface modified drug nanoparticles. U.S. Pat. US5145684.

Liversidge, G.G., Cundy, K.C., 1995. Particle size reduction for improvement of oral bioavailability of hydrophobic drugs: I. Absolute oral bioavailability of nanocrystalline danazol in beagle dogs. Int. J. Pharm. 125, 91–97.

Mannheim, V., 2011. Empirical and scale-up modeling in stirred ball mills. Chem. Eng. Res. Des. 85, 405–409.

Mende, S., Schwedes, J., 2006. Mechanical production and stabilization of nanoparticles by wet comminution in stirred media mills. Powder Handl. Process. 18, 366–373.

Mende, S., Stenger, F., Peukert, W., Schwedes, J., 2003. Mechanical production and stabilization of submicron particles in stirred media mills. Powder Technol. 132, 64–73.

Meng, X., Yang, D., Keyvan, G., Michniak-Kohn, B., Mitra., S., 2011. Stabilizing dispersions of hydrophobic drug molecules using cellulose ethers during anti-solvent synthesis of micro-particulates. Coll. and Surf. B: Biointer. 70, 7–14.

Merisko-Liversidge, E., Liversidge, G.G., Cooper, E.R., 2003. Nanosizing: a formulation approach for poorly-water soluble compounds. Eur. J. Pharm. Sci. 18, 113–120.

Merisko-Liversidge, E., Liversidge, G.G., 2011. Nanosizing for oral and parenteral drug delivery: A perspective on formulating poorly-water soluble compounds using wet media milling technology. Adv. Drug Deliv. Rev. 63, 427–440.

Monteiro, A., Afolabi, A., Bilgili, E., 2013. Continuous production of drug nanoparticle suspensions via wet stirred media milling: a fresh look at the Rehbinder effect. Drug Dev. Ind. Pharm. 39, 266–283.

Muller, R.-H., Moschwitzer, J., Bushrab, F.N., 2006. Manufacturing of nanoparticles by milling and homogenization techniques. Nanopart. Technol. Drug Deliv. 159, 21–51.

Muller, R.H., Peters, K., 1998. Nanosuspensions for the formulation of poorly soluble drugs: I. Preparation by a size reduction technique. Int. J. Pharm. 160, 229–237.

Napper, D.H., 1970. Colloid stability. Ind. Eng. Chem. Prod. Res. Develop. 9, 467–477.

Napper, D.H., 1977. Steric stabilization. J. Colloid Interface Sci., 58, 390–407.

Niwa, T., Miura, S., Danjo, K., 2011. Design of dry nanosuspension with highly spontaneous dispersible characteristics to develop solubilized formulation for poorly water-soluble drugs. Pharm. Res. 28, 2339–2249.

Noyes, A.A., Whitney, W.R., 1897. The rate of solution of solid substances in their own solutions. J. Am. Chem. Soc. 19, 930–934.

Ohnishi, H., 1995. effective surface potential and double-layer interaction of colloidal particles. . J Colloid Interface Sci., *174*, 45 - 52.

Ohnishi, H., Takeuchi, M., Sekino, T., Ikuhara, Y., Niihara, K., 2010. Wear resistance of SiO(2)-doped Y-TZP grinding media during wet milling. Int. J. Appl. Ceram.Technol. 7, 502–511.

Panmai, S., Deshpande, S., 2003. Development of nanoformulations: selection of polymeric stabilizers based on adsorption isotherm. PMSE Preprints 89, 808–809.

Park, C., Youn, H., Lee, J., Lee, K., Park, J., Koh, E., Kim, H., 2009. Improved efficacy of appetite suppression by lipoic acid particles prepared by nanocomminution. Drug. Dev. Ind. Pharm. 35, 1305–1311.

Patel, C.M., Murthy, Z.V.P., Chakraborty, M., 2012. Effects of operating parameters on the production of barium sulfate nanoparticles in stirred media mill. J. Ind. Eng. Chem. 18, 1450–1457.

Peltonen, L., Hirvonen, J., 2010. Pharmaceutical nanocrystals by nanomilling: critical process parameters, particle fracturing and stabilization methods. J. Pharm. Pharmacol. 62, 1569–1579.

Persson, H., Forssberg, E., 1994. Aufbereitungs Technik 35 (6), 307–320.

Peukert, W., Schwarzer, H.C., Stenger, F., 2005. Control of aggregation in production and handling of nanoparticles. Chem. Eng. Process. 44, 245–252.

Ploehn, H.J., Russel, W.B., 1990. Interactions between colloidal particles and soluble polymers. Adv. Chem. Eng. 15, 137–228.

Rao, V.M., Lin, M., Larive, C.K., Southard, M.Z., 1997. A mechanistic study of griseofulvin dissolution into surfactant solutions under Laminar flow conditions. J. Pharm. Sci. 86, 1132–1137.

Rehbinder, P.A., 1958. Formation and aggregative stability of disperse systems. Colloids J. USSR. 20, 493–502.

Rehbinder, P.A., Shchukin, E.D., 1972. Surface phenomena in solids during deformation and fracture processes. Prog. Surf. Sci. 3, 97–104.

Rosensweig, R. E., 1985. Ferrohydrodynamics. Cambridge University Press, New York, NY, pp 46.

Russel, W. B., Saville, D. A., Schowalter, W. R., 1989. Colloidal Dispersions. Cambridge University Press, New York, NY, pp 135.

Ryde, N., Ruddy, S., 2002. Solid dose nanoparticulate compositions comprising a synergistic combination of a polymeric surface stabilizer and dioctyl sodium sulfosuccinate, US Pat. 6375986.

Sadler III, L.Y., Stanley, D.A., Brooks, D.R., 1975. Attrition mill operating characteristics. Powder Technol. 12, 19–28.

Sangani, A.S., Mo, G.B., Tsao, H.K., Koch, D.L., 1996. Simple shear flows of dense gas–solid suspensions at finite Stokes numbers. J. Fluid. Mech. 313, 309–341.

Schramm, G., 2000. A practical approach to rheology and rheometry. Gebrueder HAAKE GmbH, D-76227 Karlsruhe, Dieselstrasse, Germany, pp. 20–25.

Schubert, M.A., Harms, M., Müller-Goymann, C.C., 2006. Structural investigations on lipid nanoparticles containing high amounts of lecithin, Eur. J. Pharm. Sci. 27, 226–236.

Schwedes, J., Bunge, F., 1993. Operation of agitated bead mill. Hung J. Ind. Chem. Veszprem. 21, 129–147.

Sepassi, S., Goodwin, D.J., Drake, A.F., Holland, S., Leonard, G., Martini, L., Lawrence, M.J., 2007. Effect of polymer molecular weight on the production of drug nanoparticles. J. Pharm. Sci. 96, 2655–2666.

Sharma, P., Denny, W.A., Garg, S., 2009. Effect of wet milling process on the solid state of indomethacin and simvastatin. Int. J. Pharm. 380, 40–48.

Shchukin, E.D., 1999. Physical–chemical mechanics in the studies of Peter A. Rehbinder and his school Colloids Surf. A, 149, 529–537.

Shchukin, E.D., 2006. The influence of surface-active media on the mechanical properties of materials. Adv. Colloid Interface Sci. 123, 33–47.

Shegokar, R., Müller,R.H. 2010. Nanocrystals: Industrially feasible multifunctional formulation technology for poorly soluble actives, Int. J. Pharm. 399, 129–139.

Sievens-Figueroa, L., Bhakay, A., Jerez-Rozo, J.I., Pandya, N., Romanach, R., Michniak-Kohn, B., Iqbal, Z., Bilgili, E., Davé, R.N., 2012. Preparation and characterization of hydroxypropyl methyl cellulose films containing stable BCS Class II drug nanoparticles for pharmaceutical applications. Int. J. Pharm. 423, 496–508.

Singare, S.D., Marella, S., Gowthamrajan, K., Kulkarni, T.G., Vooturi, R., Rao, P.S., 2010. Optimization of formulation and process variable of nanosuspension: An industrial perspective. Int. J. Pharm. 402, 213–220.

Singh, S.K., Srinivasan, K.K., Gowthamrajan, K., Singare, S.D., Prakash, D., Gaikwad, B.N., 2011. Investigation of preparation parameters of nanosuspension by top-down media milling to improve the dissolution of poorly water-soluble glyburide. Eur. J. Pharm. Biopharm. 78, 441–446.

Sommer, M., Stenger, F., Peukert, W., Wagner, N.J., 2006. Agglomeration and breakage of nanoparticles in stirred media mills - a comparison of different methods and models. Chem. Eng. Sci. 61, 135–148.

Srikar, V.T., Turner, K.T., Ie, T.Y.A., Spearing, S.M., 2004. Structural design considerations for micromachined solid-oxide fuel cells. J. Power Sources 125, 62–69.

Stehr, N., 1982. Zerkleinerung u. Materialtransport in einer Ruhrwerkskugelmuhle. Dissertation. TU Braunschweig, Germany.

Stehr, N., 1984. Residence time distribution in a stirred ball mill and their effect on comminution. Chem. Eng. Process.18, 73–83.

Stehr, N., Schwedes, J., 1983. Investigation of the grinding behaviour of a stirred ball mill. Ger. Chem. Eng. 6, 337–343.

Stein, J., Fuchs, M., Mattern, Ch., 2010. Advanced milling and containment technologies for superfine active pharmaceutical ingredients. Chem. Eng. Technol. 33, 1464–1470.

Stenger, F., Mende, S., Schwedes, J., Peukert, W., 2005. The influence of suspension properties on the grinding behavior of alumina particles in the submicron size range in stirred media mills. Powder Technol. 156, 103 – 110.

Strazisar, J., Runovc, F., 1996. Kinetics of comminution in micro- and sub-micrometer ranges. Int. J. Miner. Process. 44, 673–682.

Stuart C.M.A.,1991. Adsorbed polymers in colloidal system: from static to dynamic. Polym. J. 23, 669–682.

Su, J.C., Liang, S.Y., Liu, W.L., Jan, T.C., 2004. Ceramic micro/nanoparticle size evolution in wet grinding in stirred ball mill. J. Manuf. Sci. Eng. 126, 779–786.

Suzuki, M., Machida, M., Adachi, K., Otabe, K., Sugimoto, T., Hayashi, M., Awazu, S., 2000. Histopathological study of the effects of a single intratracheal instillation of surface active agents on lung in rats, J. Toxicol. Sci. 25, 49–55

Tadros, T.F., 1994. Surfactants in Agrochemicals. Marcel Dekker, New York, pp. 130.

Tanaka, Y., Inkyo, M., Yumoto, R., Nagai, J., Takano, M., Nagata, S., 2009. Nanoparticulation of poorly water soluble drugs using a wet-mill process and physicochemical properties of the nanopwders. Chem. Pharm. Bull. 57, 1050–1057.

Tatsumi, S., Murayama, Y., Hayakawa, H., Sanol, M., 2009. Experimental study on the kinetics of granular gases under microgravity. J. Fluid Mech. 641, 521–539.

Tüzün, M.A., Loveday, B.K., Hinde, A.L., 1995. Effect of pin tip velocity, ball density and ball size on grinding kinetics in a stirred ball mill, Int. J. Miner. Process. 43, 179-191.

Van Eerdenbrugh, B., Froyen, L., Martens, J.A., Blaton, N., Augustijns, P., Brewster,M., Van den Mooter, G., 2007. Characterization of physico-chemical properties and pharmaceutical performance of sucrose co-freeze-dried solid nanoparticulate powders of the anti-HIV agent loviride prepared by media milling. Int. J. Pharm. 338, 198–206.

Van Eerdenbrugh, B., Van den Mooter, G., Augustijns, P., 2008. Top-down production of drug nanocrystals: Nanosuspension stabilization, miniaturization and transformation into solid products. Int. J. Pharm. 364, 64–75.

Van Eerdenbrugh, B., Vermant, J., Martens, J.A., Froyen, L., Humbeeck, J.V., Augustijns, P., Van den Mooter, G. 2009. A screening study of surface stabilization during the production of drug nanocrystals. J. Pharm. Sci. 98, 2091–2103.

Vanarase, A.U., Alcala, M., Rozo, J.I., Muzzio, F.J., Romanach, R.J., 2010a. Real-time monitoring of drug concentration in a continuous powder mixing process using NIR spectroscopy. Chem. Eng. Sci. 65, 5728–5733.

Vanarase, A.U., Muzzio, F.J., 2010b. Effect of operating conditions and design parameters in a continuous powder mixer. Powder Technol. 208, 26–36.

Varinot, C., Berthiaux, H., Dodds, J., 1999. Prediction of the product size distribution in associations of stirred bead mills. Powder Technol. 105, 228–236.

Verhoff, F.H., Snow, R.A., Pace, G.W., 2003. Media milling. US Pat. 6604698.

Verma, S., Gokhale, R., Burgess, D.J., 2009. A comparative study of top-down and bottom-up approaches for the preparation of micro/nanosuspensions, Int. J. Pharm. 380, 216–222.

Verwey, E.J.W., Overbeek. J.T.G., 1948. Theory of the stability of lyophobic colloids: The interaction of sol particles having an electrical double layer. Elsevier, New York, NY.

Vital, A., Zürcher, S., Dittmann, R., Trottmann, M., Lienemann, P., Bommer, B., Graule, T., Apel, E., Höland, W., 2008. Ultrafine comminution of dental glass in a stirred media mill. Chem. Eng. Sci. 63, 484–494.

Wang, Y., Forssberg, E., 2006. Production of carbonate and silica nano-particles in stirred bead milling. Int. J. Miner. Process. 81, 1–14.

Watanabe, A., 2002. Study of crystalline drugs by means of a polarizing microscope. XIX. A trial production of a table of the optical crystallographic characteristics of crystalline drugs including crystal habits. Yakugaku Zasshi 122, 595–606.

Winnik, F.M., Winnik, M.A., 1990. The interaction of sodium dodecylsulfate with (hydroxypropyl)cellulose. Polym. J. 22, 482–488.

Wu, L., Zhang, J., Watanabe, W., 2011. Physical and chemical stability of drug nanoparticles. Adv. Drug Delivery Rev. 63, 456–69.

Wylie, J.J., Koch, D.L., Ladd, A.J.C., 2003. Rheology of suspensions with high particle inertia and moderate fluid inertia, J. Fluid Mech. 480, 95–118.

Xiong, R., Lu, W., Li, J., Wang, P., Xu, R., Chen, T., 2008. Preparation and characterization of intravenously injectable nimodipine nanosuspension, Int. J. Pharm. 350, 338–343.

Zarow, A., Zhou, B., Wang, X., Pinal, R., Iqbal, Z., 2011. Spectroscopic and X-ray diffraction study of structural disorder in cryomilled and amorphous griseofulvin. Appl. Spectrosc. 65, 135–143.